Goldstone Boson Condensation and Effects of the Axial Anomaly in Color Superconductivity

Vom Fachbereich Physik
der Technischen Universität Darmstadt

zur Erlangung des Grades
eines Doktors der Naturwissenschaften
(Dr. rer. nat.)

genehmigte Dissertation von
Dipl.-Phys. Hannes Gregor Steffen Basler
aus Bad Soden a. T.

Darmstadt 2011
D17

Referent: Priv. Doz. Dr. Michael Buballa
Korreferent: Prof. Dr. Jochen Wambach

Tag der Einreichung: 16. 11. 2010
Tag der Prüfung: 12. 01. 2011

Contents

Zusammenfassung v

1. Introduction 1

2. Color superconductivity 7
   - 2.1. Pairing patterns in color superconductors 8
     - 2.1.1. The two-flavor color superconducting phase 8
     - 2.1.2. The color-flavor locked phase 9
     - 2.1.3. Other pairing patterns 10
   - 2.2. Gapless phases 11

3. The Nambu–Jona-Lasinio model 13
   - 3.1. Lagrangian 14
     - 3.1.1. Four-point interactions 14
     - 3.1.2. Six-point interaction 14
   - 3.2. Mean-field approximation 15
   - 3.3. Thermodynamic potential 16
     - 3.3.1. Thermodynamic potential of the quarks 16
     - 3.3.2. Thermodynamic potential of the leptons 18
   - 3.4. Gap equations 18
   - 3.5. Neutron star constraints 20
     - 3.5.1. Charge neutrality 20
     - 3.5.2. β equilibrium 21
   - 3.6. Parameters 21

4. Goldstone boson condensation 23
   - 4.1. Goldstone bosons in the CFL phase 23
     - 4.1.1. Masses of Goldstone bosons 24
     - 4.1.2. The condensation point 26
   - 4.2. Pseudoscalar diquark condensates 27
     - 4.2.1. Axial flavor transformations 28
     - 4.2.2. Including pseudoscalar diquark condensates 29

4.3. Phase diagram of neutral quark matter 30
  4.3.1. The gapless CFLK^0 phase 34
  4.3.2. The gCFL window 39
  4.3.3. The p2SC phase 42
4.4. Neutrino trapping 46
  4.4.1. Varying μ_Q 47
  4.4.2. Lepton chemical potential 50
  4.4.3. The $\mu_{L_e} - T$ phase diagram 51
  4.4.4. The $T - \mu$ phase diagram at $\mu_{L_e} = 200$ MeV, 400 MeV 53

5. $U(1)_A$ breaking in color superconductors 55
5.1. The Ginzburg-Landau ansatz 56
5.2. The $U(1)_A$ breaking in the diquark sector 58
  5.2.1. Effects of the transformed six-point interaction 59
  5.2.2. Parameters 60
5.3. The low-temperature critical end point 60
  5.3.1. Equal quark masses 61
  5.3.2. Realistic strange quark mass 67
5.4. Bose-Einstein condensate of diquarks 68
5.5. Connection to the Ginzburg-Landau results 71
  5.5.1. A GL example of CFL vs. 2SC 73

6. $U(1)_A$ breaking and meson condensates 75
6.1. The K^0 mass at non-zero K' 75
6.2. Pseudoscalar diquark condensates and non-zero K' 80
6.3. The phase diagram with non-zero K' 81

7. Summary, conclusions and outlook 89

A. Conventions 92

B. Parameter sets 94

C. The transformed six-point interaction 95

D. On the numerical details 96
D.1. Momentum integrals in the gCFL/gCFLK^0 phase 96
D.2. Solving the gap equations in the gCFLK^0 phase 97

E. The accidental axial symmetry in the (p)2SC phase 100

Zusammenfassung

In dieser Arbeit untersuchen wir das Phasendiagramm neutraler Quark-Materie bei Dichten, die im Inneren eines Neutronensterns auftreten können. Bei diesen hohen Dichten finden wir eventuell freie Quarks und Gluonen. Als Fermionen mit einer anziehenden Wechselwirkung werden die Quarks einen Farbsupraleiter formen. Um Aussagen über die Phasenstruktur eines solchen Farbsupraleiters machen zu können, verwenden wir das Nambu–Jona-Lasinio-Modell in *Mean-field*-Näherung. Bei ausreichend hohem chemischen Potential der Quarks bildet sich eine besonders symmetrische farbsupraleitende Phase, die *Color-Flavor-Locked*-Phase (CFL-Phase). Bei geringerem chemischen Potential verhindert die hohe Masse des Strange-Quarks eine CFL-Phase und die weniger symmetrische *Two-Flavor-Color-Superconducting*-Phase (2SC-Phase) entsteht. Aufgrund der spontanen Brechung der Symmetrie durch Diquark-Kondensate entstehen in der CFL-Phase Goldstonebosonen als mögliche Anregungen. Wir untersuchen die Möglichkeit der Kondensation dieser Goldstonebosonen in pseudoskalaren Diquark-Kondensaten und stellen fest, dass ein großer Teil der CFL-Phase durch eine CFL-Phase mit einem Kondensat aus neutralen Kaonen ersetzt wird. Des Weiteren untersuchen wir dieses Phasendiagramm im Detail und beleuchten die Unterschiede zu vorherigen Phasendiagrammen, in denen nur skalare Diquark-Kondensate berücksichtigt worden sind. Weiterhin untersuchen wir den Effekt einer erhaltenen Leptonenzahl. Diese Situation ist von Interesse, da sie bei Berücksichtigung von elektrischer Ladungsneutralität zur Kondensation von geladenen Kaonen führt.

Im zweiten Teil der Arbeit untersuchen wir den Einfluss der axialen Anomalie auf das Zusammenspiel von chiralen Kondensaten und Diquark-Kondensaten, sowie den dadurch entstehenden Effekt auf den chiralen Phasenübergang. Das Brechen der axialen $U(1)$-Symmetrie wird im NJL-Modell üblicherweise durch eine Sechspunkt-Wechselwirkung erreicht, dem sogenannten ’t Hooft-Term. Die Mean-field-Näherung bewirkt allerdings, dass dessen Wirkung auf die chiralen Kondensate beschränkt bleibt. Durch das Einführen einer transformierten Sechspunkt-Wechselwirkung erreichen wir, dass sich der Einfluss der $U(1)_A$-brechenden Wechselwirkung auf den Diquark-Sektor ausdehnt. Dieser Term gehört zu den vielen Termen mit passenden Symmetrien, die im NJL-Modell eingefügt werden können. Motiviert wird dieser Term durch eine Ginzburg-Landau-Analyse, in der gezeigt werden konnte, dass ein solcher Term zur Entstehung eines zweiten Endpunkts am Niedertemperatur-Ende des chiralen Phasenübergangs führen kann. Die Parameter des NJL-Modells können wir besser bestimmen als die Koeffizienten einer Ginzburg-Landau-Analyse. Außerdem können wir im NJL-Modell einfacher auch weniger symmetrische Situationen behandeln. Damit erhalten wir einen Überblick über den Effekt der axialen Anomalie auf die Phasenstruktur. Es zeigt sich, dass die 2SC Phase einen *Crossover* zwischen chiral gebrochener Phase und CFL-Phase verhindert.

Im letzen Teil der Arbeit führen wir unsere Erkenntnisse aus den beiden vorangegangen Teilen zusammen und untersuchen die Auswirkungen der transformierten Sechspunkt-Wechselwirkung auf das Phasendiagramm neutraler Quarkmaterie. Wir sehen, dass die Entstehung eines Goldstoneboson-Kondensates unterdrückt wird, da die transformierte Sechspunkt-Wechselwirkung die Kopplung im pseudoskalaren Quark-Quark-Kanal schwächt.

1. Introduction

In all times mankind has been fascinated by stars, planets, nebula and other celestial objects. The study of the objects in the sky is the oldest of the natural sciences. The time and length scales needed to describe the origin and the movement of these objects are among the largest in physics. On the other hand, many of the properties of these large objects are determined by the behavior of the very small things in nature. So is, for instance, the life cycle of a star a sequence of different nuclear reactions. When all nuclear fuel is burned, the star may transform into a white dwarf or, depending on its mass, collapse in a supernova explosion, forming a neutron star or a black hole. Among these objects neutron stars are of particular interest, since their properties might actually be connected to the smallest particles we know today, the quarks.

Neutron stars are relatively small compared with other astrophysical objects but extremely dense. Within a radius of about ten to fifteen kilometers they contain up to two times the mass of our sun. Any denser system will collapse into a black hole.

The idea that there might exist stars which mainly consist of neutrons was formulated in 1933 by Baade and Zwicky [1], shortly after the discovery of the neutron in 1932 [2]. It was not until 1967, that the first observation of a neutron star was made accidentally by Hewish [3]. Today we know about 2000 neutron stars. Due to their pulsating emissions of electromagnetic radiation we have very precise measurements of their rotation frequencies. For some of the stars there are also measurements of the masses, radii and temperatures. These measurements are not as accurate as one would like them to be, hence they can give only rough restrictions for the equation of state and the cooling behavior of a neutron star.

In a simple model we can describe the structure of a neutron star as four layers, the outer crust, the inner crust, the outer core and the inner core, cf. Fig. 1.1. The outer crust, which builds the neutron star's surface, is a few hundred meters thick, it mainly consists of ions and electrons. The electrons form a degenerate Fermi gas and with increasing density the electron capture rate rises making the nuclei more neutron rich. The transition to the inner crust can be defined by the neutron drip point ρ_{ND}, the density where neutrons start to drip out of the nuclei. Going deeper into the neutron star a density is reached where neutrons are uniformly distributed in space and no longer concentrated in the nuclei. This happens in a

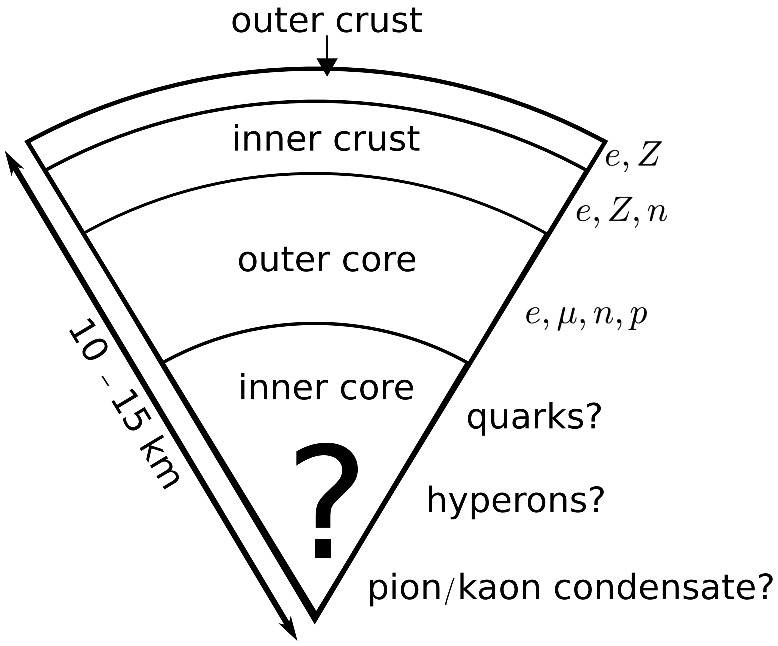

Figure 1.1.: Schematic sketch of the basic structure of a neutron star.

depth of about one to two kilometers where the density reaches approximately half of nuclear saturation density ($\rho_0 = 0.16\,\mathrm{fm}^{-3}$). When the individual nuclei have disappeared, the resulting matter consists mainly of neutrons, electrons, muons and a small fraction of protons. This region inside a neutron star is called the outer core. These three layers of a neutron star can be described more or less successfully by models based on data from nuclear experiments. However, we know very little on the behavior of matter at the even larger densities occurring in the inner core. Possible phenomena are the appearance of hyperons, pion and kaon condensates or the existence of deconfined quarks.

Before going on with the possible quark core of a neutron star, we would like to mention that this is a simplified picture of a neutron star's structure and the structure becomes more complicated when one considers the fast rotation of a neutron star, where the crust and core may rotate with different velocities. Further on there might be small liquid and plasma phases at the surface of the star called ocean and atmosphere, which are relevant for the observed radiation spectrum. The boundaries between the different layers and phases inside the neutron star may not be sharp transitions, but mixed or inhomogeneous phases might be formed.

Back to the inner core; when nuclei or other baryons are compressed to very high densities there is a point when they will start to overlap. From this simple picture it is clear that, when it is no longer possible to distinguish the individual baryons, one has to consider their internal degrees of freedom. In 1964 it was proposed by

Gell-Mann [4] and Zweig [5] that quarks and gluons are these basic building blocks of all hadrons. The interactions between quarks and gluons are described by quantum chromodynamics (QCD). There are six different quark flavors in QCD: up, down, strange, charm, bottom and top. But only the lightest three of them can be relevant for the description of a neutron star's core. Therefore we will neglect the charm, bottom and top quarks completely and work with so-called three-flavor quark matter. Each quark carries one of three gauge charges, these charges are named colors and they are labeled as red, green and blue. No colored object has ever been directly observed, all measured particles are colorless (white) bound states of three quarks (baryons) or quark-antiquark states (mesons)[1]. The absence of any free color charge is one of the essential features of QCD, it is called "color confinement". At large temperature or chemical potential one assumes that a system undergoes a transition to a deconfined phase which contains "free" quarks and gluons [6, 7]. Besides heavy-ion collisions, the only known places in nature where deconfined quarks and gluons might exist are the inner cores of neutron stars. By changing the energy scale also the coupling strength varies, the so-called "running coupling". On larger momenta and shorter distances the coupling becomes weaker and vanishes at asymptotically high momenta, this effect is called "asymptotic freedom" [8, 9]. The arbitrarily weak coupling strength at short distances allows for a perturbative treatment of QCD at these energies. On the other hand, the coupling grows at larger distances making the perturbative approach useless and one has to use non-perturbative techniques, models or lattice calculations (at zero chemical potential). Another important feature of QCD is the spontaneous breaking of chiral symmetry. Chiral symmetry is the symmetry under which left-handed and right-handed fields transform independently. Neglecting the small bare quark masses this symmetry is realized in the QCD Lagrangian. However it is, in vacuum, spontaneously broken by the formation of antiquark-quark condensates. This spontaneous symmetry breaking is accompanied by the emergence of "Goldstone" bosons [10, 11, 12]. At high temperature and/or large chemical potential chiral symmetry is expected to be restored.

One of the central objects of interest in many QCD studies is the QCD phase diagram, the behavior of quark matter in dependence of temperature and chemical potential. In Fig. 1.2 we show a simple sketch of the present-day standard picture of the phase diagram. At small chemical potential and small temperature chiral symmetry is spontaneously broken and hadrons are the relevant degrees of freedom. There are strong indications from heavy-ion experiments and lattice calculations that this changes smoothly at low chemical potential and at temperatures around 150 to 200 MeV, where quarks and gluons become the relevant degrees of freedom. Going to (asymptotically) high chemical potentials and low temperatures we come to a regime where perturbative QCD works. Here we know from first principles that

---

[1] Colorless bound states of more quarks and antiquarks might also be possible.

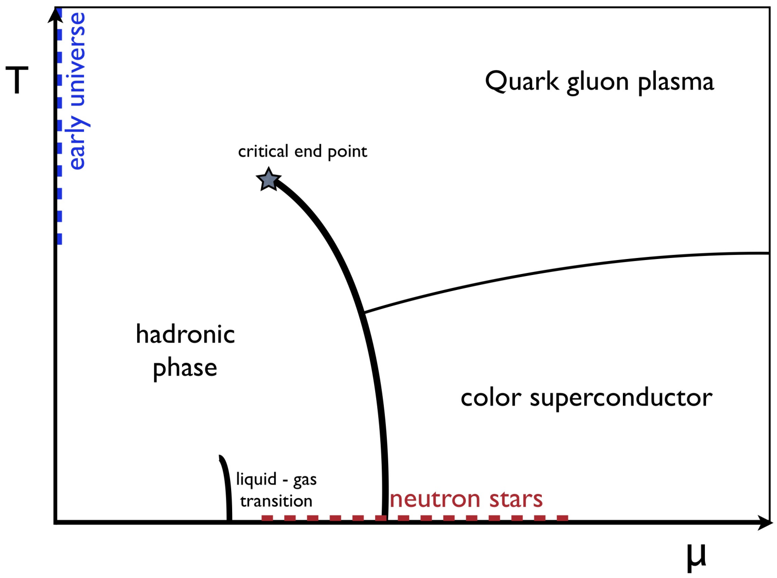

Figure 1.2.: Schematic phase diagram showing today's standard picture of the QCD phase diagram .

deconfined quarks are weakly interacting and form a color superconductor. A color superconductor is the QCD analog of an ordinary electromagnetic superconductor. While in an electromagnetic superconductor the Cooper-pairs are formed from electrons, the pairs in a color superconductor consist of quarks. Since there is only one flavor of electrons in nature, there is no flavor structure involved in the formation of Cooper-pairs in an electromagnetic superconductor. In contrast, the different quark flavors allow for a large variety of pairing patterns in a color superconductor, this can lead to a rich phase structure[2]. If there exist deconfined quarks in the inner core of a neutron star, it is expected that they form a color superconductor, although the chemical potential is not asymptotically high and the densities are more moderate. A more detailed introduction on color superconductivity is given in Chapter 2.

In the region between zero and asymptotically high quark chemical potential perturbative and lattice QCD do not work and obtaining a phase diagram from the Dyson-Schwinger approach is technically involved. In this situation one usually relies on model calculations. Most of these model calculations show a first order phase transition separating the hadronic phase from the quark-gluon plasma. To be consistent with the lattice calculations this first order phase transition has to end at a critical end point. Although this is the standard picture today, we can be relatively sure that the phase diagram has a richer structure, especially at low temperatures where inhomogeneous, quarkyonic[3] or other structures might be realized. As a possible modification of the standard picture we will later discuss the appearance of a second critical end point on the low-temperature end of the chiral phase transition.

---

[2] Different spin configurations may lead to additional pairing patterns, also in the electromagnetic superconductor.

In this work we will use the Nambu−Jona-Lasinio (NJL) model [14, 15] to investigate the phase structure of the color superconducting phase. The NJL model has the same global symmetries as QCD and can be used as a model for QCD. However, there are some important differences between QCD and the NJL model. The NJL model is not a gauge theory, hence the local $SU(3)$ gauge symmetry of QCD has to be modeled by a global $SU(3)$ color symmetry. Also the breaking of the axial $U(1)$ symmetry by quantum effects in QCD has to be put in by hand in the NJL Lagrangian. Although the NJL model is not QCD, it provides a good way to learn about the basic mechanisms and processes in a region of the phase diagram where other methods are not applicable (perturbation theory, lattice QCD) or are technically very involved (Dyson-Schwinger approach).

In this work we are interested in the phase structure of the color superconductor indicated in Fig. 1.2 under the conditions of a neutron star's core. Among the three different quarks used in our NJL-type model, one species, the strange quarks, has a significantly larger mass than the other quarks (up and down). It is this mass difference that is responsible for most of the phase structures of color superconducting quark matter. At large quark chemical potentials, where the mass difference is negligible, all quark flavors participate in the formation of the color superconductor (color-flavor locked (CFL) phase). At lower quark chemical potential, the mass difference plays an important role and allows only up and down quarks to form a color superconductor (two-flavor color superconductor, 2SC phase). These two phases share the feature that they consist of scalar diquark condensates. The phase diagram involving color superconducting phases with only scalar condensates has been extensively studied [16, 17, 18, 19]. In the first part of the work we will extend these investigations by also allowing for pseudoscalar condensates. The formation of pseudoscalar condensates might be the result of the condensation of Goldstone bosons. These Goldstone bosons originate from the symmetry breaking in the CFL phase. This mechanism works in complete analogy to the spontaneous symmetry breaking in the vacuum. The resulting Goldstone bosons (pseudoscalar mesons) carry the same quantum numbers in vacuum and in the CFL phase. The Goldstone bosons are of interest since they allow the CFL phase to inherit some of their properties. This enables the CFL phase to react to stress, induced, for example, by charge neutrality or the large strange quark mass, by forming different Goldstone boson condensates. Of particular interest is the formation of a K^0 condensate since it reduces the strangeness content of the system. Central in this part will be the resulting phase diagram of neutral quark matter, we will discuss its features and the differences to the phase diagram containing only scalar condensates in detail.

---

[3] There might be space in the phase diagram for a so-called quarkyonic phase. This phase is the conceptual idea of a confined phase where the degrees of freedom combine the properties of quarks and baryons (quarkyonic = quark + baryon) [13].

In the second part we will extend the six-point interaction of our NJL-type model to the diquark sector. Here we are motivated by results of a Ginzburg-Landau analysis [20, 21, 22] predicting that such an interaction can lead to the appearance of a low-temperature end point on the chiral phase transition. While the Ginzburg-Landau analysis can only show the principle possibility of such a second end point, in the NJL model we can investigate under what conditions such an end point exists. Further on the Ginzburg-Landau analysis in Refs. [20, 21, 22] was done only for a very symmetric situation: equal quark masses, equal diquark condensates, CFL pairing. In our NJL model, on the other hand, we are able to study the role of less symmetric pairing patterns, as well as the effect of a more realistic strange quark mass. To compare the results with the Ginzburg-Landau analysis we will not consider charge neutrality and possible Goldstone boson condensates in this part.

Goldstone bosons and charge neutrality come back into the game in the third part. Here we will study the effect of extending the six-point interaction to the diquark sector on the phase diagram of neutral quark matter and the condensation of Goldstone bosons. The only previous results [21] on this topic are considerations in the framework of a low-energy effective theory telling us that the Goldstone bosons should become heavier. We are able to calculate the masses of the Goldstone bosons explicitly within the NJL model. The Goldstone bosons masses directly effect the phase structure.

This thesis is organized in the following way; after this introduction we will give a short overview of color superconductors in Chapter 2 and introduce our NJL-type model in Chapter 3. The phase diagram of charge neutral quark matter in β-equilibrium with possible meson condensates is presented in Chapter 4, in this context we also discuss the effects of a conserved lepton number as it may occur in the very first moments of a neutron star's life. In the next chapters we will study the effect of the axial $U(1)$ breaking on the color superconductor. At first we will investigate the interplay between the chiral and diquark condensates and the effect on the chiral phase transition (Chapter 5), and later (Chapter 6) study the effect on kaon condensates and on the phase diagram under neutron star conditions. We summarize and conclude in Chapter 7.

Parts of the results shown in the Chapters 4 and 5 have already been published in Ref. [23] and Ref. [24].

2. Color superconductivity

In matter at high densities quarks and gluons are the relevant degrees of freedom. As any fermionic system quarks form a superconductor if there is an attractive interaction between them and the temperature is below a critical value. At these low temperatures fermions form a degenerate liquid. For non-interacting particles, the free energy, at zero temperature, is given by

$$\Omega = E - \mu N \tag{2.1}$$

with the total energy E, the particle number N and the chemical potential $\mu = E_F$. Adding one particle to the system requires the energy E_F and will therefore keep the free energy unchanged. With an attractive interaction the creation of pairs lowers the potential energy and it is preferable for the system to create as many fermion pairs as possible from the quarks near the Fermi surface. The Cooper-pairs will condense and create a gap in the excitation spectrum. With this gap creating a new Cooper pair will cost some energy and the system stabilizes. This mechanism was first described by Bardeen, Cooper and Schrieffer [25, 26] (BCS theory).

In quark matter, where at asymptotically high densities the one-gluon exchange[1] and at more moderate densities instanton induced interactions are attractive, it is unavoidable to form Cooper pairs. Since pairs of two quarks can not be color singlets the color gauge symmetry is broken, hence the name "color superconductor". For reviews on color superconductivity see Refs. [27, 28, 29, 30, 31, 32, 33, 34, 35, 36, 16, 37, 38, 39].

In the system we want to describe, a neutron star, the energy scale is not so high that charm, bottom and top quarks appear. Therefore we work only with the three lightest flavors. These three flavor degrees of freedom allow for a large variety of pairing patterns.

---

[1] The one-gluon exchange is attractive in the anti-triplet channel and repulsive in the sextet channel. We will therefore consider the anti-triplet channel for the formation of a color superconductor.

2.1. Pairing patterns in color superconductors

The Pauli principle limits the pairing to antisymmetric operators,

$$\langle q\,\mathcal{O}\,q\rangle \qquad \text{with}\,\mathcal{O}\,\text{antisymmetric}\,. \tag{2.2}$$

To correspond to the attractive anti-triplet channel we choose the antisymmetric Gell-Mann matrices $\lambda_2\,\lambda_5$ and λ_7 as operators in color space. Since we only include the preferred spin-0 condensates the operator structure in Dirac space is limited to the use of $C\,(=i\,\gamma^2\,\gamma^0)$ and $C\gamma^5$. To get an overall antisymmetric operator we use the antisymmetric Gell-Mann matrices τ_2, τ_5 and τ_7 for the flavor structure. With these operators it is possible to define scalar

$$s_{AA'} = \langle q^T C\gamma_5 \tau_A \lambda_{A'} q\rangle\,, \qquad\qquad A,\,A' \in \{2,5,7\} \tag{2.3}$$

and pseudoscalar

$$p_{AA'} = \langle q^T C \tau_A \lambda_{A'} q\rangle\,, \qquad\qquad A,\,A' \in \{2,5,7\} \tag{2.4}$$

diquark condensates.

The two most important phases are the 2SC phase (two-flavor color superconducting) and the CFL (color-flavor locked) phase.

2.1.1. The two-flavor color superconducting phase

The two-flavor color superconducting (2SC) phase [40, 27, 41, 42] is the most simple pairing pattern. Here only quarks of two flavors (usually up and down quarks) are paired, forming scalar condensates. At a quark chemical potential where no strange quarks exist or when the Fermi surfaces of the up/down and strange quarks have a large separation, preventing the formation of pairs including strange quarks, the 2SC phase is realized. This situation can be described by

$$\langle q_i^\alpha C\gamma_5 q_j^\beta\rangle \propto \Delta_{2\mathrm{SC}}^\gamma\,\epsilon^{\alpha\beta\gamma}\epsilon_{ij3} \tag{2.5}$$

with the gap parameters $\Delta_{2\mathrm{SC}}^\gamma$ and the color (flavor) indices $\alpha, \beta, \gamma\,(i, j)$ running from 1 to 3. Beside using 1, 2 and 3 for the color indices, we will often refer to them as "red" (1), "green" (2) and "blue" (3). The free color index γ shows an arbitrariness in choosing the color structure of the 2SC phase.

Using the above defined condensates (Eq. (2.3)), 2SC-pairing leads to the scalar diquark condensates

$$s_{2A'} = \langle q^T C\gamma_5 \tau_2 \lambda_{A'} q\rangle, \qquad A' \in \{2,5,7\}\,. \tag{2.6}$$

Usually a color rotation is used to rotate the condensates in the $A' = 2$ direction (meaning $\Delta_{2\mathrm{SC}}^\gamma = \Delta_{2\mathrm{SC}}\delta^{\gamma 3}$ in Eq. (2.5)) leaving only the s_{22} condensate with a non-zero value. With this choice the blue quarks are not involved in the pairing and therefore they do not develop a gap in their excitation spectrum. This makes them responsible for all low-energy excitations and thereby also for the transport properties. The 2SC pairing pattern breaks the QCD symmetry (assuming massless up and down quarks and heavy strange quarks)

$$\begin{aligned} &SU(3)_{\text{color}} \times SU(2)_L \times SU(2)_R \times U(1)_B \times U(1)_S \\ &\qquad \to SU(2)_{\text{rg}} \times SU(2)_L \times SU(2)_R \times U(1)_{\tilde{B}} \times U(1)_S \,. \end{aligned} \tag{2.7}$$

This symmetry breaking pattern gives rise to five massive gluons through the Anderson-Higgs mechanism [43, 44]. On the other hand all global symmetries are preserved. In the non-strange sector the baryon number symmetry is broken, but it can be replaced with a "rotated" baryon number. The generator of this rotated baryon number $\tilde{B}$ is a linear combination of the unrotated baryon number generator $B = \mathbb{1}$ and the color generator λ_8

$$\tilde{B} = B - \sqrt{3}\lambda_8 \,. \tag{2.8}$$

This also rotates the generator $Q = \text{diag}_f\,(2/3,\, -1/3)$ of the electromagnetism into

$$\tilde{Q} = Q - \frac{1}{2\sqrt{3}}\tau_8 \,. \tag{2.9}$$

Therefore the 2SC phase is neither an electromagnetic superconductor nor a superfluid. Since some of the unpaired quarks carry non-zero $\tilde{Q}$ charge the 2SC phase is a $\tilde{Q}$-conductor.

2.1.2. The color-flavor locked phase

In three-flavor quark matter where all quarks have the same mass the most symmetric pairing pattern is the color-flavor locked (CFL) phase [45]. As a result the CFL phase is the ground state of three-flavor quark matter at asymptotically high densities. The pairing can be described by

$$\langle q_i^\alpha C\gamma_5 q_j^\beta \rangle \propto \Delta_{\text{CFL}}\epsilon^{\alpha\beta A}\epsilon_{ijA} + \Delta_{\text{CFL}}\kappa\left(\delta_i^\alpha\delta_j^\beta + \delta_j^\alpha\delta_i^\beta\right) \tag{2.10}$$

with the color (flavor) indices $\alpha, \beta\,(i,\, j)$ running from 1 to 3 and the CFL gap parameter Δ_{CFL}. The first term on the right hand side of Eq. (2.10) transforms as an anti-triplet and the second term as a sextet. It turns out, that κ is in general non-zero but small [45, 46, 47], therefore we will neglect the sextet contribution in the following, as it is usually done.

In the notation of the scalar diquark condensates (Eq. (2.3)), the (ideal) CFL phase can be characterized by

$$s_{22} = s_{55} = s_{77} \neq 0 \,. \tag{2.11}$$

These condensates break the original symmetry (for massless quarks)

$$SU(3)_{\text{color}} \times SU(3)_L \times SU(3)_R \times U(1)_V \rightarrow SU(3)_{\text{color}+V} \tag{2.12}$$

with the combined color-flavor locked symmetry

$$SU(3)_{\text{color}+V} : q \rightarrow e^{i\theta_a\left(\tau_a - \lambda_a^T\right)} q\,. \tag{2.13}$$

The breaking of the color gauge symmetry leads to massive gluons through the Anderson-Higgs mechanism, while the breaking of the chiral symmetry gives rise to pseudoscalar Goldstone bosons, which will be discussed in detail in Sect. 4.1. The global baryon number symmetry is also broken making the CFL phase a superfluid and giving rise to a massless scalar Goldstone boson. Electromagnetism survives as a linear combination of the original generator $Q = \text{diag}_f\,(2/3, -1/3, -1/3)$ and the color generators λ_3 and λ_8

$$\tilde{Q} = Q - \frac{1}{2}\lambda_3 - \frac{1}{2\sqrt{3}}\lambda_8\,. \tag{2.14}$$

Two of the gluons mix with the original photon[2], since the mixing angles are small one says that the rotated gluons are the original gluons with a small admixture of the photon, whereas the (massless) $\tilde{Q}$-photon is a combination of the original photon with a small fraction of the gluons. Since there are no gapless $\tilde{Q}$-modes the CFL phase is a $\tilde{Q}$ - insulator.

2.1.3. Other pairing patterns

The 2SC and the CFL phase are the two most important homogeneous phases. If one neglects charge neutrality, they are the preferred phases at a very large, respectively small, strange quark mass. At intermediate strange quark mass or under the influence of charge neutrality other phases might be preferred. With the condensates defined in Eq. (2.3) and Eq. (2.4) there are more combinations possible than the presented 2SC and CFL pairing. In this work we will consider the combinations of scalar and pseudoscalar diquark condensates given in Table 2.1. We will discuss these phases in the context of the phase diagram of neutral quark matter in Sect. 4.3, the CFL phase with meson condensates in Sect. 4.1.2 and the p2SC phase in Sect. 4.3.3. In addition to the phases containing homogeneous spin-0 condensates there exists a large variety of possible pairing structures. These phases are spin-1 pairing [40, 49, 50], inhomogeneous [51, 52, 53, 54] and mixed phases [55], gluon condensation [56] and the formation of a meson supercurrent [57]. Although these phases may also be realized in some parts of the phase diagram we neglect them here for simplicity.

---

[2] In the chiral limit ($m_u = m_d = m_s = 0$) only the 8th gluon mixes with the photon [48].

	s_{22}	s_{55}	s_{77}	p_{25}	p_{52}	p_{27}	p_{72}	p_{57}	p_{75}
2SC	×	-	-	-	-	-	-	-	-
uSC	×	×	-	-	-	-	-	-	-
p2SC	×	-	-	×	-	-	-	-	-
CFL	×	×	×	-	-	-	-	-	-
CFLK^0	×	×	×	×	×	-	-	-	-
CFLK$^\pm$	×	×	×	-	-	×	×	-	-
CFL$\pi^\pm$	×	×	×	-	-	-	-	×	×

Table 2.1.: The different phases considered in this work, condensates taking a non-zero value are marked by ×.

2.2. Gapless phases

In this section we will give a brief introduction on gapless [58] color superconducting phases.

There are no different pairing patterns in gapless phases compared with the associated standard BCS solutions. The difference is manifested in the quasi-particle dispersion relations. While in the standard BCS solution all quasi-particle modes show an energy gap in their dispersion relation this is not the case in a gapless phase. Here, for one or more modes the gap vanishes. With the gap gone a "blocking region" emerges, this blocking region is the momentum space region between the two points where the quasi-particle mode becomes zero. It is called blocking region, since for the momenta inside this region no BCS pairing is possible. The vanishing gap has a large effect on the low-energy behavior of the phase. The low-energy excitations of a gapless mode have more similarities with the excitations in a non-superconducting phase than with the ones of the gapped modes in the corresponding superconducting phase.

A gapless phase is the result of shifted Fermi surfaces of the quarks in one pair. This difference can come from requiring charge neutrality or from different masses of the involved quarks.

In Fig. 2.1(a) we, exemplarily, show two modes from a gapless CFL phase ($T = 0$, $\mu = 460$ MeV, no leptons present, in Sect. 4.3.1 we will discuss this situation in detail), one of them fully gapped, one gapless with a blocking region between $p_1 = 368$ MeV and $p_2 = 473$ MeV. These modes are associated with the pairing of blue down (bd) and green strange (gs) quarks. Figure 2.1(b) shows the occupation numbers $f(p)_{f,c}$ for the involved quarks, also at $T = 0$, $\mu = 460$ MeV. The occupation number relates to the number density in the following way

$$n_{f,c} \propto \int d^3p\, f(p)_{f,c}\,. \tag{2.15}$$

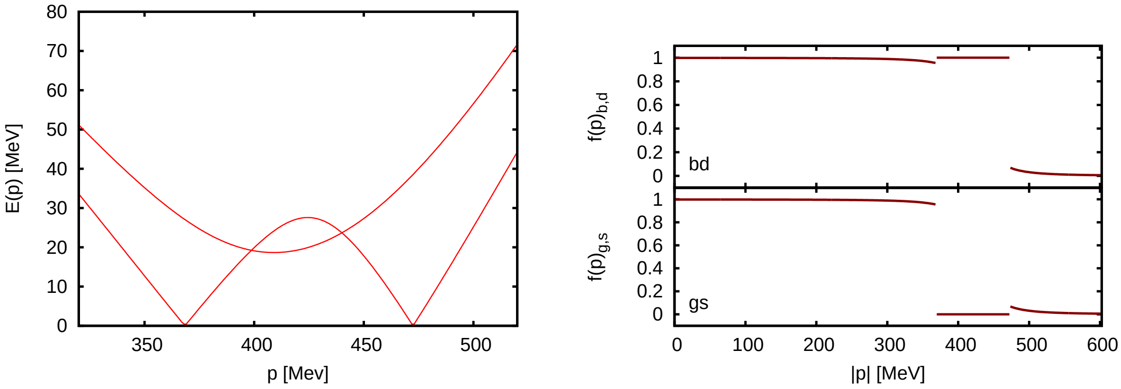

(a) quasi-particle modes (b) occupation number

Figure 2.1.: The modes associated with bd–gs pair in a gapless CFL phase (a) and the related occupation number (b), for blue down quarks in the upper and for green strange quarks in the lower part.

For all momenta outside the blocking region we see the same occupation number for the blue down and the green strange quarks, allowing for the formation of BCS-pairs. Close to the blocking region we see that, even neglecting the blocking region, the occupation number is not the step function as one would get for unpaired fermions, but it gets smeared out due to the pairing. In the vicinity of the Fermi-momentum we find the blocking region. In the CFL phase the shifted Fermi surfaces originate from the large strange quark mass. As a result there are no green strange quarks present in the blocking region, while all states for blue down quarks are occupied by unpaired quarks.

In the context of color superconductivity gapless phases where first discussed in the 2SC phase [59, 60] and later in the CFL phase [61, 62, 63, 64]. These studies show that gapless phases may suffer from chromomagnetic instabilities, the emergence of imaginary Meissner masses. These instabilities hint to an energetically preferred, unknown ground state.

3. The Nambu–Jona-Lasinio model

In the context of color superconductivity the Nambu–Jona-Lasinio (NJL) model is frequently used. Invented in 1961, before QCD, by Yoichiro Nambu and Giovanni Jona-Lasinio [14, 15] to model the nucleon-nucleon interaction, it was later used to describe effective quark-quark interactions [65, 66, 67] (for reviews see e.g. [68, 69, 70, 16]).

The NJL model has the same global symmetries as QCD, it successfully describes the spontaneous breaking of chiral symmetry, the appearance of Goldstone bosons and parts of the meson mass spectrum. However, the NJL model is not a gauge theory, it does not include gauge bosons and can not describe confinement. For the study of color superconductivity this lack of confinement is of minor importance since color superconductors can only exist in the deconfined phase. By adding a Polyakov loop potential [71] one can model the deconfinement transition. Since the parameters of the Polyakov loop potential have been fitted to lattice results at zero quark chemical potential, this gives good results in the crossover region at large temperature and low quark chemical potential. However, it is not even clear if the Polyakov loop, with this parameterization, can give useful results at low temperatures and large quark chemical potentials. On the other hand, we work at large quark chemical potential where quark matter is expected to be deconfined[1], therefore it is not necessary to include the Polyakov loop in our calculations.

The NJL model is not renormalizable, therefore one has to regularize momentum integrals. There are several methods for doing this, each method has its advantages and disadvantages. But for most applications it is sufficient to use a sharp cutoff for the three-momentum, as we will do here.

In this chapter we will introduce the model in the form it is used in Refs. [16, 17, 18, 19]. We use this form as our starting point and will add the treatment of pseudoscalar condensates in Chapter 4 and extend the six-point interaction to the diquark sector in Chapter 5. The principle way of handling the model will not be affected by these extensions, therefore we show the general strategy here with the "basic version" of the model.

---

[1] Admittedly, this is an assumption, it excludes the formation of a quarkyonic phase, where the "opposite" assumption is needed. Our assumption allows free quarks to exists at all quark chemical potentials above the chiral phase transition.

3.1. Lagrangian

The Lagrangian for the NJL-type model we use reads

$$\mathcal{L} = \bar{q}(i\partial\!\!\!/ - \hat{m} + \gamma_0 \hat{\mu})q + \mathcal{L}_\chi^{(4)} + \mathcal{L}_d^{(4)} + \mathcal{L}_\chi^{(6)} \,. \tag{3.1}$$

It is based on Lagrangians used in Refs. [16, 17, 18]. The quark field q has three color (r, g, b) and three flavor (u, d, s) degrees of freedom. The current quark masses enter through the diagonal mass matrix $\hat{m} = \mathrm{diag}_f\,(m_u, m_d, m_s)$ and the quark chemical potentials through the diagonal matrix $\hat{\mu}$ (more details on $\hat{\mu}$ are given in Sect. 3.5). The interaction terms in Eq. (3.1) contain four-point interactions as well as a six-point interaction.

3.1.1. Four-point interactions

The term

$$\mathcal{L}_\chi^{(4)} = G \sum_{a=0}^{8} \left[(\bar{q}\tau_a q)^2 + (\bar{q} i\gamma_5 \tau_a q)^2 \right] \tag{3.2}$$

is the *usual* NJL four-point interaction in the quark-antiquark channel, the first term describes scalar interactions and the second one pseudoscalar interactions.

In the quark-quark channel the interaction reads

$$\mathcal{L}_d^{(4)} = H \sum_{A,B=2,5,7} \left[\left(\bar{q} i\gamma_5 \tau_A \lambda_B C \bar{q}^T\right) \left(q^T C i\gamma_5 \tau_A \lambda_B q\right) + \left(\bar{q}\tau_A \lambda_B C \bar{q}^T\right) \left(q^T C \tau_A \lambda_B q\right) \right] . \tag{3.3}$$

As before τ_a (λ_a) are the Gell-Mann matrices acting in flavor (color) space with $\tau_0 = \sqrt{2/3}\mathbb{1}$. $C = i\gamma^2\gamma^0$ is the charge conjugation operator, G and H are dimensionful coupling constants. The first term in Eq. (3.3) describes scalar, the second one pseudoscalar interactions in the color anti-triplet, flavor anti-triplet quark-quark channel. To respect chiral symmetry it is important to include both terms, although we first only consider scalar diquark condensates and introduce the pseudoscalar diquark condensates later.

The four-point interactions (Eq. (3.2) and Eq. (3.3)) are invariant under $U(3)_R \times U(3)_L$ transformations. To break the $U(1)_A$ symmetry we add a six-point interaction term.

3.1.2. Six-point interaction

It was shown in 1970 by Kobayashi and Maskawa that the $\eta - \eta'$ mass splitting could be explained by a six-point interaction of determinantal form that breaks the

$U(1)$ axial symmetry [73, 74]. Later, in 1976, 't Hooft related the form of this six-point interaction term to the instanton interaction [75]. The term is therefore called *'t Hooft* or *Kobajashi–Maskawa–'t Hooft* interaction, it reads

$$\mathcal{L}_\chi^{(6)} = -K \ \left\{\det{}_f \left[\bar{q}\,(1+\gamma_5)\,q\right] + \det{}_f \left[\bar{q}\,(1-\gamma_5)\,q\right]\right\} \,, \tag{3.4}$$

where the determinant $\det_f$ has to be taken in flavor space and K is a dimensionful coupling constant. This term connects three incoming fields with three outgoing fields. It can couple three quark-antiquark channels like $(\bar{u}u)(\bar{d}d)(\bar{s}s)$ or one quark-quark channel to one antiquark-antiquark channel and one quark-antiquark channel, e.g. $(ud)(\bar{u}\bar{d})(\bar{s}s)$. However only the first case will survive the mean-field (Hartree) approximation we apply later. We will continue at this point in Chapter 5, where we will extend the six-point interaction to also allow for the coupling of quark-quark channels in mean-field approximation.

3.2. Mean-field approximation

In the following we will work in mean-field approximation. Since we are not interested in critical phenomena this is a valid approximation.

For the mean-field approximation we introduce the quark-antiquark condensates

$$\phi_f = \langle \bar{q}_f q_f \rangle, \qquad f \in \{u, d, s\}\,, \tag{3.5}$$

and the scalar

$$s_{AA} = \langle q^T C \gamma_5 \tau_A \lambda_A q \rangle\,, \qquad A \in \{2, 5, 7\} \tag{3.6}$$

diquark condensates. Other possible scalar and all pseudoscalar condensates are, so far, neglected. Using these condensates we linearize the Lagrangian (Eq. (3.1)) with

$$XY \approx \langle X \rangle Y + X \langle Y \rangle - \langle X \rangle \langle Y \rangle \tag{3.7}$$

$$XYZ \approx \langle X \rangle \langle Y \rangle Z + \langle X \rangle Y \langle Z \rangle + X \langle Y \rangle \langle Z \rangle - 2 \langle X \rangle \langle Y \rangle \langle Z \rangle \tag{3.8}$$

and obtain the mean-field Lagrangian

$$\mathcal{L}_{\mathrm{MF}} = \bar{\Psi} S^{-1} \Psi - \mathcal{V}\,. \tag{3.9}$$

To write the Lagrangian in this compact form we use Nambu–Gorkov spinors

$$\Psi = \frac{1}{\sqrt{2}} \begin{pmatrix} q \\ C\bar{q}^T \end{pmatrix}, \qquad \bar{\Psi} = \frac{1}{\sqrt{2}} \left(\bar{q},\, q^T C\right)\,, \tag{3.10}$$

and the inverse propagator in momentum space

$$S^{-1}(p) = \begin{pmatrix} \not{p} + \mu\gamma_0 - \hat{M} & \sum_A \Delta_{AA}^{(s)}\, \tau_A\, \lambda_A\, \gamma_5 \\ -\sum_A \Delta_{AA}^{(s)\star}\, \tau_A\, \lambda_A\, \gamma_5 & \not{p} - \mu\gamma_0 - \hat{M} \end{pmatrix}. \tag{3.11}$$

Due to 4 Dirac, 3 flavor, 3 color and 2 Nambu-Gorkov degrees of freedom this is a 72 by 72 matrix.

On the diagonal of the matrix $\hat{M}$ we find the dynamical quark masses

$$M_a = m_a - 4G\phi_a + K\phi_b\phi_c\,. \tag{3.12}$$

Here (a, b, c) is any permutation of (u, d, s).

Furthermore the off-diagonal elements in Nambu-Gorkov space of the inverse propagator (Eq. (3.11)) include

$$\Delta^{(s)}_{AA} = -2H\, s_{AA}\,. \tag{3.13}$$

All terms that do not depend on the fields are collected in the constant term

$$\mathcal{V} = 2G\left(\phi_u^2 + \phi_d^2 + \phi_s^2\right) - 4K\phi_u\phi_d\phi_s + \sum_{A=2,5,7} H|s_{AA}|^2\,. \tag{3.14}$$

3.3. Thermodynamic potential

To obtain the phase structure of the color superconductor the central object of interest is the thermodynamic potential. Here we will change our definition of the thermodynamic potential and from now on actually mean the thermodynamic potential per volume when stating “thermodynamic potential”. This is defined by

$$\Omega \equiv \frac{T}{V}\ln Z\,. \tag{3.15}$$

For a consistent description of a neutron stars interior we also include massless electrons and massive muons in our system

$$\Omega = \Omega_{\text{quark}} + \Omega_{\text{electron}} + \Omega_{\text{muon}}\,. \tag{3.16}$$

For the construction of a phase diagram we minimize the thermodynamic potential in the presence of different condensates and compare the pressure $p = -\Omega$ of the different phases. The phase with the highest (lowest) pressure (thermodynamic potential) is realized.

3.3.1. Thermodynamic potential of the quarks

From the linearized Lagrangian (Eq. (3.9)) the mean-field thermodynamic potential for the quark part of the system can be written as

$$\Omega\left(T, \{\mu_i\}\right)_{\text{quark}} = -T\sum_n \int \frac{d^3p}{(2\pi)^3}\frac{1}{2}\text{Tr}\ln\left(\frac{S^{-1}\left(i\omega_n, \vec{p}, \{\mu_i\}\right)}{T}\right) + \mathcal{V}\,, \tag{3.17}$$

with the fermionic Matsubara frequencies $\omega_n = (2n+1)\,\pi T$. After applying the relation $\mathrm{Tr}\ln S^{-1} = \ln\det S^{-1}$ the determinant of the inverse propagator can be transformed

$$\det S^{-1} = \det\left(\gamma_0\gamma_0 S^{-1}\right) = \det\gamma_0 \det\left(\gamma_0 S^{-1}\right) = \det\left(\gamma_0 S^{-1}\right) \,. \tag{3.18}$$

It is useful to split the inverse Propagator in two parts

$$\gamma_0 S^{-1}\left(i\omega_n, \vec{p}\right) = i\omega_n - A\left(\vec{p}\right) \tag{3.19}$$

and calculate the determinant as the product of the eigenvalues

$$\det\frac{S^{-1}}{T} = \frac{1}{T^{72}}\prod_{1}^{72}\left(i\omega_n - \epsilon(\vec{p})\right) \,, \tag{3.20}$$

where ϵ_i are the 72 eigenvalues of A. This, and the fact that each eigenvalue has a partner with the same magnitude but opposite sign, enables us to use the relation [76]

$$\sum_{n=-\infty}^{\infty}\ln\left[\frac{1}{T^2}\left(\omega_n^2+\epsilon^2\right)\right] = \frac{|\epsilon|}{T} + \ln\left[1+\exp\left(-\frac{|\epsilon|}{T}\right)\right] \tag{3.21}$$

to evaluate the Matsubara sum analytically. Since the numerical algorithms for finding eigenvalues scale badly with the size of the matrix it is advantageous to decompose the large 72 × 72 matrix into smaller blocks.

One observes that each eigenvalue of A (and thereby of S^{-1}) is twofold degenerate. This degeneracy comes from the two possible spin states. We exploit this feature to halve the dimension of our eigenvalue problem by decomposing S^{-1} into two matrices S_+^{-1} and S_-^{-1} using the spin-projectors

$$P_\pm = \frac{1}{2}\left(1 \pm \sigma^i p_i\right) \,, \qquad i \in \{1,2,3\} \tag{3.22}$$

with the Pauli-matrices σ^i and write

$$\gamma_0 S^{-1} = P_+ S_+^{-1} + P_- S_-^{-1} \,. \tag{3.23}$$

The determinant of the matrices S_+^{-1} and S_-^{-1} are equal [77]

$$\det S_+^{-1} = \det S_-^{-1} \,, \tag{3.24}$$

so that it is sufficient to calculate only one of them.

The remaining 36 × 36 matrix can be brought into a block diagonal form, the size of these blocks depends on the phase structure. This leads to four 4 × 4 and ten 2 × 2 blocks in the 2SC, two 6 × 6, four 4 × 4 and four 2 × 2 blocks in the uSC and one 12 × 12 block and six 4 × 4 blocks in the CFL phase.

3.3.2. Thermodynamic potential of the leptons

Beside quarks we also include two kinds of leptons[2] in our system, massless electrons and massive muons

$$m_e = 0.0 \text{ MeV}\,, \tag{3.25}$$

$$m_\mu = 105.66 \text{ MeV}\,. \tag{3.26}$$

Neglecting the mass of the electron, which actually is 511 keV, can only have an effect when the temperature and the chemical potential for the electrons both are small. Later, in our analysis of gapless CFL/CFLK^0 phases (Sect. 4.3.1), we will encounter such a situation and comment on the choice of zero electron mass.

We treat the leptons as a non-interacting gas of fermions where the thermodynamic potential is given by

$$\Omega_{leptons} = -2T \sum_{l\in\{e^-,\mu\}} \sum_{\pm} \int \frac{d^3p}{(2\pi)^3} \ln\left[1 + \exp\left(-\frac{E_l \pm \mu_l}{T}\right)\right] \tag{3.27}$$

with $E_l = \sqrt{\vec{p}^{\,2} + m_l^2}$. The charged leptons are sensitive to the lepton number chemical potential μ_{L_l} and the electric charge chemical potential μ_Q,

$$\mu_l = \mu_{L_l} - \mu_Q\,. \tag{3.28}$$

A neutron star is transparent for neutrinos, therefore lepton number is not a conserved quantity. Hence for most of this work we will use $\mu_{L_l} = 0$. Lepton number might only be conserved in the very first moments of a neutron star's existence, we will comment on this situation in Sect. 4.4.

3.4. Gap equations

The ground state is the minimum of the thermodynamic potential and is fulfilling the so called gap equations

$$\frac{\partial\Omega}{\partial\Delta_{AB}^{(s)}} = 0 \quad \text{and} \quad \frac{\partial\Omega}{\partial\phi_i} = 0 \tag{3.29}$$

for all condensates.

---

[2] The τ-lepton is much heavier than any energy scale in the system, so that we can neglect it safely.

The derivative of the quark thermodynamic potential with respect to a condensate X is given by

$$\frac{\partial}{\partial X}\Omega_{\text{quark}} = -T\sum_n \int \frac{d^3p}{(2\pi)^3}\frac{1}{2}\mathrm{Tr}\left[S\gamma_0 \underbrace{\left(\frac{\partial}{\partial X}\gamma_0 S^{-1}\right)}_{\Gamma}\right] + \frac{\partial \mathcal{V}}{\partial X}\,. \tag{3.30}$$

We diagonalize S^{-1}

$$S^{-1} = \gamma_0 U\, D\, U^\dagger \tag{3.31}$$

with the diagonal matrix $D_{kl} = (i\omega_n + \epsilon_k)\,\delta_{kl}$ with the eigenvalues ϵ_k of A and get the propagator

$$S = U\, D^{-1} U^\dagger \gamma_0 \tag{3.32}$$

and after a cyclic permutation we write

$$\begin{aligned}\frac{\partial}{\partial X}\Omega_{\text{quark}} &= -\frac{T}{2}\sum_n \int \frac{d^3p}{(2\pi)^3}\mathrm{Tr}\left[D^{-1}\underbrace{U^\dagger \Gamma U}_{\tilde{\Gamma}}\right] + \frac{\partial \mathcal{V}}{\partial X} && (3.33)\\ &= -\frac{T}{2}\sum_n \int \frac{d^3p}{(2\pi)^3}\sum_{j=1}^{72}\frac{1}{i\omega_n + \epsilon_j}\left(\tilde{\Gamma}\right)_{jj} + \frac{\partial \mathcal{V}}{\partial X}\,. && (3.34)\end{aligned}$$

The residue theorem gives us the useful relation

$$-\sum_n f\left((2n+1)\,\pi i\right) = \oint_C \frac{dx}{2\pi i}\frac{f(x)}{e^x + 1}\,, \tag{3.35}$$

where the closed path C encloses all poles on the imaginary axis. We use Eq. (3.35) to turn the Matsubara-sum into an integral

$$\frac{\partial}{\partial X}\Omega_{\text{quark}} = \frac{1}{2}\oint \frac{dz}{2\pi i}\int \frac{d^3p}{(2\pi)^3}\sum_{j=1}^{72}\frac{1}{z+\epsilon_j}\left(\tilde{\Gamma}\right)_{jj}\frac{1}{e^{z/T}+1} + \frac{\partial \mathcal{V}}{\partial X}\,. \tag{3.36}$$

By bending the integration path outwards, so that it only encloses one pole at $z = -\epsilon_j$, and by applying the residue theorem again we can evaluate the z-integration

$$\frac{\partial}{\partial X}\Omega_{\text{quark}} = \frac{1}{2}\int \frac{d^3p}{(2\pi)^3}\sum_{j=1}^{72}\left(\tilde{\Gamma}\right)_{jj}\frac{1}{e^{-\epsilon_j/T}+1} + \frac{\partial \mathcal{V}}{\partial X}\,. \tag{3.37}$$

For the numerical calculations it is beneficial to decompose the 72 × 72 matrices into the small blocks mentioned in Sect. 3.3.1.

3.5. Neutron star constraints

In this work we are interested in quark matter, particular color superconducting matter, under the conditions of a neutron star's inner core. That implies electric and color charge neutrality as well as equilibrium concerning weak processes, namely β-equilibrium.

3.5.1. Charge neutrality

A neutron star is an electric and color charge neutral object. All particles in the system (quarks and leptons) carry electric charge, we therefore introduce an electric charge chemical potential μ_Q, that will be adjusted to make the system electrically neutral.

QCD requires that the neutron star is in a color singlet state, but since we are not working in a gauge theory we will only require color neutrality, meaning an equal amount of red (n_r), green (n_g) and blue (n_b) color charges. It has been shown that there is no significant difference in the free energy between a color singlet and a color neutral state in the thermodynamic limit [78]. For this purpose we use the two color charges

$$n_3 = n_r - n_g \,, \tag{3.38}$$

$$n_8 = \frac{1}{\sqrt{3}} \left(n_r + n_g - 2n_b \right) \,, \tag{3.39}$$

and introduce the corresponding color charge chemical potentials μ_3 and μ_8. With these charge chemical potentials and the quark number chemical potential[3] μ we can write the diagonal chemical potential matrix $\hat{\mu}$ in our Lagrangian (Eq. (3.1)) as

$$\hat{\mu} = \mu + \mu_3 \lambda_3 + \mu_8 \lambda_8 + \mu_Q \hat{Q} \tag{3.40}$$

with the electric charge matrix in flavor space $\hat{Q} = \mathrm{diag}_f \left(2/3, -1/3, -1/3 \right)$. The components of this matrix give the chemical potentials for the individual quarks ($\mu_{f,c}$).

To have a charge neutral ground state we tune the charge chemical potentials μ_3, μ_8 and μ_Q so that the charges

$$n_3 = -\frac{\partial \Omega}{\partial \mu_3} \,, \qquad n_8 = -\frac{\partial \Omega}{\partial \mu_8} \quad \text{and} \quad n_Q = -\frac{\partial \Omega}{\partial \mu_Q} \tag{3.41}$$

---

[3] We will often refer to the quark number chemical potential as quark chemical potential even though the chemical potential for the individual quark might differ from μ due to the neutrality constrains.

vanish. Further on we check that there is no color charge hidden in the off-diagonal charge densities

$$n_i = \frac{\partial \Omega}{\partial \mu_i}\,, \qquad i \in \{1, 2, 4, 5, 6, 7\}\,. \tag{3.42}$$

It has been shown that, for some pairing patterns, color charges from n_3 and n_8 get rotated in off-diagonal charges [79]. Since all color charge has to vanish this situation has to be avoided, or one has to include additional, off-diagonal color charge chemical potentials (μ_i), that eliminate these charges.

3.5.2. β equilibrium

The time scale of the existence of a neutron star is much longer than any scale for strong or weak processes, therefore the star's matter content is in the ground state. Hence, there are no processes that lower the free energy and therefore the β decay and its inverse process need to be in equilibrium. For quark matter this means the reaction rates

$$u_c + l \rightleftarrows d_c + \nu_l\,, \tag{3.43}$$

$$u_c + l \rightleftarrows s_c + \nu_l \tag{3.44}$$

need to equilibrate, with the charged leptons $l \in \{e^-,\, \mu,\, \tau\}$. On the level of chemical potential this equilibrium means

$$\mu_{u,\,c} + \mu_l = \mu_{d,\,c} + \mu_{\nu_l}\,, \tag{3.45}$$

$$\mu_{u,\,c} + \mu_l = \mu_{s,\,c} + \mu_{\nu_l}\,. \tag{3.46}$$

With the neutrinos only sensitive to the lepton number chemical potential and μ_l from Eq. (3.28), β equilibrium manifests in the relations of the chemical potentials

$$\mu_u - \mu_Q = \mu_d\,, \tag{3.47}$$

$$\mu_u - \mu_Q = \mu_s\,. \tag{3.48}$$

We made sure that these relations are automatically fulfilled by choosing one common quark number chemical potential in Eq. (3.40) and not individual chemical potentials for the different quark flavors.

3.6. Parameters

The Lagrangian (Eq. (3.1)) contains six parameters, the three bare quark masses (m_u, m_d, m_s), the two four-point coupling constants (G, H) and the six-point coupling constant (K). Further on, since the NJL model is not renormalizable, we need to regularize the momentum integrals. Therefore we use a sharp three-momentum cut-off (Λ).

The parameters not connected to quark-quark interactions can be fitted to measured meson masses and decay constants in vacuum [80]

$$\begin{aligned} m_u &= m_d = 5.5 \text{ MeV}\,, \\ m_s &= 140.7 \text{ MeV}\,, \\ \Lambda &= 602.3 \text{ MeV}\,, \\ G &= 1.835/\Lambda^2\,, \\ K &= 12.36/\Lambda^5\,. \end{aligned} \tag{3.49}$$

The values for the diquark coupling constant H can not be deduced from vacuum meson properties. By performing a Fierz transformation of the one-gluon exchange term one can relate the diquark coupling to the quark-antiquark coupling [16], obtaining $H = 3/4\,G$. Since there is no more rigid method for the determination of H also other values are used for it. To get an impression how the color superconductor reacts to changes of the diquark coupling, we will also use $H = G$.

Sometimes, we are interested in the situation of equal bare quark masses, then we set m_s also to 5.5 MeV and adjust the coupling G in a way that the dynamical vacuum quark mass for the up and down quarks remains at $M_{u/d} = 367.6$ MeV. This method gives $G = 1.918/\Lambda^2$.

For easier reference we define different sets of parameters. Combining the values from Eq. (3.49) with $H = 3/4\,G$ we call set I. The same set for equal bare quark masses, hence $m_s = 5.5$ MeV and $G = 1.918/\Lambda^2$ is named set II. Set III is the same as set I but with the stronger diquark coupling ($H = G$). An overview of all parameter sets used in this work is given in Table B.1 in Appendix B.

4. Goldstone boson condensation

In this chapter we will discuss the condensation of Goldstone bosons in the color-flavor locked (CFL) phase for electric and color charge neutral quark matter. The CFL phase was introduced in Chapter 2 as a very symmetric way of forming quark pairs. If all quarks have the same Fermi momenta this works well and therefore CFL is the preferred pairing pattern at asymptotically high densities in three-flavor quark matter [47, 82]. But at more “moderate” densities, relevant for the description of a neutron star’s inner core, the mass of the strange quark has a value comparable to the quark chemical potential and can not be neglected. The strange quark mass then shifts the Fermi surfaces and BCS pairing is only possible as long as the gain in condensation energy is larger than the energy needed to readjust the Fermi surfaces. There are different possibilities how the system can react when simple BCS pairing is no longer possible. Here we will investigate the formation of a K^0 condensate in the CFL phase. Although we focus on the condensation of Goldstone bosons it is unavoidable to consider also gapless phases.

The K^0 carries negative strangeness (-1) and so it can reduce the strangeness content of the system, allowing for CFL pairing at lower quark chemical potential. The CFL phase is charge neutral by itself and the condensation of the neutral K^0 will clearly not change this. However in situations where it is preferable for the system to have a charged quark part (neutrino trapping, mixed phases), the condensation of charged Goldstone bosons ($\mathrm{K}^{\pm}$, $\pi^{\pm}$) may occur.

In the following section we will calculate the masses of the relevant Goldstone bosons and calculate the phase diagram of electric and color charge neutral quark matter taking the condensation of Goldstone bosons into account.

4.1. Goldstone bosons in the CFL phase

As already mentioned in Sect. 2.1.2, the presence of the diquark condensates in the CFL phase breaks the original

$$SU(3)_{\text{color}} \times SU(3)_L \times SU(3)_R \times U(1)_V \, (\times U_A(1)) \tag{4.1}$$

symmetry[1] to a remaining combined color and flavor

$$SU(3)_{\text{color}+V} \ (\times \mathbb{Z}_2) \ , \qquad SU(3)_{\text{color}+V} : q \to e^{i\theta_a\left(\tau_a - \lambda_a^T\right)} q \, , \tag{4.2}$$

symmetry. The breaking of chiral symmetry gives rise to eight pseudoscalar Goldstone bosons. One additional pseudoscalar Goldstone boson comes from the breaking of the axial $U_A(1)$ symmetry. The breaking of the baryon number symmetry $U\,(1)_V$ leads to one scalar Goldstone boson.

At low energies, where the Goldstone modes are the only relevant degrees of freedom, it is possible to use the so-called low-energy effective theory [85, 86, 87] to study the features of the Goldstone bosons. The first prediction of a K^0 condensate in the CFL phase was made in this framework [88, 89].

4.1.1. Masses of Goldstone bosons

The masses of the Goldstone bosons in CFL phase within the NJL model can be calculated by solving the Bethe-Salpeter equation [90]

$$\hat{T} = \hat{K} + \hat{K}\hat{J}\hat{T} \, . \tag{4.3}$$

This has be done in the chiral limit in Refs. [94, 95] and for static quark masses in Refs. [91, 92, 93]. We will add the self-consistent treatment of the quark masses to obtain the exact result for our model.

To write Eq. (4.3) as a matrix equation we need the scattering vertices. For the quark-antiquark part this is the situation described in Refs. [68, 69, 80], with the specialty that we work in Nambu-Gorkov space and need to convert the vertices according to

$$\Gamma \to (\Gamma)_{\text{NG}} \equiv \begin{pmatrix} \Gamma & 0 \\ 0 & -C\Gamma^T C \end{pmatrix} \, . \tag{4.4}$$

From the Lagrangian we extract the pseudoscalar operators for the quark-quark interaction

$$\Gamma^{p\uparrow}_{AA'} \equiv \begin{pmatrix} 0 & \tau_A\,\lambda_{A'} \\ 0 & 0 \end{pmatrix} , \qquad \Gamma^{p\downarrow}_{AA'} \equiv \begin{pmatrix} 0 & 0 \\ \tau_A\,\lambda_{A'} & 0 \end{pmatrix} \, . \tag{4.5}$$

To shorten the notation we define[2]

$$\bar{\Gamma}_i \equiv \gamma^0 \Gamma_i^\dagger \gamma^0 \, , \tag{4.6}$$

which basically flips the direction of the arrow in the vertices (Eq. (4.5)).

---

[1] $U(1)_A$ is a classical symmetry of the QCD Lagrangian, but in QCD it is broken by quantum effects [83, 84], in the NJL model this symmetry is explicitly broken by the six-point interaction (Eq. (3.4)).

[2] The γ_0's will only be needed for the scalar counterparts of Eq. (4.5).

Modes with the same quantum numbers will mix, we therefore have to consider three vertices for each mode we are interested in [96, 97, 91]

$$\pi^+ : \qquad \frac{1}{2\sqrt{2}}\left(\tau_1 + i\tau_2\right), \qquad \Gamma^{p\uparrow}_{57}, \qquad \Gamma^{p\downarrow}_{75}, \tag{4.7}$$

$$\pi^- : \qquad \frac{1}{2\sqrt{2}}\left(\tau_1 - i\tau_2\right), \qquad \Gamma^{p\uparrow}_{75}, \qquad \Gamma^{p\downarrow}_{57}, \tag{4.8}$$

$$K^+ : \qquad \frac{1}{2\sqrt{2}}\left(\tau_4 + i\tau_5\right), \qquad \Gamma^{p\uparrow}_{27}, \qquad \Gamma^{p\downarrow}_{72}, \tag{4.9}$$

$$K^- : \qquad \frac{1}{2\sqrt{2}}\left(\tau_4 - i\tau_5\right), \qquad \Gamma^{p\uparrow}_{72}, \qquad \Gamma^{p\downarrow}_{27}, \tag{4.10}$$

$$K^0 : \qquad \frac{1}{2\sqrt{2}}\left(\tau_6 + i\tau_7\right), \qquad \Gamma^{p\uparrow}_{25}, \qquad \Gamma^{p\downarrow}_{52}, \tag{4.11}$$

$$\bar{K}^0 : \qquad \frac{1}{2\sqrt{2}}\left(\tau_6 - i\tau_7\right), \qquad \Gamma^{p\uparrow}_{52}, \qquad \Gamma^{p\downarrow}_{25}. \tag{4.12}$$

States related to quark-antiquark scattering we will call $\bar{q}q$ meson states and states related to quark-quark scattering CFL mesons. However these states can not be separated clearly in the CFL phase since they mix. In vacuum such a mixing is not possible since these states carry different baryon numbers, but in the CFL phase the baryon number symmetry is broken.

Now we can write

$$\hat{T} = \bar{\Gamma}_i T_{ij} \Gamma_j \,, \tag{4.13}$$

$$\hat{K} = \bar{\Gamma}_i K_{ij} \Gamma_j \,. \tag{4.14}$$

The scattering kernel for the quark-antiquark scattering can directly be taken from the literature (e.g. Ref. [80])

$$\left(K_{\pi^\pm}\right)_{ij} = 2\left(G - \frac{1}{2}K\langle\bar{s}s\rangle\right)\delta_{ij} \qquad \text{for the pion modes}\,, \tag{4.15}$$

$$\left(K_{K^\pm}\right)_{ij} = 2\left(G - \frac{1}{2}K\langle\bar{d}d\rangle\right)\delta_{ij} \qquad \text{for the charged kaons modes}\,, \tag{4.16}$$

$$\left(K_{K^0,\bar{K}^0}\right)_{ij} = 2\left(G - \frac{1}{2}K\langle\bar{u}u\rangle\right)\delta_{ij} \qquad \text{for the neutral kaon modes}\,. \tag{4.17}$$

The scattering kernel for the quark-quark scattering is

$$\left(K_{qq}\right)_{ij} = 4H\delta_{ij}\,. \tag{4.18}$$

The second crucial ingredient for the Bethe-Salpeter equation (Eq. (4.3)) is the polarization loop

$$J_{ij}\left(q\right) = -T\sum_n \int \frac{d^3k}{\left(2\pi\right)^3}\frac{1}{2}\mathrm{Tr}\left[\bar{\Gamma}_i S\left(k+q\right)\Gamma_j S\left(k\right)\right]\,. \tag{4.19}$$

Where $k = (i\omega_n, \vec{k})^T$ contains the fermionic Matsubara frequency ω_n and the three-momentum $\vec{k}$. Interested in the mass of a zero-momentum meson we set $q = (i\omega_m, \vec{q} = 0)^T$ where ω_m is a bosonic Matsubara frequency.

Since we always have three operators that mix, the T-matrix is a 3×3 - matrix in operator space and can be written as

$$T\,(q) = K\;[\mathbb{1} - J\,(q)\,K]^{-1}\;. \tag{4.20}$$

To extract the mass and chemical potential we solve for the poles of $T\,(q)$

$$\det\,[T(q)]^{-1} = \det\left\{[\mathbb{1} - J\,(q)\,K]\,K^{-1}\right\} = 0\,. \tag{4.21}$$

In the vicinity of the poles we can parameterize a mode as a free boson with the mass m_i and the chemical potential μ_i (for zero three-momentum)

$$T(q)_i \propto \frac{1}{(q_0 + \mu_i)^2 - m_i^2}\,. \tag{4.22}$$

With the locations of two poles, ω_1 and ω_2, for a mode we can extract the mass

$$m_i = \frac{1}{2}\,(\omega_1 - \omega_2) \tag{4.23}$$

and the chemical potential

$$\mu_i = -\frac{1}{2}\,(\omega_1 + \omega_2)\;. \tag{4.24}$$

4.1.2. The condensation point

As already mentioned above we expect the CFL phase to develop a K^0 condensate at moderate densities to reduce the strangeness content of the system. In this section we will study the onset of kaon condensation in the CFL phase exemplarily for one point of the phase diagram and present a full phase diagram for neutral quark matter in the next section.

For our investigation we choose[3] $\mu = 500$ MeV and $T = 0.1$ MeV. If one neglects pseudoscalar condensates, this point lies deep in the CFL phase [17, 18]. At this point we solve the gap equations Eq. (3.29) and the neutrality conditions Eq. (3.41) for the charge neutral CFL solution with self-consistent dynamical quark masses and then use the Bethe-Salpeter equation to construct the meson masses and chemical potentials. Interpolating[4] between the parameter sets I and II we get the meson masses and chemical potentials as functions of the bare strange quark mass, shown in Fig. 4.1. Comparing the mass and the chemical potential for the K^0 (K^+) meson, Fig. 4.2(a), we see that for bare strange quark masses larger than 63.6 MeV

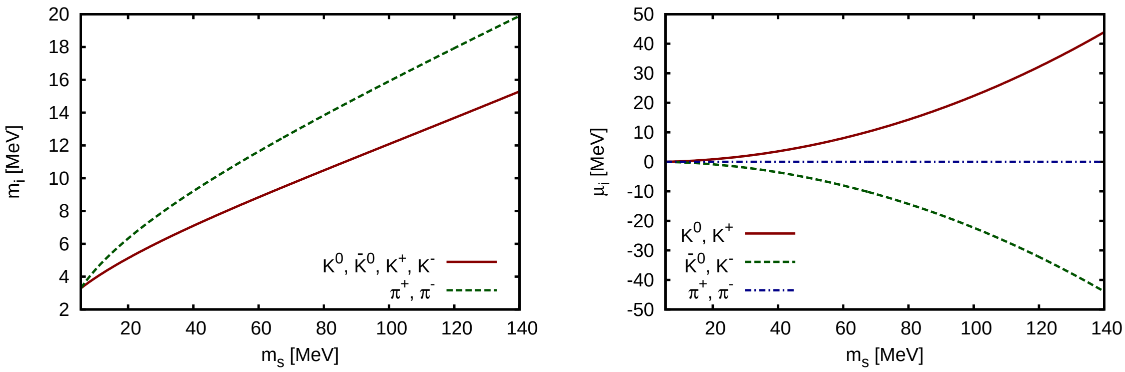

(a) (b)

Figure 4.1.: The mass (a) and the chemical potential (b) of the Goldstone bosons (K^0, $\bar{K}^0$, K^+, K^-, π^+, π^-) in the CFL phase at $\mu = 500$ MeV, $T = 0.1$ MeV as functions of the bare strange quark mass. (Interpolation between parameter sets II and I.)

the chemical potential exceeds the meson mass and K^0 (K^+) condensation is possible. The condensation of electrically charged kaons will not take place under the neutrality conditions in the charge neutral CFL phase, since the electric charge of the kaons needs to be compensated by leptons and the necessary electric charge chemical potential prevents the charged kaons from condensing.

It is also possible to find the condensation point by looking for the appearance of pseudoscalar diquark condensates. We will discuss this in detail in the next section. As a preview Fig. 4.2(b) shows the values of the pseudoscalar diquark condensates associated with K^0 condensation in dependence of the bare strange quark mass. The results for the condensates are obtained by solving the gap equations and give, independently, also a value of $m_s = 63.6$ MeV for the onset of K^0 condensation.

4.2. Pseudoscalar diquark condensates

Besides mentioning the possible existence of pseudoscalar diquark condensates in Sect. 2.1, up to this point we have only used scalar diquark condensates. In this section we will show the connection of the pseudoscalar condensates to the condensation of Goldstone bosons and modify the mean-field Lagrangian (Eq. (3.9)) so that we can treat the pseudoscalar diquark condensates in the same way as the scalar condensates.

---

[3] The small but nonzero temperature simplifies the numerical evaluation.

[4] See Appendix B for details on this interpolation between parameter sets.

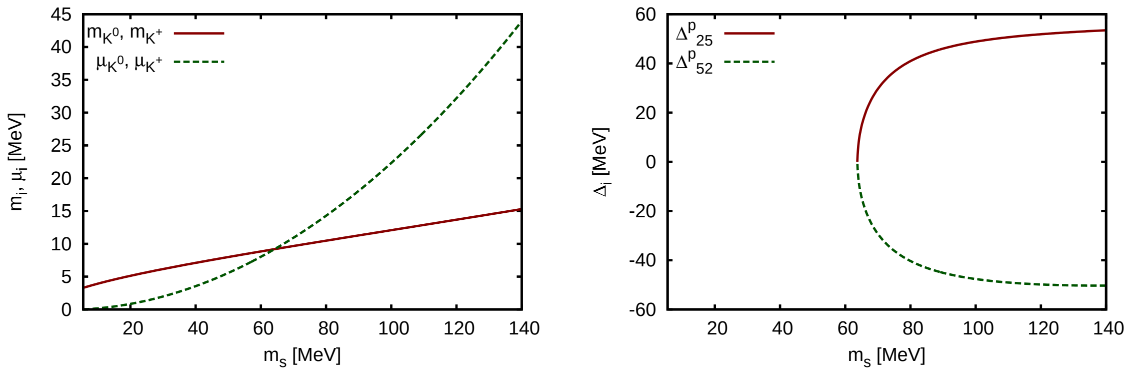

(a) (b)

Figure 4.2.: The onset of K^0/K^+ condensation by increasing the strange quark mass in the CFL phase at $\mu = 500$ MeV and $T = 0.1$ MeV with the meson mass and chemical potential (a) or the appearance of pseudoscalar condensates (b). (Interpolation between set II and I.)

As a reminder (Eq. (2.4)), we use

$$p_{AA'} = \langle q^T C \tau_A \lambda_{A'} q \rangle \,, \qquad\qquad A,\ A' \in \{2,5,7\} \tag{4.25}$$

for the pseudoscalar diquark condensates.

4.2.1. Axial flavor transformations

The first investigations on the Goldstone boson condensation in the CFL phase within the NJL model were done by making use of axial flavor rotations [98, 99]. In the chiral limit the symmetry Eq. (4.1) is exact. Then the axial flavor transformations, where the quark field q is transformed as

$$q \longrightarrow \exp\left(i\theta_a \frac{\tau_a}{2}\gamma_5\right) \,, \tag{4.26}$$

connect a continuous set of ground states. Applying one of the transformations (Eq. (4.26)) rotates one or more of the the scalar diquark condensates (s_{22}, s_{55}, s_{77}) into pseudoscalar condensates ($p_{AA'}$).

In the more realistic situation, where Eq. (4.1) is not an exact symmetry, the CFL phase may become unstable and a phase with non-zero values of $p_{AA'}$ might be preferred. This corresponds to the condensation of Goldstone bosons. According to their quantum numbers one can connect the transformations with pseudoscalar mesons:

$a = 1,\, 2$	charged pions:	$\pi^+,\, \pi^-$,
$a = 4,\, 5$	charged kaons:	$K^+,\, K^-$,
$a = 6,\, 7$	neutral kaons:	$K^0,\, \bar{K}^0$,
$a = 0, 3, 8$	hidden flavor mesons:	$\pi^0,\, \eta,\, \eta'$.

Since the hidden flavor mesons (π^0, η, η') are not sensitive to the chemical potentials relevant in this study we will neglect them.

For the electrically and strangeness charged modes the rotations transform the scalar diquark condensates in the following way:

$$\begin{array}{lll} \pi^+,\, \pi^- : & s'_{22} = s_{22} & \\ & s'_{55} = \cos\frac{\theta}{2} s_{55} & p'_{75} = i \sin\frac{\theta}{2}\left(\hat{\theta}_1 - i\hat{\theta}_2\right) s_{55} \\ & s'_{77} = \cos\frac{\theta}{2} s_{77} & p'_{57} = i \sin\frac{\theta}{2}\left(\hat{\theta}_1 + i\hat{\theta}_2\right) s_{77} \end{array} \tag{4.27}$$

$$\begin{array}{lll} K^+,\, K^- : & s'_{22} = \cos\frac{\theta}{2} s_{22} & p'_{72} = i \sin\frac{\theta}{2}\left(\hat{\theta}_4 - i\hat{\theta}_5\right) s_{22} \\ & s'_{55} = s_{55} & \\ & s'_{77} = \cos\frac{\theta}{2} s_{77} & p'_{27} = i \sin\frac{\theta}{2}\left(\hat{\theta}_4 + i\hat{\theta}_5\right) s_{77} \end{array} \tag{4.28}$$

$$\begin{array}{lll} K^0,\, \bar{K}^0 : & s'_{22} = \cos\frac{\theta}{2} s_{22} & p'_{52} = i \sin\frac{\theta}{2}\left(\hat{\theta}_6 - i\hat{\theta}_7\right) s_{22} \\ & s'_{55} = \cos\frac{\theta}{2} s_{55} & p'_{25} = i \sin\frac{\theta}{2}\left(\hat{\theta}_6 + i\hat{\theta}_7\right) s_{55} \\ & s'_{77} = s_{77} & \end{array} \tag{4.29}$$

with $\theta = \sqrt{\theta_a^2 + \theta_{a'}^2}$ and $\hat{\theta}_a = \theta_a/\theta$. When Eq. (4.1) is not an exact symmetry the rotation (Eq. (4.26)) does not give the exact ground state of the system. In this case one has to solve the gap equations (Eq. (3.29)) for both the scalar and pseudoscalar condensates and calculate the pressure. For that it is necessary to include the pseudoscalar diquark condensates in the thermodynamic potential.

4.2.2. Including pseudoscalar diquark condensates

In analogy to the scalar diquark gap parameter (Eq. (3.13)), we define the gap parameter for the pseudoscalar diquark condensates as

$$\Delta^{(p)}_{AB} = -2H\, p_{AB}\,. \tag{4.30}$$

The evaluation of the thermodynamic potential and the gap equations work in complete analogy to the procedure presented in Sect. 3.3 and Sect. 3.4. The pseudoscalar diquark condensates give a contribution to the inverse propagator, cf. Eq. (3.11),

$$S^{-1}(p) = \begin{pmatrix} \not{p} + \mu\gamma_0 - \hat{M} & \sum_{A,B} \left(\Delta^{(s)}_{AB}\gamma_5 - \Delta^{(p)}_{AB}\right) \tau_A \lambda_B \\ \sum_{A,B} \left(-\Delta^{(s)\star}_{AB}\gamma_5 - \Delta^{(p)\star}_{AB}\right) \tau_A \lambda_B & \not{p} - \mu\gamma_0 - \hat{M} \end{pmatrix} . \tag{4.31}$$

This also effects the block diagonal structure of S^{-1}. It is now only possible to reduce S^{-1} to one 20×20 and two 8×8 blocks[5]. There are field independent terms that contribute to $\mathcal{V}$ (Eq. (3.14)). This term now reads

$$\mathcal{V} = 2G\left(\phi_u^2 + \phi_d^2 + \phi_s^2\right) - 4K\phi_u\phi_d\phi_s + \sum_{A,B=2,5,7} H\left[|s_{AB}|^2 + |p_{AB}|^2\right] . \tag{4.32}$$

To find the minimum of the thermodynamic potential we now have to solve also the gap equation for the pseudoscalar condensates

$$\frac{\partial\Omega}{\partial\Delta^{(p)}_{AB}} = 0 . \tag{4.33}$$

We will consider CFL-like phases with a single Goldstone boson condensate, therefore we have to include two pseudoscalar diquark condensates at a time, cf. Sect. 4.2.1. This gives us eight gap equations, three for the chiral condensates, three for scalar and two for pseudoscalar diquark condensates, together with the three neutrality conditions (Eq. (3.41)) this makes eleven equations that have to be solved simultaneously.

4.3. Phase diagram of neutral quark matter

We will now construct the phase diagram for electric and color charge neutral quark matter in β equilibrium. Here we work with "realistic" parameter sets, using $m_s = 140.7$ MeV. To find the ground state we solve the gap equations and neutrality conditions for each phase in Table 2.1 and compare the pressures. In addition to the color superconducting phases listed in Table 2.1 we find at least one solution where all diquark condensates vanish. Where the self-consistently determined quark-antiquark condensates are small we call this phase "normal quark" (NQ) phase and where the quark-antiquark condensates are large we label this phase with "χSB" (chiral symmetry spontaneously broken) even though chiral symmetry is broken explicitly in our model.

---

[5] In the presence of two pseudoscalar diquark condensates

Let us first consider the case of an "intermediate" diquark coupling strength ($H = 3/4\,G$, parameter set I). As a starting point we have calculated the phase diagram neglecting pseudoscalar diquark condensates. This phase diagram is shown in Fig. 4.3(a). Here we find the chirally broken phase, at low chemical potential and temperature, and the normal quark phase at larger chemical potential. The two phases are separated by a first-order phase transition at low temperatures and connected by a smooth crossover at high temperatures and low chemical potentials. This is the standard picture of the chiral phase transition. Color superconducting phases exist only at temperatures smaller than ≈ 50 MeV on the chirally restored side of the chiral phase transition. First, at quark chemical potentials where no strange quarks are present, a 2SC phase emerges. In the 2SC phase, where only up and down quarks are present, ideally there are as many down quarks as there are up quarks. This would give the 2SC a positive electric charge. To compensate this charge a negative electric charge chemical potential is needed, leading to a surplus of down quarks and introducing electrons. This will neutralize the system, but on the other hand, split up the Fermi surfaces of up and down quarks. At low temperatures the separation gets so large, that 2SC-pairing is no longer possible and the normal quark phase is realized. When the quark chemical potential is sufficiently large to allow for strange quarks, uSC and CFL phases appear. The uSC phase is a result of the electric charge neutrality splitting of the Fermi surfaces of the up and down quarks and therefore allows for up−strange pairing at lower quark chemical potential than for down−strange pairing. This phase diagram agrees exactly with the phase diagram of Ref. [17].

In the next step we also allow for pseudoscalar diquark condensates. The resulting phase diagram is presented in Fig. 4.3(b). At temperatures lower than ≈ 25 MeV pseudoscalar condensates appear, the CFL phase turns into a CFLK^0 phase. Except for a few differences our results also agree with Ref. [72], where the same model was used for the same parameters. In contrast to the results of Ref. [72] we find a gapless CFLK^0 phase at very low temperatures and quark chemical potentials lower than 457.2 MeV, whereas in Ref. [72] no gapless CFLK^0 phase exists. The uSC reaching down to zero temperature in Ref. [72] is replaced by a gCFL phase for temperatures lower than ≈ 7 MeV in our calculation. Further on we have strong evidences that the p2SC phase found in Ref. [72] is an artifact of the mean-field approximation. We therefore did not indicate this phase in the phase diagram (Fig. 4.3(b)) even though our numerical results confirm the results of Ref. [72]. We will discuss these points in more detail below.

In Fig. 4.4 we show values for the quark masses, charge chemical potentials and diquark condensates as functions of the quark chemical potential for three selected temperatures for the phase diagram Fig. 4.3(b).

For the stronger diquark coupling ($H = G$, parameter set III) we proceed in the same way. Figure 4.5(a) shows the phase diagram only taking scalar condensates into

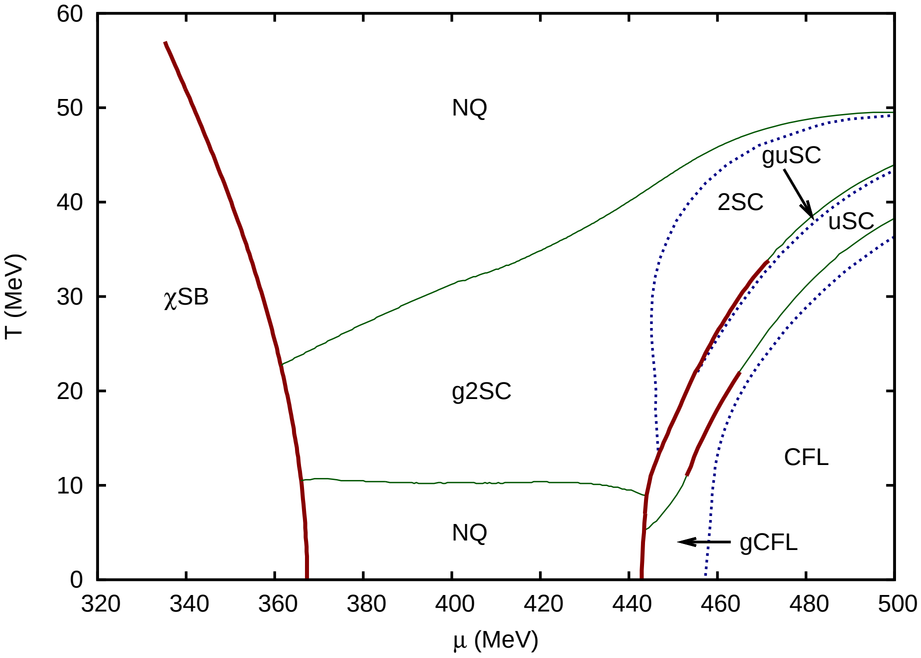

(a) only scalar diquark condensates

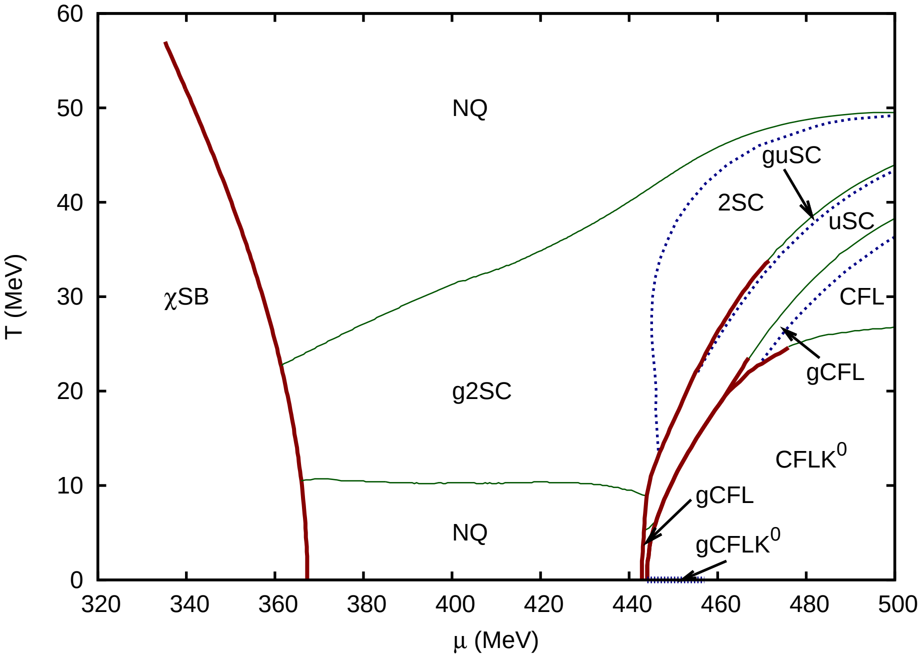

(b) with pseudoscalar diquark condensates

Figure 4.3.: The phase diagram of electric and color charge neutral quark matter with the intermediate diquark coupling strength $H = 3/4\,G$. The upper panel (a) shows the phase diagram considering only scalar diquark condensates, pseudoscalar diquark condensates are included in the lower panel (b). Thick (red) lines denote first-order phase transitions, thin (green) lines second-order phase transitions and the dotted (blue) lines the (dis)appearance of the gap in the excitation spectrum (transition to a gapless phase). (parameter set I)

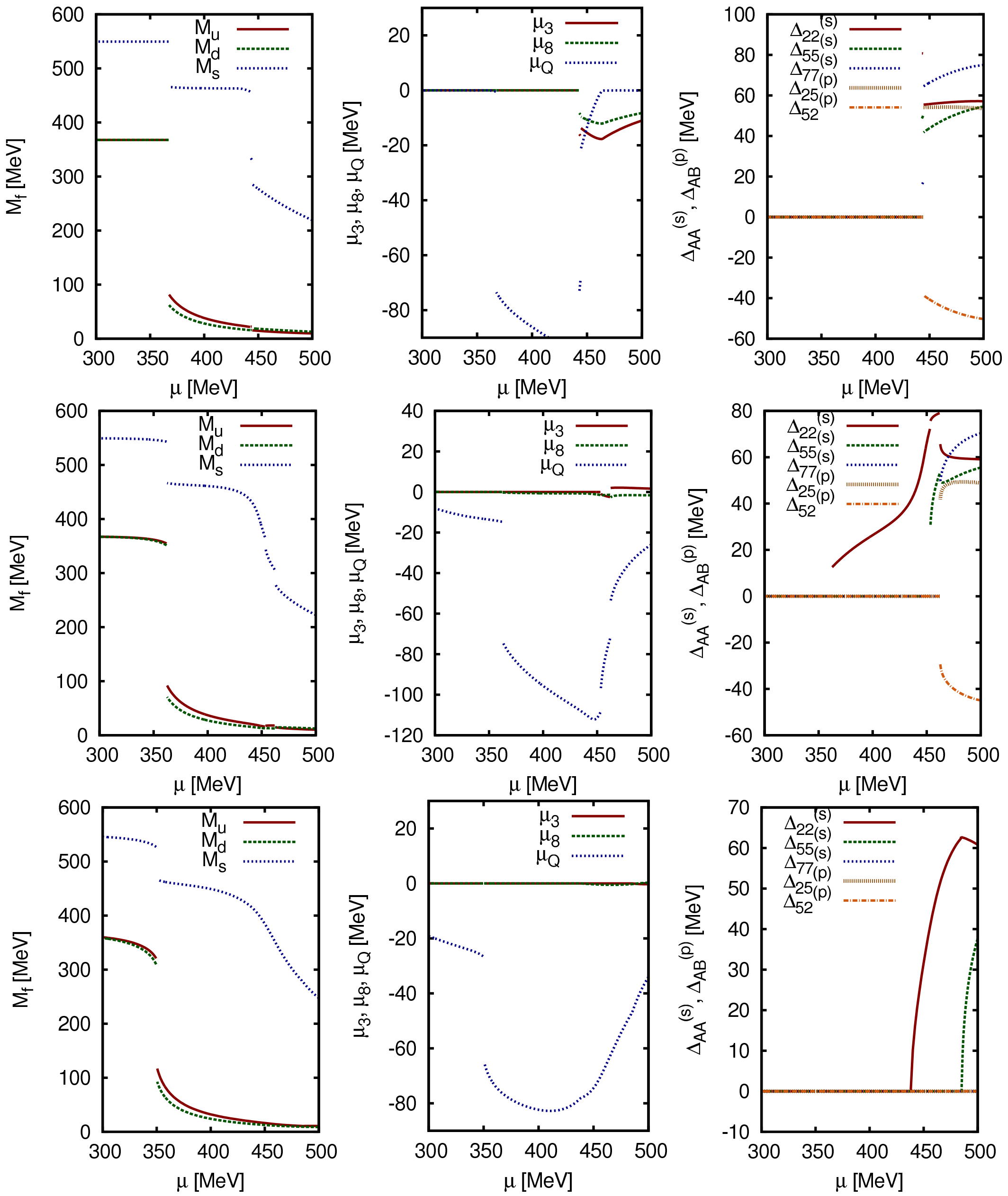

Figure 4.4.: The quark masses (left), the charge chemical potentials (center) and the gap parameters (right) from the phase diagram Fig. 4.3(b) at $T = 0$ (top), $T = 20$ MeV (middle) and $T = 40$ MeV (bottom) for the intermediate diquark coupling $H = 3/4\,G$. (parameter set I)

account. Due to the stronger diquark coupling the domains of color superconducting matter grow compared with Fig. 4.3(a). The basic structure, 2SC at lower quark chemical potential and CFL at higher quark chemical potential, is kept. With the stronger diquark coupling the 2SC phase is also realized at small temperatures replacing the normal quark phase. This phase diagram is in very good agreement with the results of Ref. [17].

In Fig. 4.5(b) we show the phase diagram, including pseudoscalar condensates. Similar to the "intermediate" coupling case, a large part of the CFL phase is replaced by the CFLK^0 phase. The CFLK^0 phase becomes gapless at very low temperatures and $\mu < 415.6$ MeV. The stronger diquark coupling is not discussed in Ref. [72].

In Fig. 4.6 we show values for the quark masses, charge chemical potentials and diquark condensates as functions of the quark chemical potential for three selected temperatures, for the phase diagram Fig. 4.5(b).

4.3.1. The gapless CFLK^0 phase

Both phase diagrams (Fig. 4.3(b) and Fig. 4.5(b)) contain a gapless CFLK^0 phase. At very low temperature and a quark chemical potential lower than a critical value, $\mu_c = 457.2$ MeV for $H = 3/4\,G$ and $\mu_c = 415.6$ MeV for $H = G$, the gap in the excitation spectrum vanishes. This only happens for temperatures so small ($T < 0.01$ MeV) that is was not possible to resolve the gCFLK^0 /CFLK^0 transition temperature numerically[6]. In the following we will study the situation with the "intermediate" diquark coupling ($H = 3/4\,G$, parameter set I), but there is no qualitative difference to the case $H = G$ (parameter set III).

As already mentioned, the gCFLK^0 phase only appears at very small temperatures. To illustrate this behavior we show the size of the gap in the excitation spectrum as a function of quark chemical potential for different temperatures in the upper part of Fig. 4.7. For $T = 1$ MeV, which is usually a good approximation for the zero-temperature case, the gap still takes a value of several MeV. Even for $T = 0.01$ MeV the gap keeps a finite, although small, value. Finally, for zero temperature a gapless phase is realized[7]. In the lower part of Fig. 4.7 the electric charge chemical potential is shown as a function of the quark chemical potential. At zero temperature in the fully gapped, color and electric charge neutral CFLK^0 phase the electric charge chemical potential has to be zero. We therefore expect only small values of μ_Q for the temperatures shown in Fig. 4.7 in the fully gapped CFLK^0 phase. However, for all non-zero temperatures in Fig. 4.7, we see derivations from this behavior that are characteristic for a gapless phase, even though the gap keeps a finite value. For $T = 0.01, 0.1$ and 1 MeV we observe, that the excitation gap as

---

[6] More details on the numerical difficulties are given in Appendix D.

[7] From this observation we conclude that the transition temperature must lie in the interval $[0, 0.01]$ MeV.

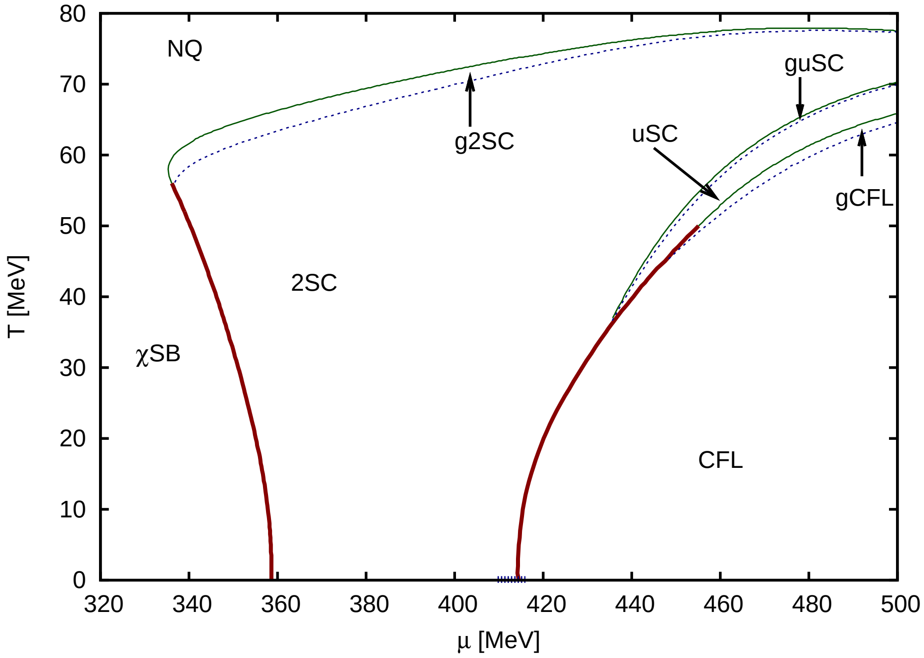

(a) only scalar diquark condensates

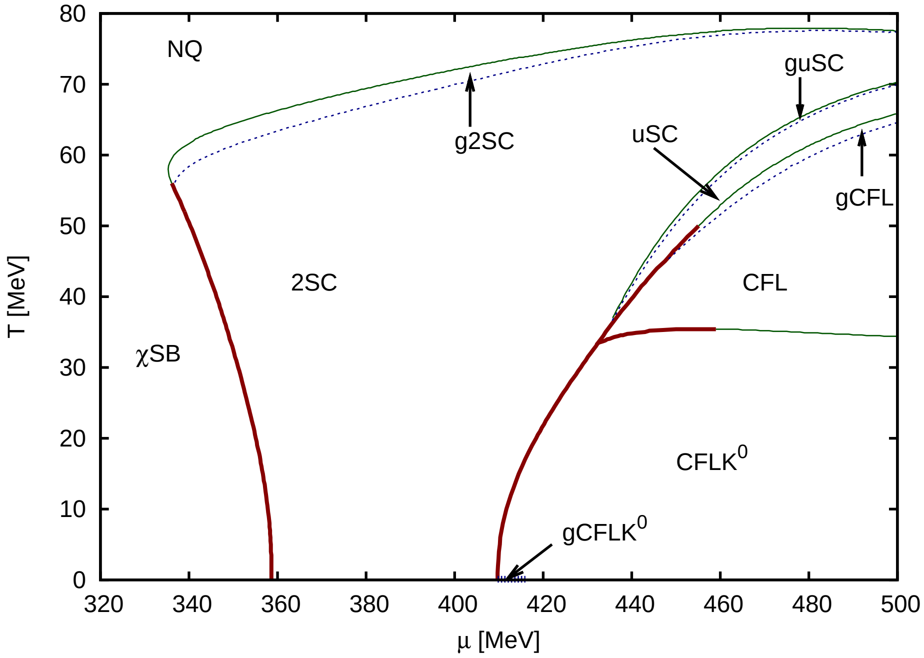

(b) with pseudoscalar diquark condensates

Figure 4.5.: The phase diagram of electric and color charge neutral quark matter for the stronger diquark coupling $H = G$. The upper panel (a) shows the phase diagram considering only scalar diquark condensates, pseudoscalar diquark condensates are included in the lower panel (b). Thick (red) lines denote first-order phase transitions, thin (green) lines second-order phase transitions and the dotted (blue) lines the (dis)appearance of the gap in the excitation spectrum (transition to a gapless phase). (parameter set III)

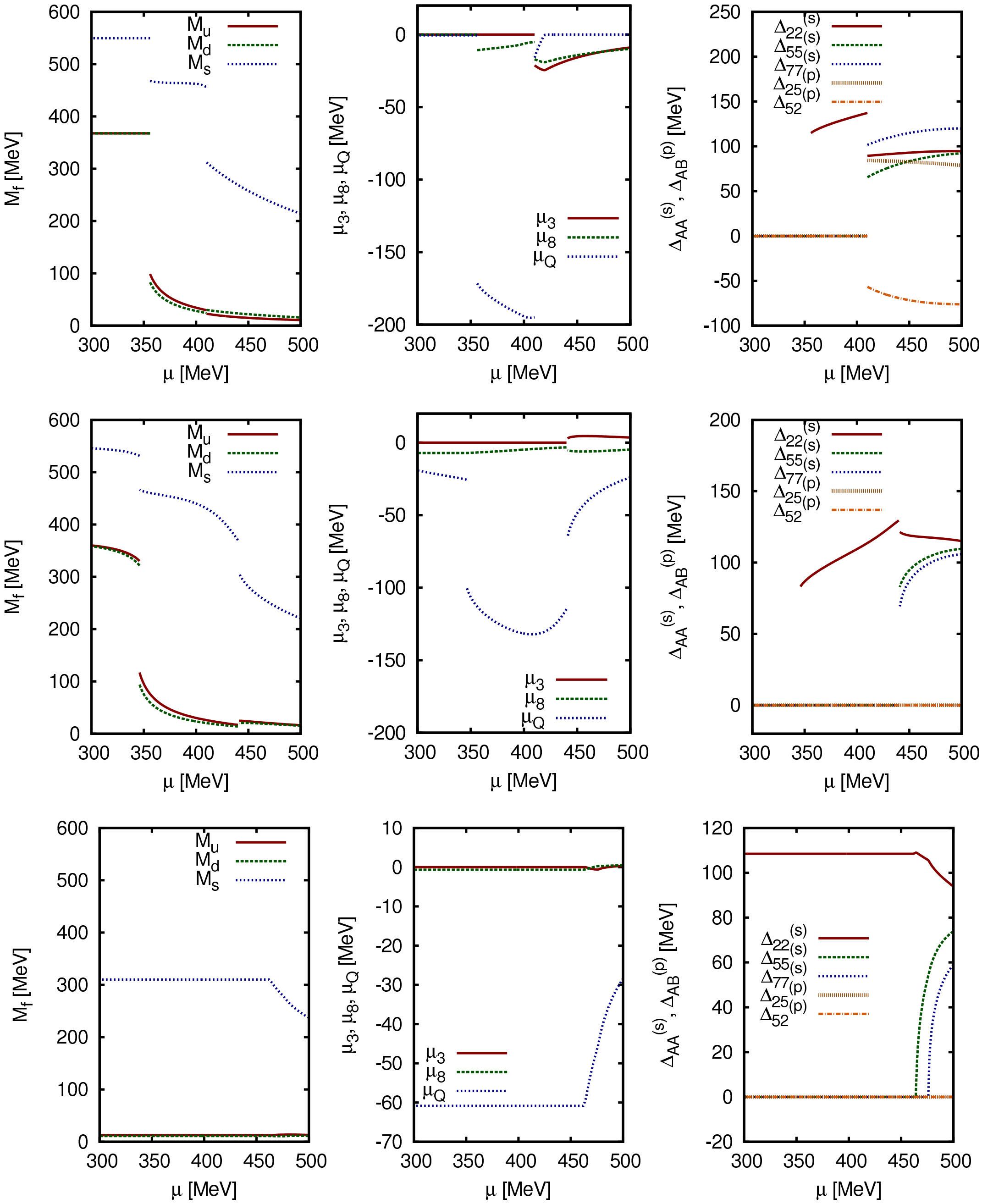

Figure 4.6.: The quark masses (left), the charge chemical potentials (center) and the gap parameters (right) from the phase diagram Fig. 4.5(b) at $T = 0$ (top), $T = 40$ MeV (middle) and $T = 60$ MeV (bottom) for the stronger diquark coupling $H = G$. (parameter set III)

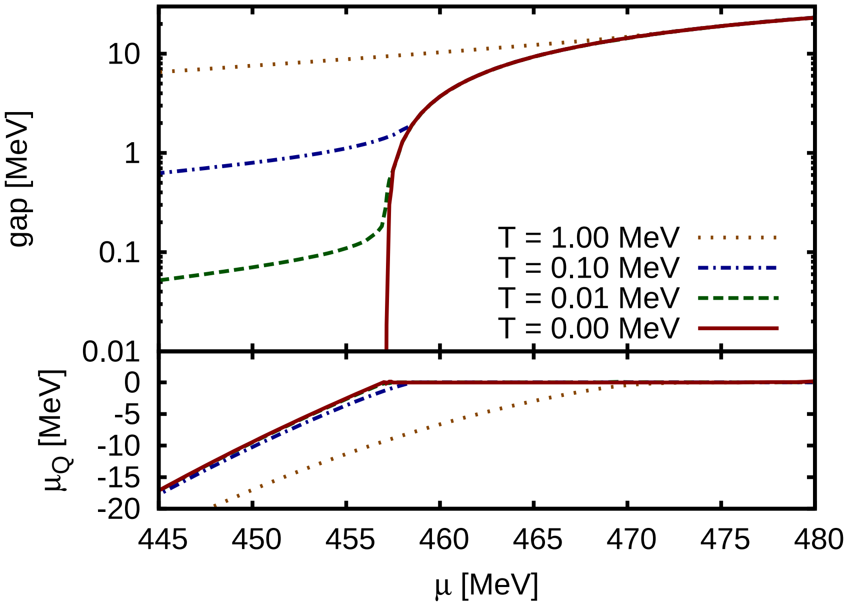

Figure 4.7.: The gap in the excitation spectrum and the electric charge chemical potential μ_Q as functions of the quark chemical potential for various temperature around the onset of the gCFLK^0 phase. (parameter set I)

a function of the quark chemical potential bends away from the zero-temperature value at the point where the electric charge chemical potential starts to take a non-zero value. We will see that charge neutrality is crucial for the mechanisms which are relevant here.

Figure 4.8 is the counterpart of Fig. 4.7 showing the gap in the excitation spectrum as a function of temperature for two different quark chemical potentials. At $\mu = 460$ MeV we see that the value of the gap bends and remains finite at zero temperature, whereas at $\mu = 450$ MeV it decreases constantly and reaches zero at (or slightly above) $T = 0$.

To understand this behavior it is instructive to take a look on the more familiar and slightly simpler situation in the (g)CFL phase. The characteristics of the gCFL phase have been worked out in Ref. [61] for a simpler model neglecting quark masses.

In Fig. 4.9 we show the quasi-particle dispersion relations at $\mu = 450$ MeV for the gCFL phase at $T = 0$ (Fig. 4.9(a)), $T = 5$ MeV (Fig. 4.9(b)), the (g)CFLK^0 phase at $T = 0$ (Fig. 4.9(c)) and $T = 5$ MeV (Fig. 4.9(d)). For the gapless CFL phase at $T = 0$ one finds two modes that are gapless (Fig. 4.9(a)). Since the rotated charge $\tilde{Q}$ (Eq. (2.14)) is a good, conserved quantum number, each mode carries a defined $\tilde{Q}$-charge. The bd-particle–gs-hole mode carries $\tilde{Q} = 0$ and develops an approximately 100 MeV wide “blocking region” (cf. Sect. 2.2). On the contrary, the bu-particle–

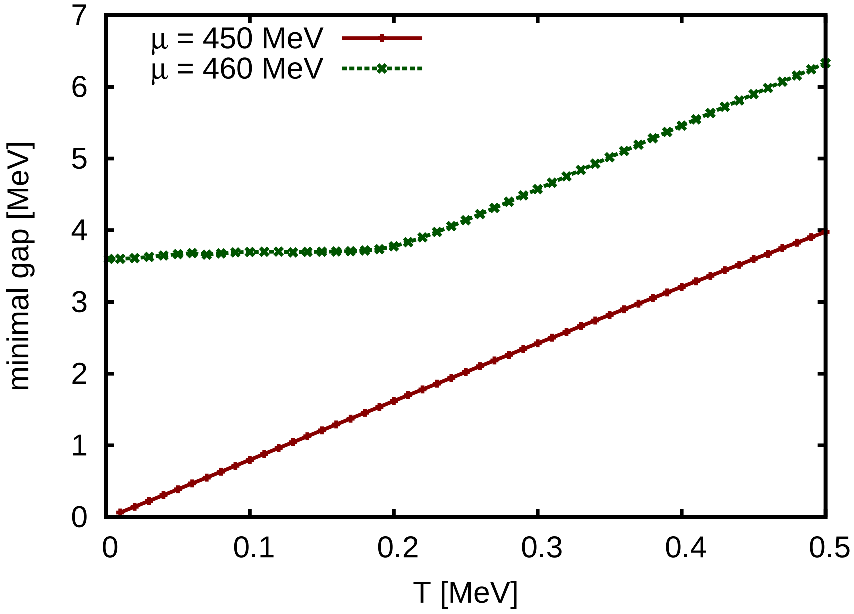

Figure 4.8.: The gap in the excitation spectrum as function of the temperature in the CFLK^0 phase for two different values of the quark chemical potential. (parameter set I)

rs-hole mode, which carries $\tilde{Q} = +1$ vanishes at two points, only separated by a very small blocking region, so that the mode looks almost quadratic [62] on the scale of Fig. 4.9. In neutral CFL matter, at $T = 0$, the difference in chemical potential for the bd–gs and bu–rs quark pairs is equal, $\mu_{d,b} - \mu_{s,g} = \mu_{u,b} - \mu_{s,r}$, further on $M_u - M_s = M_d - M_s$. Therefore the separation of the Fermi surfaces is the same in both pairs. This means that both modes become gapless at the same point[8] if one decreases the quark chemical potential at $T = 0$ starting in the fully gapped CFL phase. However after the gap vanished they behave very differently. The emergence of the blocking region in the bu–rs mode leads to unpaired bu quarks and thereby introduces positive charges in the quark part of the system. These positive charges need to be compensated by leptons and the appearing negative electric charge chemical potential reduces the stress on the bu–rs pairs, keeping the blocking region small. Obviously this mechanism does not work for the $\tilde{Q}$ neutral bd–gs mode and here the blocking region grows with decreasing quark chemical potential. At higher temperature, $T = 5$ MeV is shown in Fig. 4.9(b), the situation changes. While the bd–gs mode is still gapless the gu–rs mode develops a gap of a few MeV. That a gapless mode develops a non-zero gap when the temperature is increased above a certain value, is a known behavior of gapless modes [60]. Our numerical analysis shows that the narrow blocking region at the *bd*–*gs* mode vanishes already when the temperature rises slightly above zero.

---

[8] See also Appendix D.1 particularly Eq. (D.2) therein.

In the CFLK^0 phase at $T = 0$ we also find a mode, carrying $\tilde{Q} = +1$, which becomes gapless with a very narrow blocking region, but there is no gapless $\tilde{Q} = 0$ mode. This means, that the gCFLK^0 phase is generated exclusively by the $\tilde{Q} = +1$ mode. Hence the mechanism working in the gCFLK^0 phase is comparable to the one in the gCFL phase, only the missing $\tilde{Q} = 0$ mode limits the gCFLK^0 phase to very low temperatures whereas we find the gCFL phase everywhere on the boundary to the uSC phase in Fig. 4.3(a) ($H = 3/4\,G$) and only at large temperatures in Fig. 4.5(a) ($H = G$). The situation in the CFLK^0 phase is more complicated compared to the CFL phase, since the $\tilde{Q} = +1$ quasi-particle modes consist of four quarks and not only of two quarks like in the CFL phase. The $\tilde{Q} = +1$ mode of interest is a *gu*–*rs*–*rd*–*bu* mixture (see Fig. 4.10), where the fraction of *rd* holes is negligible small.

Finding a numeric solution for the gap equations (Eq. (3.29)) and neutrality conditions (Eq. (3.41)) in the vicinity of a mode with a narrow blocking region is challenging, we present the techniques used in Appendix D.

From effective theories [112] we know that there exists also a gCFLK^0 phase with a gapless $\tilde{Q} = 0$ mode, we will denote this phase with "gCFLK^{0*}". We find that this phase emerges when the gCFL phase develops a K^0 condensate, but it is never the preferred phase and never present in the phase diagram, we therefore do not consider this phase in detail.

Finally we would like to make a short comment on the use of massless electrons in our model. In the regime where $|\mu_Q| \gg m_e$ or where no leptons are allowed, the influence of a finite electron mass can be neglected. Using $m_e = 0$ has the advantage that the solution for the electric neutrality condition in the CFL/CFLK^0 phase at $T = 0$ lies at exactly $\mu_Q = 0$, whereas with a finite electron mass every value in the interval $|\mu_Q| < m_e$ would be allowed with the appropriate values of μ_3 and μ_8. Finding the one $\mu_Q = 0$ solution is numerically easier than to find one of the many possible solutions in the $|\mu_Q| < m_e$ interval, even for a small value of m_e like $m_e = 0.511$ MeV. However a finite electron mass certainly has an influence on the small region at the onset of the gapless CFL/CFLK^0 phase where $|\mu_Q| < m_e$. Allowing for a small non-zero μ_Q in a gapped CFLK^0 phase can shift the onset of the gCFLK^0 phase approximately 0.4 MeV downwards in quark chemical potential compared to the point indicated in Fig. 4.7.

4.3.2. The gCFL window

In both phase diagrams (Fig. 4.3(b) and Fig. 4.5(b)) a large part of the (g)CFL phase is replaced by the CFLK^0 phase. As hinted at the beginning of this chapter the K^0 condensate reduces the strangeness content of the phase which is advantageous at

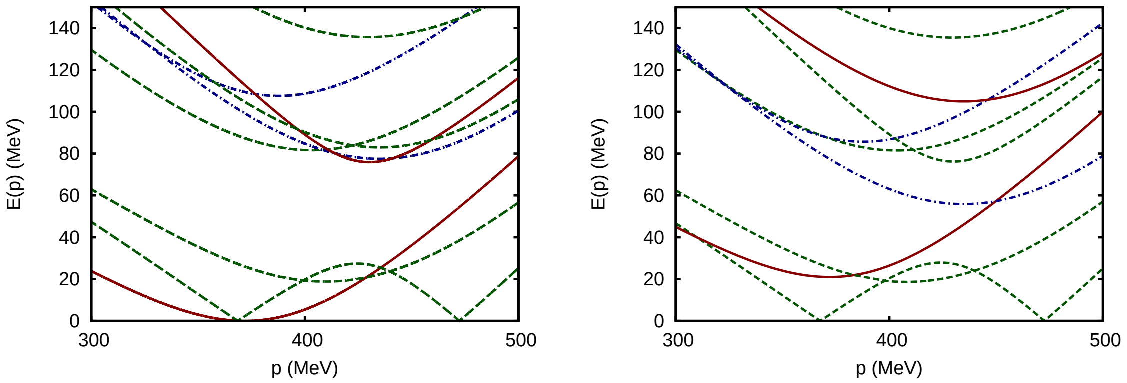

(a) gCFL: $T = 0$ (b) gCFL: $T = 5$ MeV

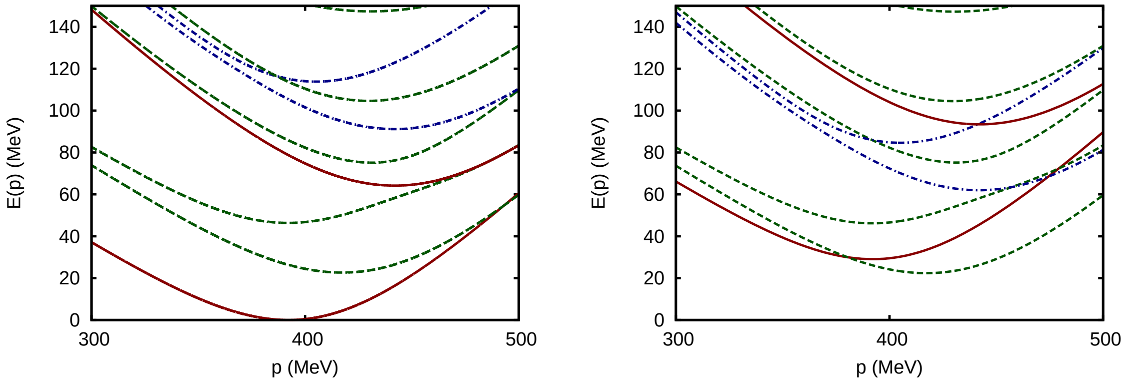

(c) gCFLK^0 : $T = 0$ (d) CFLK^0 : $T = 5$ MeV

Figure 4.9.: The quasi-particle dispersion relations in the gCFL phase (top) and the (g)CFLK^0 phase (bottom) for $\mu = 450$ MeV at two different temperatures for $H = 3/4G$. The solid (red) lines mark modes with $\tilde{Q}$-charge $+1$, the dashed (green) lines $\tilde{Q} = 0$ and the dashed-dotted (blue) $\tilde{Q} = -1$. (parameter set I)

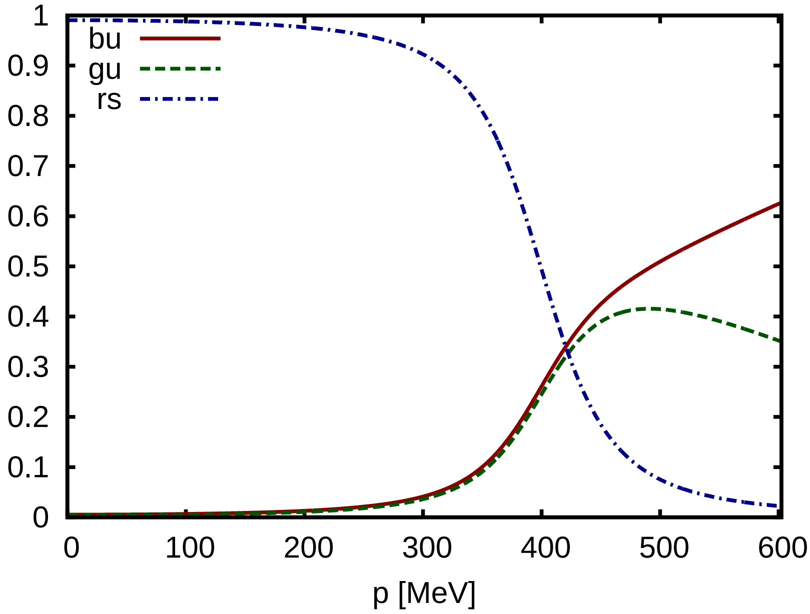

Figure 4.10.: Composition of the $\tilde{Q} = +1$ mode in the gCFLK^0 phase at $T = 0$ and $\mu = 450$ MeV where this mode is gapless, the fraction of *rd*-holes is very small and not shown. (parameter set I)

moderate densities. From this point of view it seems surprising to find (in Fig. 4.3(b)) a narrow band of a gCFL phase on the low quark chemical potential side of the CFLK^0 phase. In Ref. [72] this gCFL window is not found, instead the uSC phase reaches down to zero temperature. To shed some light on the situation we show the pressure difference to the normal phase for the competing phases in Fig. 4.11 at $T = 0.5$ MeV. Here we also take the gCFLK^{0*} phase (see Sect. 4.3.1) into account. In the phase diagram the CFLK^0 phase, the gCFL phase and the normal phase are realized while decreasing the quark chemical potential, whereas the uSC and gCFLK^{0*} phases are never favored.

This becomes more clear looking at the strange quark fraction n_s/n of the different phases, Fig. 4.12. In the fully gapped CFL phase at zero temperature one third of the quarks have to be strange quarks due to the symmetric pairing pattern. At $T = 0.5$ MeV (Fig. 4.12) no deviation from $n_s/n = 1/3$ is visible. When the CFL phase becomes gapless at $\mu = 457.1$ MeV the strange quark fraction drops rapidly. The small temperature of 0.5 MeV smoothes this transition. As expected in the CFLK^0 phase the strange quark fraction is clearly smaller than in the CFL phase. However the strange quark fraction is only reduced mildly in the CFLK^0 phase when the quark chemical potential is decreased while the gCFL phase reduces its strange quark content more efficiently. But for this reduction quark pairs have to be split

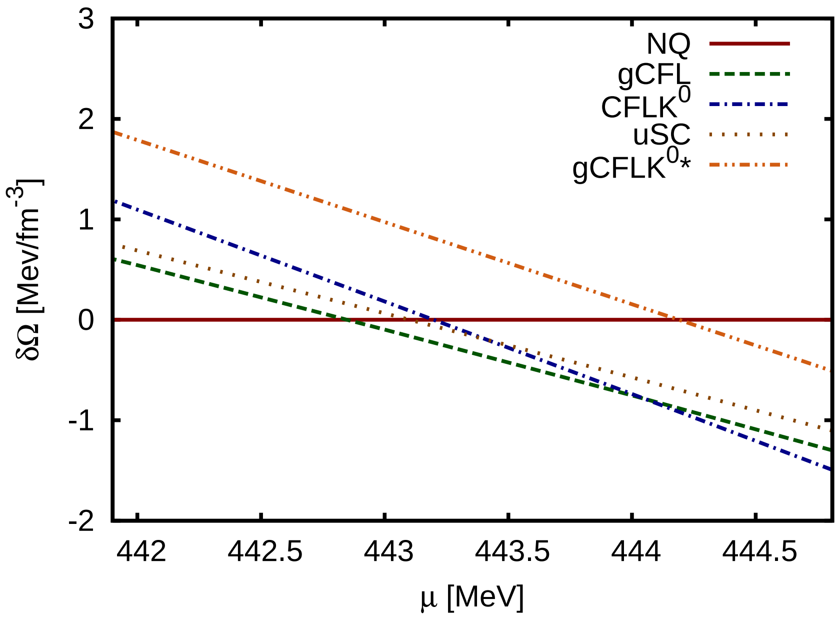

Figure 4.11.: The free energy of different solutions relative to the normal phase for $H = 3/4\,G$ and $T = 0.5$ MeV as a function of the quark chemical potential. (parameter set I)

up in the gCFL phase and the condensation energy decreases. These competing mechanisms lead to a first-order phase transition from the CFLK^0 phase to the gCFL phase at $\mu = 444.1$, giving rise to the small gCFL window found in the phase diagram, Fig. 4.3(b).

4.3.3. The p2SC phase

In Ref. [72] it was found that if one allows for pseudoscalar condensates a part of the 2SC phase is replaced by a p2SC phase. The p2SC is characterized by non-vanishing $\Delta_{22}^{(s)}$ and $\Delta_{25}^{(p)}$ condensates[9], cf. Table 2.1. In Fig. 4.13 this region is indicated for $H = 3/4\,G$. For $H = G$ this also happens at the corresponding place in the phase diagram (not shown). The difference in the free energy between the p2SC and the 2SC phase is very small, less than $1\,\mathrm{keV/fm^3}$. It was observed in Ref. [72], that the p2SC and the corresponding 2SC solution obey the relation

$$\left(\Delta_{22}^{(s)}\right)^2_{\mathrm{p2SC}} + \left(\Delta_{25}^{(p)}\right)^2_{\mathrm{p2SC}} = \left(\Delta_{22}^{(s)}\right)^2_{\mathrm{2SC}} \tag{4.34}$$

---

[9] A rotation of $\Delta_{25}^{(p)}$ into $\Delta_{27}^{(p)}$ is possible.

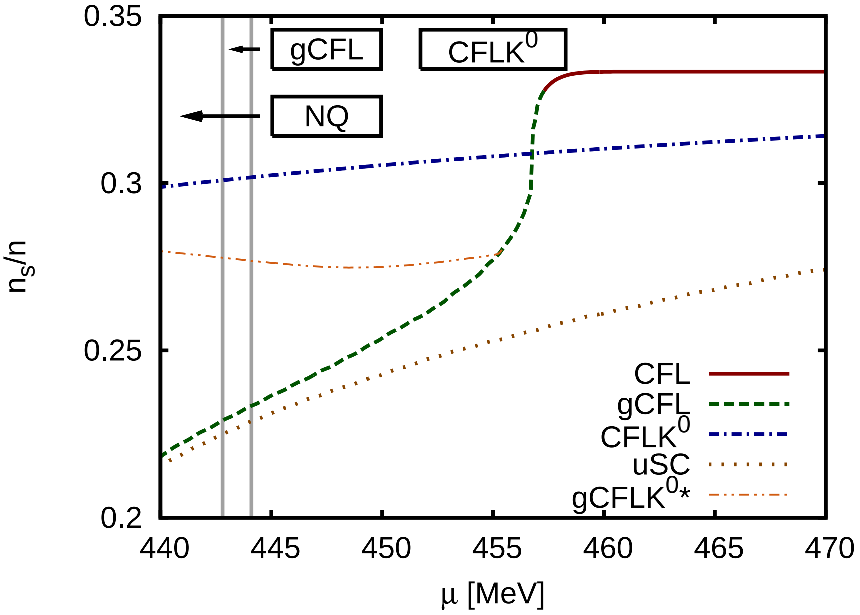

Figure 4.12.: The strange quark fraction n_s/n in the competing color superconducting phases for $H = 3/4\,G$ and $T = 0.5$ MeV as a function of the quark chemical potential. The labels in the boxes indicate which phase is actually realized in the phase diagram. (parameter set I)

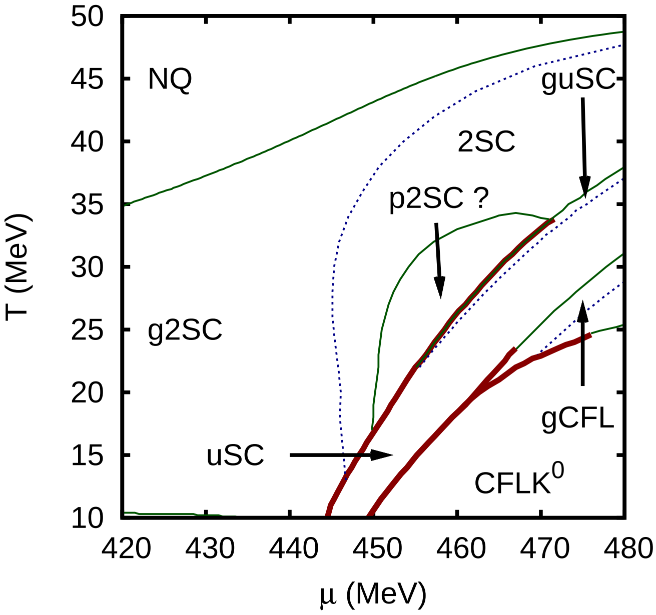

Figure 4.13.: A part of the phase diagram showing the region where the numerical results prefer a p2SC phase over the 2SC phase, for $H = 3/4\,G$. (parameter set I)

indicating that the two solutions are connected via an axial color transformation

$$q \to \exp\left(i\theta\frac{\lambda_7}{2}\gamma_5\right) q\,. \tag{4.35}$$

Our numerical calculations confirm all these results. The two following open questions are: What is the physical meaning of the p2SC phase? Why is the p2SC phase preferred over the 2SC phase.

Let us start with the physical interpretations. The appearance of pseudoscalar condensates in the CFL phase is related to the condensation of Goldstone bosons and thereby with the spontaneous breaking of global symmetries. This is different in the situation here, there is no global symmetry associated with the transformations described by Eq. (4.35) that could lead to a Goldstone mode in the 2SC phase. This means that the Goldstone mode responsible for the p2SC phase has to be of unphysical origin. We notice that the mean-field thermodynamic potential is invariant under the transformation Eq. (4.35) if one sets $M_u = M_d = 0$, allows only for the diquark condensates $\Delta_{22}^{(s)}$, $\Delta_{25}^{(p)}$ and restricts the transformation to the non-strange sector (see Appendix E for more details). This accidental symmetry is broken by the $\Delta_{22}^{(s)}$ condensate in the 2SC phase and the appearing unphysical Goldstone mode leads to the appearance of the p2SC phase. Hence the p2SC phase is an artifact of the mean-field approximation.

Nevertheless it is interesting to investigate why the p2SC is preferred over the 2SC phase. Comparing the 2SC and p2SC solution shows that the absolute values of μ_8 are smaller in the p2SC phase than in the 2SC phase and there is a non-zero value for μ_3 whereas μ_3 is exactly zero in the 2SC phase. This suggests that the pressure difference between the two phases is due to some different behavior of the color charges.

It is known from Ref. [79] that a vector color rotation

$$q \to \exp\left(i\theta_a \frac{\lambda_a}{2}\right) q \tag{4.36}$$

rotates the color charges n_3 and n_8 into the off-diagonal color charges n_1, n_4 and n_6 ($n_a = \langle q^\dagger \lambda_a q\rangle$ $a \in \{1\ldots 8\}$). If one mistakenly ignores these off-diagonal color charges, one finds that the 2SC phase can be neutralized by the transformation Eq. (4.36) and the possibility to reduce the color charge chemical potentials gives this rotated 2SC phase a lower free-energy [100]. Certainly this is not a physical way to neutralize the 2SC phase since all color charges have to vanish. The presence of the color charge chemical potentials μ_a is a peculiarity of the NJL model. In QCD the color charges n_a couple the corresponding gluon fields A_a^0 and thereby the system is neutralized in all components n_a.

The transformation Eq. (4.35) does not rotate the color charges n_3 and n_8 into off-diagonal color charges[10] but into "axial" color charges

$$n_a^{(5)} = \langle q^\dagger \gamma_5 \lambda_a q\rangle \,. \tag{4.37}$$

In the situation of the p2SC phase the color charge n_8 is rotated into

$$\begin{aligned} n_8\big|_{\mathrm{p2SC}} &= \frac{1}{4}(1+3\cos\theta)\, n_8\big|_{\mathrm{2SC}}\,, \\ n_3\big|_{\mathrm{p2SC}} &= \frac{\sqrt{3}}{4}(1-\cos\theta)\, n_8\big|_{\mathrm{2SC}}\,, \\ n_6^{(5)}\Big|_{\mathrm{p2SC}} &= -\frac{\sqrt{3}}{2}\sin\theta\, n_8\big|_{\mathrm{2SC}}\,. \end{aligned} \tag{4.38}$$

In Fig. 4.14 we show the axial color charge density in the p2SC phase. Since there is no argument that requires the "axial" color charges to vanish and the sum $\sum_a \left(n_a^2 + n_a^{(5)2}\right)$ is conserved, smaller values of the charge chemical potentials are sufficient and the p2SC phase is preferred over the 2SC phase.

At this point we like to point out, that in our numerical evaluation of the CFLK^0 phase we also find non-vanishing "axial" color charge densities, but unlike in the

---

[10] We check that for all neutral solutions of the gap equations in this work all color charges (n_a, $a \in \{1\ldots 8\}$) vanish although only μ_3 and μ_8 are used to neutralize the solution.

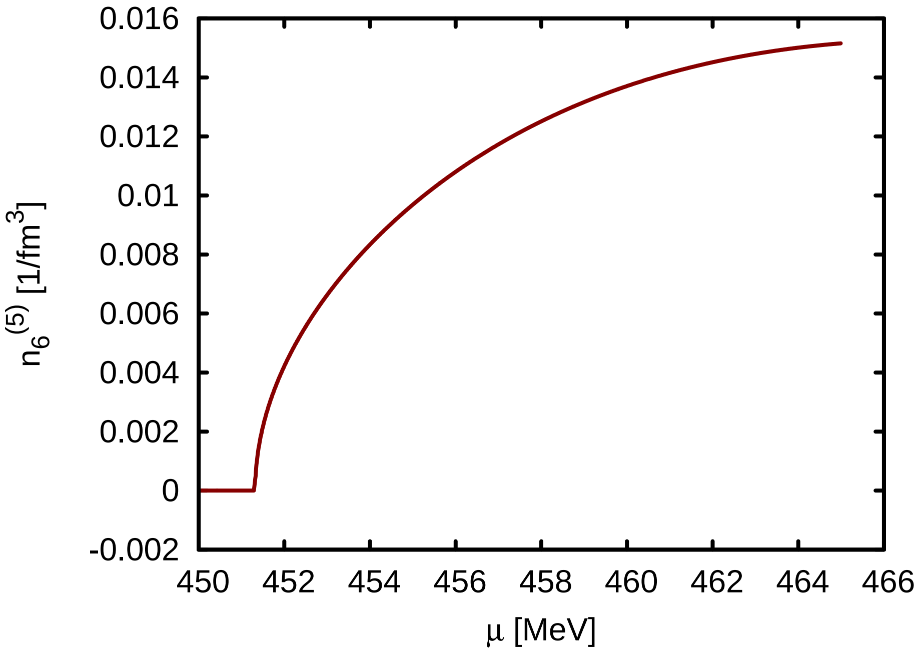

Figure 4.14.: The axial color charge density $n_6^{(5)}$ at $T = 25$ MeV in the (p)2SC phase as a function of μ. The p2SC phase and the 2SC phase are connected by a second-order phase transition at $\mu = 451.3$ MeV. (parameter set I)

p2SC phase, the Goldstone bosons in the CFLK^0 phase have a reliable physical interpretation. Further on the pressure difference between the CFL and CFLK^0 phase is much larger than the 1 keV/fm^3 difference between the 2SC and p2SC phase.

4.4. Neutrino trapping

When a neutron star is born in the aftermath of a supernova it might be a few tens of MeV hot and intransparent for neutrinos, so that the neutrinos are trapped inside the star and lepton number is a conserved quantity (see e.g. Ref. [101]). However the neutron star will cool very fast to a temperature below 1 MeV and the neutrinos will leave the star.

In this section we will study the effect of the trapped neutrinos on the phase structure of the color superconductor. Neglecting pseudoscalar condensates this has been done in Ref. [102], but in this case the condensation of charged mesons might play an important role since their electric charge can compensate the electric charge from leptons produced by introducing a lepton chemical potential.

Neglecting neutrino oscillations, the two families of leptons we use, electrons and muons, will lead to the conservation of the independent lepton numbers

$$n_{L_e} = n_e + n_{\nu_e} \,, \tag{4.39}$$

$$n_{L_\mu} = n_\mu + n_{\nu_\mu} \,. \tag{4.40}$$

To handle these additional conserved charges we have to introduce two new chemical potentials[11], the electron lepton number chemical potential μ_{L_e} and the muon lepton number chemical potential μ_{L_μ}. While the neutrinos only feel the lepton number chemical potentials

$$\mu_{\nu_e} = \mu_{L_e} \,, \tag{4.41}$$

$$\mu_{\nu_\mu} = \mu_{L_\mu} \,, \tag{4.42}$$

the other leptons are also sensitive to the electric charge chemical potential μ_Q

$$\mu_e = \mu_{L_e} - \mu_Q \,, \tag{4.43}$$

$$\mu_\mu = \mu_{L_\mu} - \mu_Q \,. \tag{4.44}$$

We assume that the lepton content of the proto-neutron star is roughly the same as in the progenitor star and we therefore set $\mu_{L_\mu} = 0$ and limit μ_{L_e} to positive values smaller than 400 MeV [102]. This assumption adds μ_{L_e} as a third axis to the $T - \mu$ phase diagram. While the proto-neutron star is loosing its neutrino content μ_{L_e} moves down from its initial value to $\mu_{L_e} = 0$ where the star is transparent for neutrinos and lepton number is no longer conserved.

In principle we need to add an additional part to the thermodynamic potential (Eq. (3.16)) taking the contribution of neutrinos into account Ω_{neutrino}. But since this contribution will only depend on the temperature and the lepton chemical potential and does not have any influence on the quark part of the system, this shifts the pressure by the same amount for every quark phase and we can neglect its contribution when calculating the phase diagram.

4.4.1. Varying μ_Q

The lepton part of the system influences the quark part via the neutrality conditions and the electric charge chemical potential. It is therefore very instructive to have a look at the behavior of the quark part under variations of the electric charge chemical potential at first, leaving the lepton number chemical potentials at zero.

In Fig. 4.15 we show the pressure difference of phases with different Goldstone boson condensates compared to the pressure of the CFL phase at $\mu_Q = 0$ for $T = 0$

---

[11] So far we always worked with $\mu_L = \mu_{L_e} = \mu_{L_\nu} = 0$.

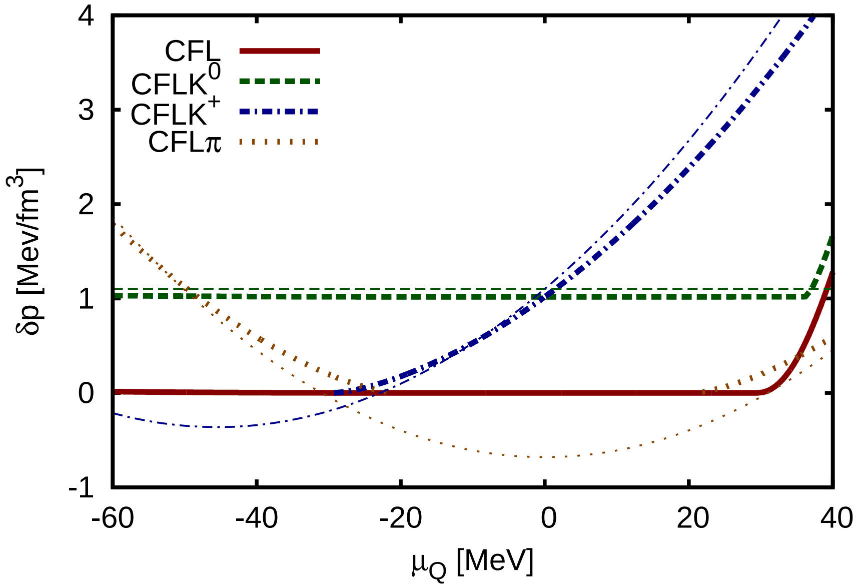

Figure 4.15.: The pressure difference of phases with different Goldstone bosons condensates to the pressure of the CFL phase at $\mu_Q = 0$ for $T = 0$ and $\mu = 500$ MeV. Thick lines denote the results of our NJL model calculations and thin lines the corresponding predictions from Ref. [89]. (parameter set I)

and $\mu = 500$ MeV. The results of our NJL model calculation (thick lines) are compared to the results from an low-energy effective theory (thin lines) obtained in Ref. [89].

From Ref. [89] we get the following relations:

(i) *Meson masses*

$$m^2_{\pi^\pm} = a(M_u + M_d)\, M_s\,, \tag{4.45}$$

$$m^2_{K^\pm} = a(M_u + M_s)\, M_d\,, \tag{4.46}$$

$$m^2_{K^0,\bar{K}^0} = a(M_d + M_s)\, M_u \tag{4.47}$$

with $a = 3(\Delta^2/\pi^2 f_\pi^2)$ and $f_\pi^2 = (21 - 8\ln 2)/(36\pi^2)\mu^2$ (for Δ we use $\Delta = \left(\Delta^{(s)}_{22} + \Delta^{(s)}_{55} + \Delta^{(s)}_{77}\right)/3$). From Ref. [91] we know that using this value for a will lead to a deviation of approximately 10% from the NJL results of the meson masses, but in our case, where we are mainly interested in the pressure and in understanding the basic mechanisms, this deviation is of minor importance.

(ii) *Effective chemical potentials* for the $\pi^\pm$, $K^\pm$, K^0 and $\bar{K}^0$ mesons

$$\mu_{\pi^\pm} = \mu_Q \pm \frac{M_d^2 - M_u^2}{2\mu}\,, \tag{4.48}$$

$$\mu_{K^\pm} = \mu_Q \pm \frac{M_s^2 - M_u^2}{2\mu}\,, \tag{4.49}$$

$$\mu_{K^0,\bar{K}^0} = \pm\frac{M_s^2 - M_d^2}{2\mu}\,. \tag{4.50}$$

(iii) *Contributions to the thermodynamic potential* by the different meson condensates

$$\delta\Omega_{\pi^\pm} = -\frac{f_\pi^2}{2}\mu^2_{\pi^\pm}\left(1 - \frac{M^2_{\pi^\pm}}{\mu^2_{\pi^\pm}}\right)\,, \tag{4.51}$$

$$\delta\Omega_{K^\pm} = -\frac{f_\pi^2}{2}\mu^2_{K^\pm}\left(1 - \frac{M^2_{K^\pm}}{\mu^2_{K^\pm}}\right)\,, \tag{4.52}$$

$$\delta\Omega_{K^0} = -\frac{f_\pi^2}{2}\mu^2_{K^0}\left(1 - \frac{M^2_{K^0}}{\mu^2_{K^0}}\right)\,. \tag{4.53}$$

Applying the above mentioned results of the low-energy effective theory to the situation at $T = 0$ and $\mu = 500$ MeV in the CFL phase we see that the equal masses of the up and down quark lead to $\mu_\pi = \mu_Q$ and the following mass ordering for the Goldstone bosons (Eqs. (4.45) - (4.47)) [86]

$$m^2_\pi > m^2_{K^\pm} = m^2_{K^0,\bar{K}^0}\,. \tag{4.54}$$

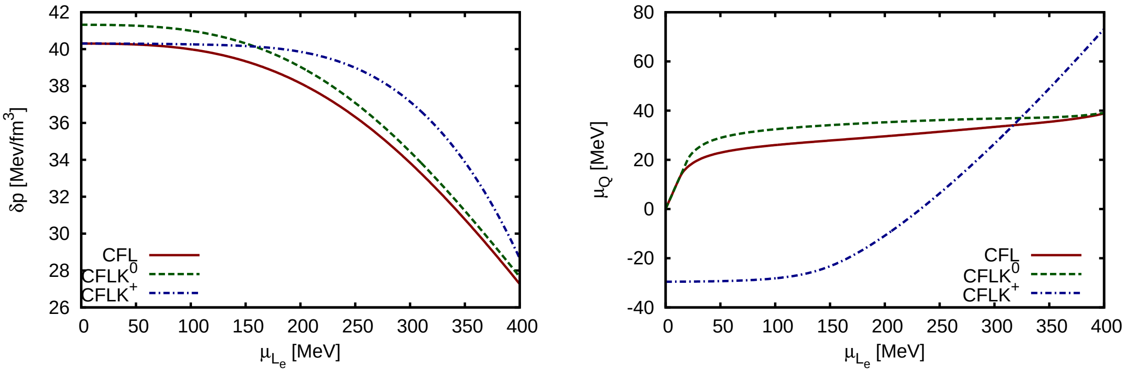

(a) pressure difference (b) electric charge chemical potential

Figure 4.16.: The pressure difference to the normal phase for the CFL, CFLK^0 and CFLK$^+$ phase (a) and the corresponding value of the electric charge chemical potential μ_Q (b) as functions of μ_{L_e}. The phase transition from CFLK^0 to CFLK$^+$ happens at $\mu_{L_e} = 157$ MeV. (parameter set I)

The large strange quark mass gives a nonzero effective strangeness chemical potential

$$\frac{M_s^2 - M_{u/d}^2}{2\mu} > 0\,. \tag{4.55}$$

This will always prefer the condensation of K^+ to the condensation of π^+ at positive values of μ_Q. At $\mu_Q = 0$ the CFLK$^+$ phase is replaced by the CFLK^0 phase and only at sufficiently large negative electric charge chemical potential, where the electric charge chemical potential compensates the strangeness chemical potential a condensate of negatively charged pions is realized, the CFLπ^- phase. These predictions from the low-energy effective theory are very well reproduced by the NJL calculation with the addition, that in the NJL calculation phases can become gapless when the pairing breaks down due to a large separation of the Fermi surfaces of the quarks in one pair. For the above mentioned case this happens at $\mu_Q = 30.2$ MeV for the CFL and $\mu_Q = 36.5$ MeV for the CFLK^0 phase, we can see these points in Fig. 4.15 where the pressures for the CFL and CFLK^0 phase suddenly start changing their value.

4.4.2. Lepton chemical potential

So far we have only considered the quark part of the system, now we will look at the situation where we allow for leptons and will increase the value of μ_{L_e}. For the numerical analysis we choose, as before, $T = 0$ and $\mu = 500$ MeV.

At zero μ_{L_e} the CFLK^0 phase is the preferred phase (Fig. 4.16(a)). Until μ_{L_e} reaches a value of 36.5 MeV the CFLK^0 phase stays charge neutral and this forces $\mu_Q = \mu_{L_e}$ (Fig. 4.16(b)). At $\mu_{L_e} = 36.5$ the stress on the quark pairs, induced by μ_Q, triggers the transition to a gapless CFLK^0 phase.

The CFLK$^+$ phase, on the other hand, starts at $\mu_{L_e} = 0$ with a negative value of μ_Q, so that the presence of electrons compensates the positive charge of the kaons. At $\mu_{L_e} = 0$ we find for the CFLK$^+$ solution that the absolute value of μ_Q is only a bit smaller than $(M_s^2 - M_u^2)/(2\mu)$ meaning that μ_{K^+} is small. This is confirmed by the observation that the pseudoscalar condensates associated with the K^+ condensate are small. As a consequence the CFLK$^+$ phase has almost the same pressure as the CFL phase (Fig. 4.16(a)). By turning up the lepton chemical potential this situation changes. The introduced electrons naturally compensate the charge of the K^+ and reduce the absolute value of μ_Q in the CFLK$^+$ phase. At some point μ_Q crosses zero and change $\mu_{K^+} > \mu_{K^0}$. In a world where the CFLK^0 phase is not gapless (in the low-energy effective theory) this would be the point where the CFLK$^+$ phase becomes the preferred phase, since all other quantities in Eq. (4.52) and Eq. (4.53) are equal. But since, with our set of parameters, the CFLK^0 phase already became gapless and weaker at lower μ_{L_e}, the transition occurred earlier at $\mu_{L_e} = 157$ MeV.

4.4.3. The $\mu_{L_e} - T$ phase diagram

As a next step we add the temperature axis to our considerations and obtain the phase diagram in Fig. 4.17.

The main effect, increasing the lepton chemical potential, is the shift of the transition to the 2SC phase to lower temperatures. The area for the uSC phase becomes smaller and finally disappears. This, and a mechanism for this effect, has been shown in Refs. [102, 103]. We see no noticeable difference to the results of Ref. [102] in the areas of the phase diagram where 2SC or uSC phase are realized.

The existence of pseudoscalar condensates, and with it the possibility for Goldstone boson condensation, was neglected in Refs. [102] and therefore the CFL phase was the low-temperature ground state at large quark chemical potential in this calculation.

Allowing for the condensation of Goldstone bosons in the CFL phase the ground state at $\mu_{L_e} = 0$ changes from CFL to CFLK^0 for temperatures lower than 26.5 MeV. This boundary does not depend on the value of μ_{L_e} since the CFL and CFLK^0 phases do not carry an electric charge. At very low temperatures the CFLK^0 phase becomes gapless for μ_{L_e} larger than 36.5 MeV (as described before in Sect. 4.4.2). Increasing μ_{L_e} further will lead to the condensation of K^+ and at even larger μ_{L_e} one observes that all CFL-like phases are pushed to lower temperatures and replaced by the 2SC phase.

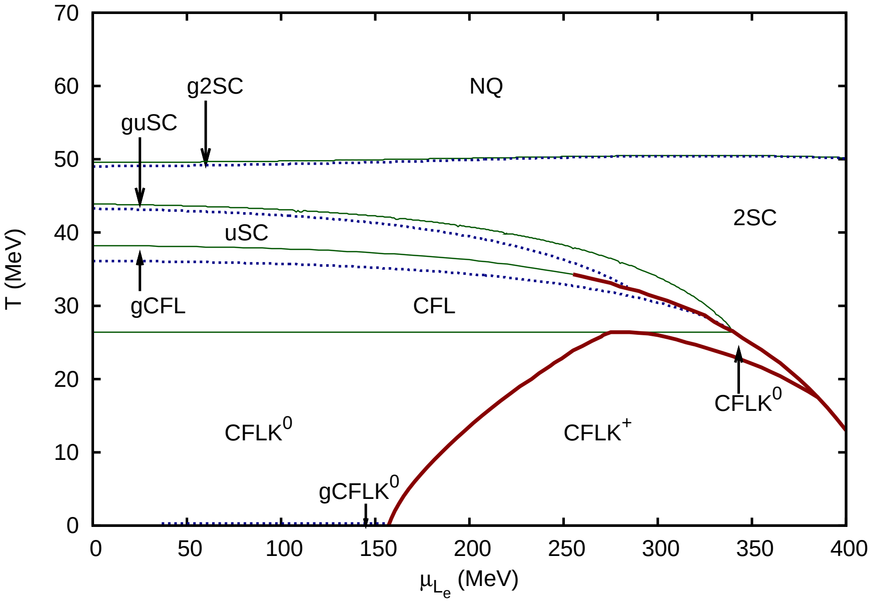

Figure 4.17.: The phase diagram of neutral quark matter in the $\mu_{L_e} - T$ plane at $\mu =$ 500 MeV. Thick (red) lines indicate first order phase transitions while thin (green) lines stand for second order phase transitions. The dashed (blue) lines indicate the (dis)appearance of the gap in the excitation spectrum. (parameter set I)

4.4.4. The $T-\mu$ phase diagram at $\mu_{L_e} = 200$ MeV, 400 MeV

In Fig. 4.18 we present the phase diagram of neutral quark matter at $\mu_{L_e} = 200$ MeV (upper panel) and $\mu_{L_e} = 400$ MeV (lower panel). For comparison the phase diagram at $\mu_{L_e} = 0$ has already been presented in Sect. 4.3 (Fig. 4.3(b)).

All parts of these phase diagrams outside the CFL, CFLK^0 or CFLK$^+$ phases are in good agreement with the results of Ref. [102].

The general structure for all three phase diagrams (Fig. 4.3(b) and Fig. 4.18) is similar, at low quark chemical potential we find a chirally broken phase, where the chiral condensate is significantly larger than in any other phase. On the high quark chemical potential side of the phase diagram a CFL-like phase is realized and the region in-between contains a 2SC phase. The main effect produced by an increasing lepton chemical potential is that the area of the 2SC phase expands and pushes the transition to the chirally broken phase to lower and the transition to a CFL-like phase to higher quark chemical potential. As already mentioned before, increasing the lepton chemical potential will lead to a CFL phase where positively charged kaons condense (CFLK$^+$) and compensate the electric charge of the electrons. At $\mu_{L_e} = 200$ MeV the CFLK$^+$ phase replaces only a part of the CFLK^0 phase, while at $\mu_{L_e} = 400$ MeV the CFLK$^+$ is the only remaining CFL-like phase.

We note that, due to the larger pressure induced by the Goldstone boson condensate, the CFLK^0 and CFLK$^+$ phases reach to a slightly lower value of the quark chemical potential, than the CFL phase in Ref. [102]. This is a small effect.

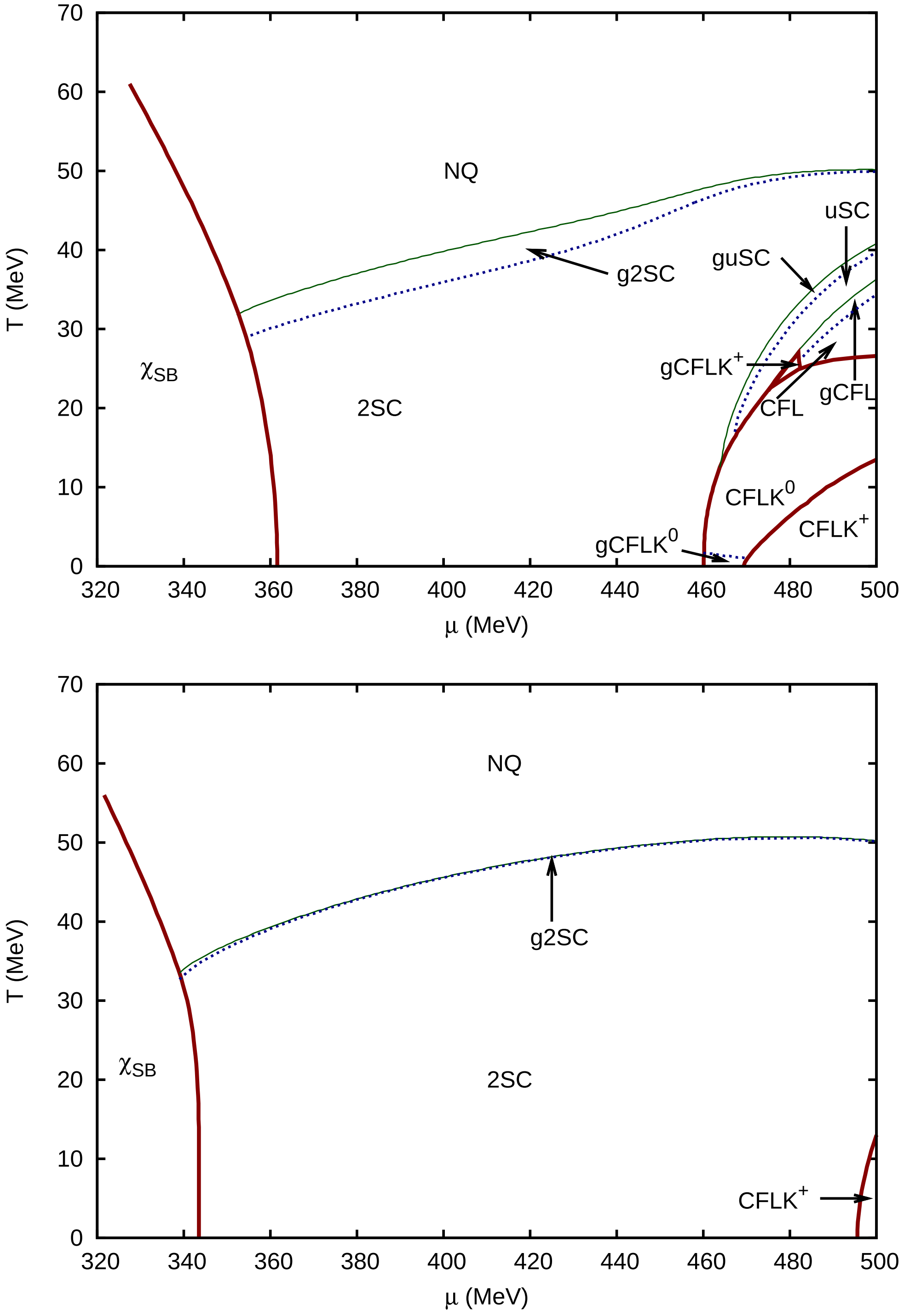

Figure 4.18.: The upper panel shows the phase diagram at $\mu_{L_e} = 200$ MeV and the lower one the situation at $\mu_{L_e} = 400$ MeV, compare with the phase diagram at $\mu_{L_e} = 0$, Fig. 4.3(b). The phase transitions are indicated as in Fig. 4.3. (parameter set I)

5. $U(1)_A$ breaking in color superconductors

In Fig. 1.2 we have shown a sketch of the standard picture of the phase diagram of strongly interacting matter. In this diagram the hadronic phase and the quark gluon plasma or the color superconducting phases are separated by a first-order phase transition at low temperatures and connected by a smooth crossover at large temperatures (and small chemical potentials). The first-order phase transition ends at a critical end point (CEP). Studies within an NJL-type model showed that this first-order phase transition becomes weaker when electric charge neutrality is imposed or vector interactions are included [104, 105, 106]. With certain choices of the parameters this will lead to the appearance of a second critical end point at low temperature near the chemical potential axis. In the following we will call this CEP the low-temperature CEP to distinguish it from the conventional CEP.

Unrelated to charge neutrality or vector interactions such a low-temperature CEP can also be induced by the axial anomaly. This has been shown first in a Ginzburg-Landau analysis [20, 21, 22] and was later confirmed in an NJL-type model [81]. The Ginzburg-Landau analysis worked with three flavors of massless quarks, while in the NJL-type model the situation for three massless quarks and three flavors of quarks with equal bare masses was investigated. With these choices of the quark masses it seems natural that the color superconductor formed is in the CFL phase. It was therefore, in both approaches, chosen two use only one common chiral and one common diquark condensate. This choice is necessary in the Ginzburg-Landau analysis to reduce the number of coefficients so that one can extract some useful informations about the pressure of the different phases. However less symmetric pairing patterns, like the 2SC phase, have not been considered in this Ginzburg-Landau approach[1]. As we have seen before in the phase diagrams for a more realistic strange quark mass (Fig. 4.3(b) and Fig. 4.5(b)), in our model the chirally broken phase and the CFL phase do not have a common phase boundary. Instead they are separated by a broad band of the 2SC phase.

---

[1] Shortly before the completion of the thesis Ref. [107] appeared. Although this study improves the treatment of quark masses and the 2SC phase in the GL approach, its results do not change the statements made here.

We will start by giving a short summary of the relevant results of the GL analysis [20, 21, 22]. Then we transfer this situation to the NJL model with equal bare quark masses and investigate how increasing the strange quark mass will effect the appearance of the low-temperature critical end point. In Sect. 5.5 we will then check the compatibility of the GL and NJL model results.

5.1. The Ginzburg-Landau ansatz

In this section we present the Ginzburg-Landau ansatz from Refs. [20, 21, 22] which leads to the prediction of the low-temperature CEP. This GL ansatz includes chiral condensates as well as diquark condensates. The $\bar{q}q$ condensates are represented by the matrix

$$\Phi_{ij} \propto \langle \bar{q}^j_{Ra} q^i_{La} \rangle \,, \tag{5.1}$$

where i, j are flavor indices and a is a color index. Here q_R (q_L) are right-handed (left-handed) quark fields. The diquarks enter through the matrices

$$\langle q^j_{Lb}\, C\, q^k_{Lc} \rangle \propto \epsilon_{abc}\epsilon_{ijk}\, d^\dagger_{L\,a\,i} \,, \tag{5.2}$$

$$\langle q^j_{Rb}\, C\, q^k_{Rc} \rangle \propto \epsilon_{abc}\epsilon_{ijk}\, d^\dagger_{R\,a\,i} \,, \tag{5.3}$$

here i, j, k (a, b, c) are flavor (color) indices. With these matrices one constructs all terms up to order four in Φ and $d_{L,R}$, which are invariant under

$$SU(3)_{\text{color}} \times SU(3)_R \times SU(3)_L \times U(1)_V \times U(1)_A \tag{5.4}$$

transformations. In addition one also includes terms that break the $U(1)_A$ symmetry.

Now the general GL ansatz (up to order four), giving the difference in free energy to the normal phase (where all condensates vanish), reads

$$\Omega\left(\Phi, d_L, d_R\right) = \Omega_\chi\left(\Phi\right) + \Omega_d\left(d_R, d_L\right) + \Omega_{\chi d}\left(\Phi, d_R, d_L\right) \tag{5.5}$$

with

$$\Omega_\chi = \frac{a_0}{2}\mathrm{Tr}[\Phi^\dagger\Phi] + \frac{b_1}{4!}\left(\mathrm{Tr}[\Phi^\dagger\Phi]\right)^2 + \frac{b_2}{4!}\mathrm{Tr}[(\Phi^\dagger\Phi)^2] - \frac{c_0}{2}\left(\det[\Phi] + \det[\Phi^\dagger]\right) \,, \tag{5.6}$$

$$\begin{aligned}\Omega_d = \;& \alpha_0 \mathrm{Tr}[d_L d_L^\dagger + d_R d_R^\dagger] \\ & + \beta_1\left((\mathrm{Tr}[d_L d_L^\dagger])^2 + (\mathrm{Tr}[d_R d_R^\dagger])^2\right) + \beta_2 \mathrm{Tr}[(d_L d_L^\dagger)^2 + (d_R d_R^\dagger)^2] \\ & + \beta_3 \mathrm{Tr}[(d_R d_L^\dagger)(d_L d_R^\dagger)] + \beta_4 \mathrm{Tr}[d_L d_L^\dagger]\,\mathrm{Tr}[d_R d_R^\dagger] \,,\end{aligned} \tag{5.7}$$

and

$$\begin{aligned}\Omega_{\chi d} = \;& \gamma_1 \mathrm{Tr}[(d_R d_L^\dagger)\Phi + (d_L d_R^\dagger)\Phi^\dagger] + \lambda_1 \mathrm{Tr}[(d_L d_L^\dagger)\Phi\Phi^\dagger + (d_R d_R^\dagger)\Phi^\dagger\Phi] \\ & + \lambda_2 \mathrm{Tr}[d_L d_L^\dagger + d_R d_R^\dagger]\cdot\mathrm{Tr}[\Phi^\dagger\Phi] + \lambda_3\left(\det[\Phi]\cdot\mathrm{Tr}[(d_L d_R^\dagger)\Phi^{-1}] + h.c.\right) \,.\end{aligned} \tag{5.8}$$

In this ansatz the terms $c_0/2\left(\det[\Phi]+\det[\Phi^\dagger]\right)$ and $\gamma_1\mathrm{Tr}[(d_R d_L^\dagger)\Phi+(d_L d_R^\dagger)\Phi]$ break the $U(1)_A$ symmetry to Z_6. All other terms in Eq. (5.5) are invariant under Eq. (5.4).

This general ansatz contains thirteen coefficients that can not be determined within the GL analysis. Further on these coefficients can depend on temperature and chemical potential. It is therefore necessary to make some simplifing assumptions to reduce the number of coefficients. To study three massless quark flavors the authors of Ref. [21] chose to use the flavor independent condensates $\Phi=\mathrm{diag}\,(\sigma,\sigma,\sigma)$ and $d_L=-d_R=\mathrm{diag}\,(d,d,d)$. In the notation we use in the NJL model this ansatz corresponds to the situation $\phi_u=\phi_d=\phi_s$ and $s_{22}=s_{55}=s_{77}$. To work with flavor independent condensates is a plausible assumption when using massless quarks, however it allows only for CFL-type pairing and excludes 2SC-like phases. This ansatz requires only seven coefficients since the free energy simplifies to[2]

$$\Omega_{3F}\left(\sigma,d\right)=\left(\frac{a}{2}\sigma^2-\frac{c}{3}\sigma^3+\frac{b}{4}\sigma^4\right)+\left(\frac{\alpha}{2}d^2+\frac{\beta}{4}d^4\right)-\gamma d^2\sigma+\lambda d^2\sigma^2 \tag{5.9}$$

where the coefficients of Eq. (5.9) are related to the coefficients of Eq. (5.6) in the following way

$$\begin{aligned}
&a=3a_0\,, && c=3c_0\,, && b=\frac{1}{2}\left(3b_1+b_2\right)\,,\\
&\alpha=12\alpha_0\,, && \beta=12\left(6\beta_1+2\beta_2+\beta_3+3\beta_4\right)\,, &&\\
&\gamma=6\gamma_1\,, && \lambda=6\left(\lambda_1+3\lambda_2-\lambda_3\right)\,. &&
\end{aligned} \tag{5.10}$$

Making some physically motivated assumptions on the signs of some coefficients the authors of Refs. [20, 21, 22] construct a phase diagram in the a-α plane, which consists of four phases. In two of these phases the diquark condensate takes a non-zero value, in the two others it vanishes. One of phases with zero diquark condensate has a large chiral condensate, the other one has no chiral condensate. In the notation of this work we would label them as χSB and NQ. The two other phases are coexistence phases, where both kinds of condensates are present. In one of them the chiral condensate is large and the diquark condensate is small. In the other coexistence phase it is the other way round, with a small diquark condensate and a large chiral condensate. It was shown, that for $\gamma>0$ the first order phase transition separating the two coexistence phases ends at a critical end point. Transferring this situation to the phase diagram in μ-T plane, where the diquark condensates exist at low temperature, this end point can correspond to the above mentioned low-temperature end point. For $\gamma=0$ no such end point was found.

To cover the two-flavor case the ansatz $\Phi=\mathrm{diag}\,(\sigma,\sigma,0)\,,\ d_L=-d_R=\mathrm{diag}\,(0,0,d)$ was chosen. This ansatz gives the free energy

$$\Omega_{2F}\left(\sigma,d\right)=\left(\frac{a'}{2}\sigma^2+\frac{b'}{4}\sigma^4\right)+\left(\frac{\alpha'}{2}d^2+\frac{\beta'}{4}d^4\right)+\lambda' d^2\sigma^2\,. \tag{5.11}$$

---

[2] It can be necessary to include a term of order six to stabilize the system.

For this ansatz no second end point was found. Here we like to point out, that this ansatz differs from the situation in the three-flavor NJL model. In Eq. (5.11) all condensates related to strange quarks are completely neglected. In our NJL model the strange quark-antiquark condensate has a large (negative) value in the 2SC phase. We will come back to this point later in Sect. 5.5, where we discuss the connection of the GL and NJL model results.

5.2. The $U(1)_A$ breaking in the diquark sector

From the Ginzburg-Landau analysis we learn that it is crucial for the intended effect to include a term that connects diquark and quark-antiquark condensates. The term related to the appearance of the low-temperature CEP also breaks the $U(1)_A$ symmetry, it is therefore clear that a low-temperature CEP in the NJL model will be related to a six-point interaction. Usually one uses the 't Hooft-term[3]

$$\mathcal{L}_{\chi}^{(6)} = -K \ \left\{ \det{}_f \left[\bar{q} \left(1+\gamma_5\right) q \right] + \det{}_f \left[\bar{q} \left(1-\gamma_5\right) q \right] \right\} \tag{5.12}$$

as a $U(1)_A$ breaking six-point interaction. It connects three incoming right-handed (left-handed) fields with three left-handed (right-handed) outgoing fields. This term has the appropriate external legs to connect the diquark condensates to the quark-antiquark condensates, however its internal structure is of such kind that within the mean-field approximation it does not couple to the diquark condensates.

We therefore include the additional term[4]

$$\mathcal{L}_{\chi d}^{(6)} = \frac{K'}{8} \sum_{\pm} \sum_{A,A',B=2,5,7} \left[\bar{q}\tau_A\lambda_B(1\pm\gamma_5)C\bar{q}^T\right] \left[q^T C(1\pm\gamma_5)\tau_{A'}\lambda_B q\right] \left[\bar{q}_{\bar{A}}(1\pm\gamma_5)q_{\bar{A}'}\right]$$
$$\times \begin{cases} -1\,, & \text{if } A=5 \text{ (exclusive) or } A'=5 \\ \ \ 1\,, & \text{all other cases, including } A=A'=5 \end{cases} \tag{5.13}$$

with reordered quark fields. Here we use $\bar{A}$ to denote the flavor not connected by the Gell-Mann matrix τ_A, i.e. $\bar{2}=s$, $\bar{5}=d$ and $\bar{7}=u$. This term has the same symmetries as Eq. (5.12) but in Eq. (5.13) the quark fields are ordered in a way that will create the intended connection of the diquark and quark-antiquark condensates also in Hartee approximation. Both terms, Eq. (5.12) and Eq. (5.13) are related to the instanton vertex via a Fierz transformation. This will also relate the coupling constants K and K'. Because of this relation we will call the new six-point interaction (Eq. (5.13)) the "transformed" six-point interaction, even though we will treat it completely independent of Eq. (5.12). Therefore we will handle K' as a free parameter. In the rest of this chapter we will now investigate the effect of the transformed six-point interaction on the color superconductor and the chiral phase transition.

---

[3] In Sect. 3.1.2 we introduced this term as Eq. (3.4)

[4] In Appendix C we show this term with the sum over A and A' evaluated, giving a better overview of the flavor structure of Eq. (5.13).

5.2.1. Effects of the transformed six-point interaction

The transformed six-point interaction does not change the general structure of the mean-field Lagrangian (Eq. (3.9)) or the inverse propagator (Eq. (3.11)). However it modifies the mass term and the gap parameter entering in the inverse propagator and gives a contribution to the field-independent term $\mathcal{V}$ (Eq. (3.14)) in the mean-field Lagrangian.

By connecting two incoming and two outgoing legs of the six-point interaction to diquark condensates a contribution to the mass term emerges, the full term now reads

$$M_a = m_a - 4G\phi_a + K\phi_b\phi_c + \frac{K'}{4}|s_{\bar{a}\bar{a}}|^2\,, \tag{5.14}$$

cf. Eq. (3.12). Here (a, b, c) is any permutation of (u, d, s) and $\bar{a}$ is the index for a diquark condensate not containing quarks of the flavor a, i.e. $\bar{u} = 7$, $\bar{d} = 5$, $\bar{s} = 2$, this is kind of the inverse of the above defined $\bar{A}$.

In Fig. 5.1(a) we show, as an example, the contribution to the up quark mass generated by the coupling to the s_{77} condensate.

There is also a contribution to the off-diagonal elements of the inverse propagator in Nambu-Gorkov space, the gap parameter now reads

$$\Delta^{(s)}_{AA} = -2\left(H - \frac{K'}{4}\phi_{\bar{A}}\right) s_{AA}\,, \tag{5.15}$$

cf. Eq. (3.13). This term effectively acts like an amplified quark-quark coupling (H') where the increase depends on the quark-antiquark condensate of the flavor not involved in the relevant quark-quark interaction (cf. Fig. 5.1(b)).

The mean-field approximation also produces terms that do not depend on the field, these terms are collected in $\mathcal{V}$, cf. Eq. (3.14),

$$\mathcal{V} = 2G\left(\phi_u^2 + \phi_d^2 + \phi_s^2\right) - 4K\phi_u\phi_d\phi_s + \sum_{A=2,5,7}\left(H - \frac{K'}{2}\phi_{\bar{A}}\right)|s_{AA}|^2\,. \tag{5.16}$$

Such a contribution of the transformed six-point interaction is diagrammatically represented in Fig. 5.1(c).

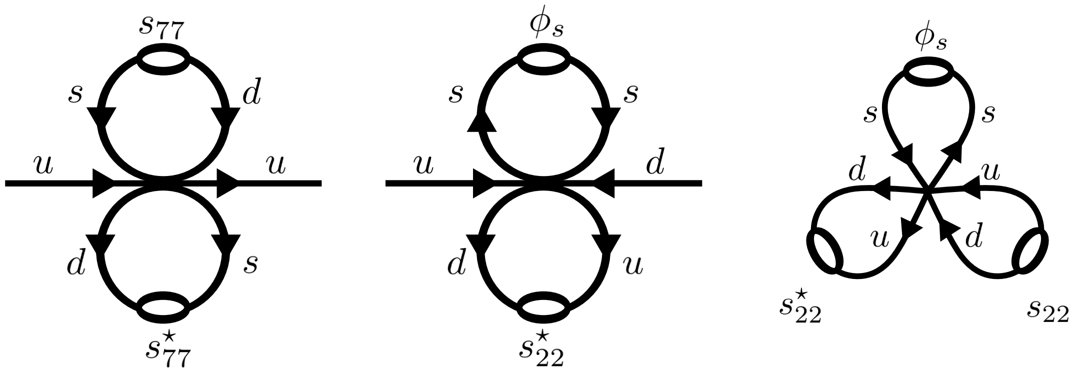

(a) mass (b) off-diagonal (c) field independent

Figure 5.1.: Diagrammatic representation of the effects of the transformed six-point interaction (a): effect on the dynamical quark mass, as an example the contribution to the up quark mass is shown (b): example for the effect on the off-diagonal components of the inverse propagator in the Nambu-Gorkov space (c): example for a field independent term

5.2.2. Parameters

With the new interaction we also introduced a new coupling constant K'. We will treat K' as a free parameter and vary it, in this chapter, between zero and $5\,K$. Further on we want to compare our results with Ref. [81] and therefore adopt the parameters used there. These parameter are the same as set II but with a stronger diquark coupling[5] $H = 1.74/\Lambda^2$. We label these parameters as set IV. Analogous to the connection between the parameter sets II and I, we also introduce a parameter set with a “realistic” strange quark mass $m_s = 140.7$ MeV in this context, we call it set V. The sets IV and V are connected by varying m_s and adjusting G so that $M_{u/d}$ stays constant. An overview of all parameter sets used in this work is given in Table B.1 in appendix B.

5.3. The low-temperature critical end point

As in the Ginzburg-Landau analysis [20, 21, 22], we neglect any neutrality constraints. Further on we start with equal bare quark masses. To calculate the phase diagram we use the same techniques as before. Later we increase the bare strange quark mass, trying to connect the equal-quark mass results with results for a more

---

[5] This value is $3/4\,G$ if K is set to zero and G is adjusted to keep $M_{u/d}$ constant. This is taken from Ref. [16]

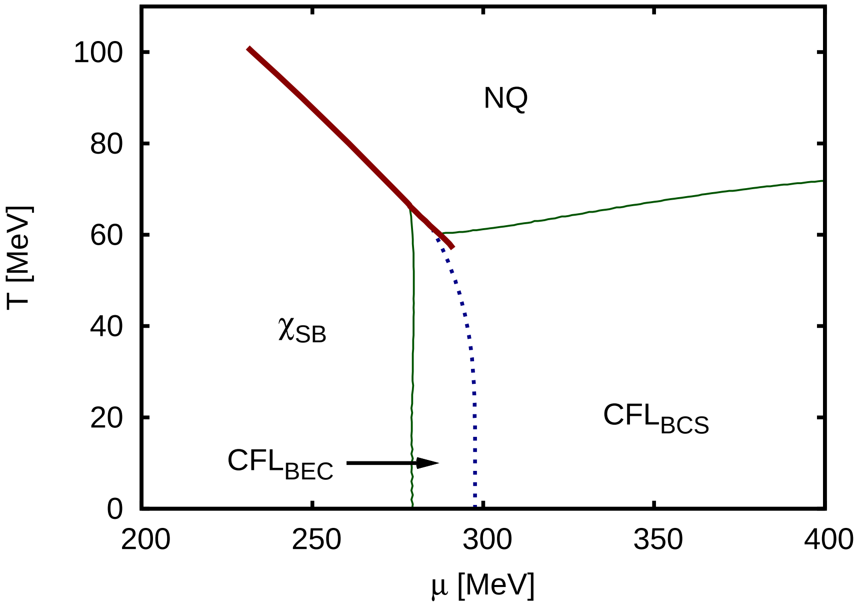

Figure 5.2.: The phase diagram in the $\mu - T$ plane for $K' = 4.2\,K$, with equal bare quark masses, one common diquark condensate $\phi_u = \phi_d = \phi_s$ and one common diquark condensate $s_{22} = s_{55} = s_{77}$. Thick (red) solid lines indicate first-order phase transition, second-order phase transitions are indicated by thin (green) lines. The dotted (blue) line indicates the BEC-BCS crossover line defined by $M\,(T,\,\mu) = \mu$. (parameter set IV)

realistic set of parameters.

5.3.1. Equal quark masses

In Ref. [81] it was found that for equal bare quark masses $m_u = m_d = m_s = 5.5$ MeV and a coupling $K' > 3.8\,K$ ($H = 1.74/\Lambda^2$, parameter set IV) the chiral phase transition ends at a low-temperature chiral end point near the chemical potential axis inside the color superconducting phase. The analysis of Ref. [81] was done assuming one common chiral condensate $\phi_u = \phi_d = \phi_s$ and one common diquark condensate $s_{22} = s_{55} = s_{77}$. With these restrictions and $K' = 4.2\,K$ we calculate the phase diagram, Fig. 5.2. This phase diagram agrees exactly with the phase diagram shown in Ref. [81]. In contrast to all phase diagrams shown before in this work, we find a phase containing a Bose-Einstein condensates (BEC) of diquarks in Fig. 5.2. Such a BEC phase can appear when the quark-quark coupling is sufficiently strong, so that strongly bound diquarks with a mass $M_D < 2{\cdot}M_{\text{quark}}$ appear. Containing two quarks these diquarks will condense when $\mu > M_D/2$ [108, 109]. The masses of these diquarks can be calculated analogously to the RPA-mesons masses (cf. Sect. 5.4). In NJL-type models such a BEC-like phase is not uncommon, when a strong quark-quark coupling (H) is used [110, 111]. By including the six-point coupling K' we increase the effective four-point quark-quark coupling so that the BEC condensates do not come as a surprise. Here we use the same notation for the different phases as before but the phases containing diquark condensates we characterize as BEC-like or BCS-like. Only increasing the four-point coupling as in Refs. [110, 111] does not give rise to a low-temperature end point. A large diquark coupling and the related appearance of a BEC condensate may weaken the chiral phase transition from the top end [110]. From this we conclude, that the low-temperature end point is an effect of the $U(1)_A$-breaking six-point interaction and not of the increased quark-quark coupling.

In Fig. 5.2 the BEC-like and BCS-like CFL phase are connected by a smooth crossover. We define the crossover line by $M(T\,,\mu) = \mu$ with M being the dynamical quark mass and μ the quark chemical potential. Note that with this definition the crossover line does not hit the low-temperature CEP exactly.

In the next step we drop the restriction to one common chiral and one common diquark condensate and allow the condensates ϕ_f, $f \in \{u, d, s\}$, and s_{AA}, $A \in \{2, 5, 7\}$ to vary independently. In the first step we keep the bare quark masses equal and obtain the phase diagram presented in Fig. 5.3. Comparing the phase diagrams in Fig. 5.2 and Fig. 5.3 a large part of the CFL phase is replaced by a 2SC phase in Fig. 5.3. With the appearance of the 2SC phase the low-temperature CEP from Fig. 5.2 has disappeared, the chiral phase transition reaches down to zero temperature and separates the BEC-like and the BCS-like 2SC phase.

The areas of non-superconducting quark phases 'NQ' and 'χSB' remain almost unchanged. This is due to the fact that the phase boundaries between the superconducting and normal-conducting phases in the phase diagrams (Fig. 5.2 and Fig. 5.3) are mostly of second order. At a second-order phase transition where all diquark condensates vanish the effect of the transformed six-point interaction also vanishes and due to the equal bare quark masses CFL and 2SC pairing is possible at the same point. For the 2SC we choose quark pairs containing up and down quarks ($s_{22} \neq 0$) leaving blue and strange quarks unpaired ($s_{55} = s_{77} = 0$). This choice breaks the $SU(3)$-flavor symmetry spontaneously. It is useful to use this standard 2SC pairing pattern, since it remains unchanged when the flavor symmetry is explicitly broken by a bare strange quark mass. The 2SC and CFL phases are necessarily separated by a first-order phase transition, since s_{55} and s_{77} vanish in the 2SC phase, but all diquark condensates take the same value in the CFL phase ($s_{22} = s_{55} = s_{77}$), due to the equal bare quark masses. Thus there can not be a second-order phase transition from the CFL to the 2SC phase, where s_{55} and s_{77} go to zero but s_{22} keeps a finite value. The only second-order phase transitions are the transition to the normal-conducting phases in Fig. 5.3. As a consequence the first-order phase tran-

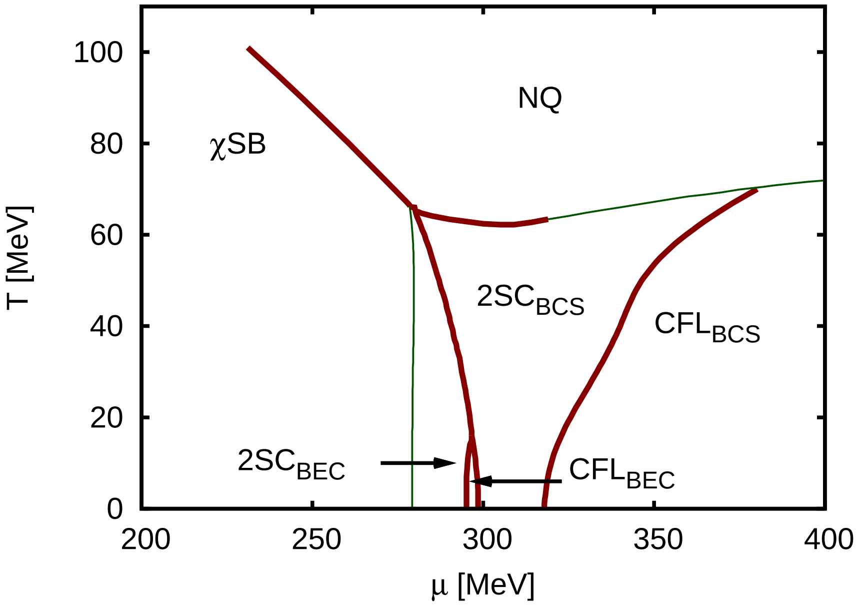

Figure 5.3.: The same situation as in Fig. 5.2 but with independent chiral condensates ϕ_u, ϕ_d, ϕ_s and diquark condensates s_{22}, s_{55}, s_{77}. (parameter set IV)

sition separating the 2SC and CFL phase ends exactly on the second-order phase transition separating the superconducting and normal-conducting phases. At low temperature ($T < 16$ MeV) there is a small window of a CFL_{BEC} phase between the the 2SC_{BEC} and the 2SC_{BCS} phase. The origin of this CFL_{BEC} window will become clear below.

In Fig. 5.4 we vary the six-point coupling K' at zero temperature and show the phase diagram in the $\mu - K'$ plane. From this diagram it is clear, that for every value of K' in the range $0\,K$ to $5\,K$ there is a first-order phase transition separating the chirally broken phase from the CFL_{BCS} phase. Thus we never find a smooth crossover at $T = 0$ and a low-temperature CEP like in the case of one common chiral and one common diquark condensate. For values of $K'/K < 3$ there is not much change in the phase structure. Then the condensation of diquarks starts on the chirally broken side of the phase transition, the 2SC_{BEC} phase appears. Soon afterwards also the CFL_{BEC} phase emerges. The first-order phase transition separating the CFL_{BEC} and CFL_{BCS} phases ends at $K' \approx 3.8\,K$, this is the point where the low-temperature CEP appears in Ref. [81]. When we cut Fig. 5.4 at $K'/K = 4.2$ it is also clear how the CFL_{BEC} window between the 2SC_{BEC} and the 2SC_{BCS} emerges. We also observe, that this window will quickly disappear when K' is varied.

To get a more complete picture of the changes in the phase diagram, when K'

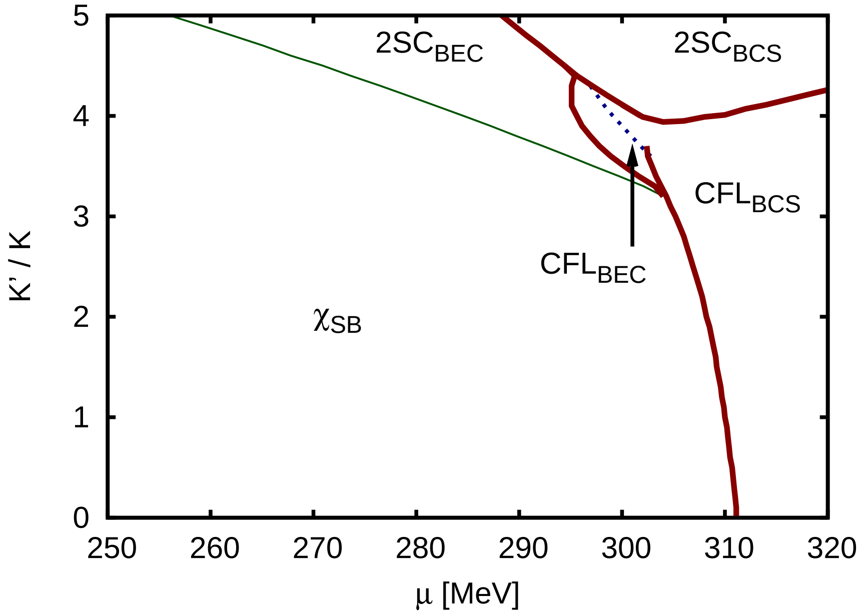

Figure 5.4.: The phase diagram in the μ-K' plane at $T = 0$ for equal bare quark masses. Thick (thin) lines indicate first (second) order phase transitions, the dotted line marks $M(\mu) = \mu$. (parameter set IV)

is varied we show the phase digram in the $\mu - T$ plane for several values of K' in Fig. 5.5. Until K' reaches approximately $3\,K$ the phase diagram does not change much, only a $2\mathrm{SC}_{\mathrm{BCS}}$ phase appears at high temperature (Fig. 5.5(b)). When K' is increased, the area of this $2\mathrm{SC}_{\mathrm{BCS}}$ phase grows quickly, $2\mathrm{SC}_{\mathrm{BEC}}$ and $\mathrm{CFL}_{\mathrm{BEC}}$ phases appear (Fig. 5.5(c)). Then the transition between the $\mathrm{CFL}_{\mathrm{BEC}}$ and the $\mathrm{CFL}_{\mathrm{BCS}}$ becomes a crossover and for a very narrow K' interval we see the low-temperature CEP from Ref. [81] (Fig. 5.5(d)) before the whole region gets covered by the $2\mathrm{SC}_{\mathrm{BCS}}$ phase (Fig. 5.5(e)). With further increased K' the 2SC regions grow, the $\mathrm{CFL}_{\mathrm{BEC}}$ phase disappears and the transition to the $\mathrm{CFL}_{\mathrm{BCS}}$ gets pushed to higher values of the quark chemical potential (Fig. 5.5(f)). In Fig. 5.5(g) and Fig. 5.5(h) we see that the part of chiral phase transition which lies in the region where it is completely surrounded by phases with diquark condensates, turns into a crossover. This starts at high temperatures (Fig. 5.5(g)) and at K' slightly larger than $5\,K$ (Fig. 5.5(h)) the first-order phase transition is completely gone. This effect is similar to the case where the $2\mathrm{SC}_{\mathrm{BEC}}$ phase is a result of a strong quark-quark coupling [110, 111].

At first sight it is a surprise to find the 2SC in the case of equal bare quark masses. Since the interplay of the chiral and diquark condensates is essential here it is not possible to make any further simplifying assumption within the NJL-model approach. We therefore try to find a rough explanation of the mechanisms fa-

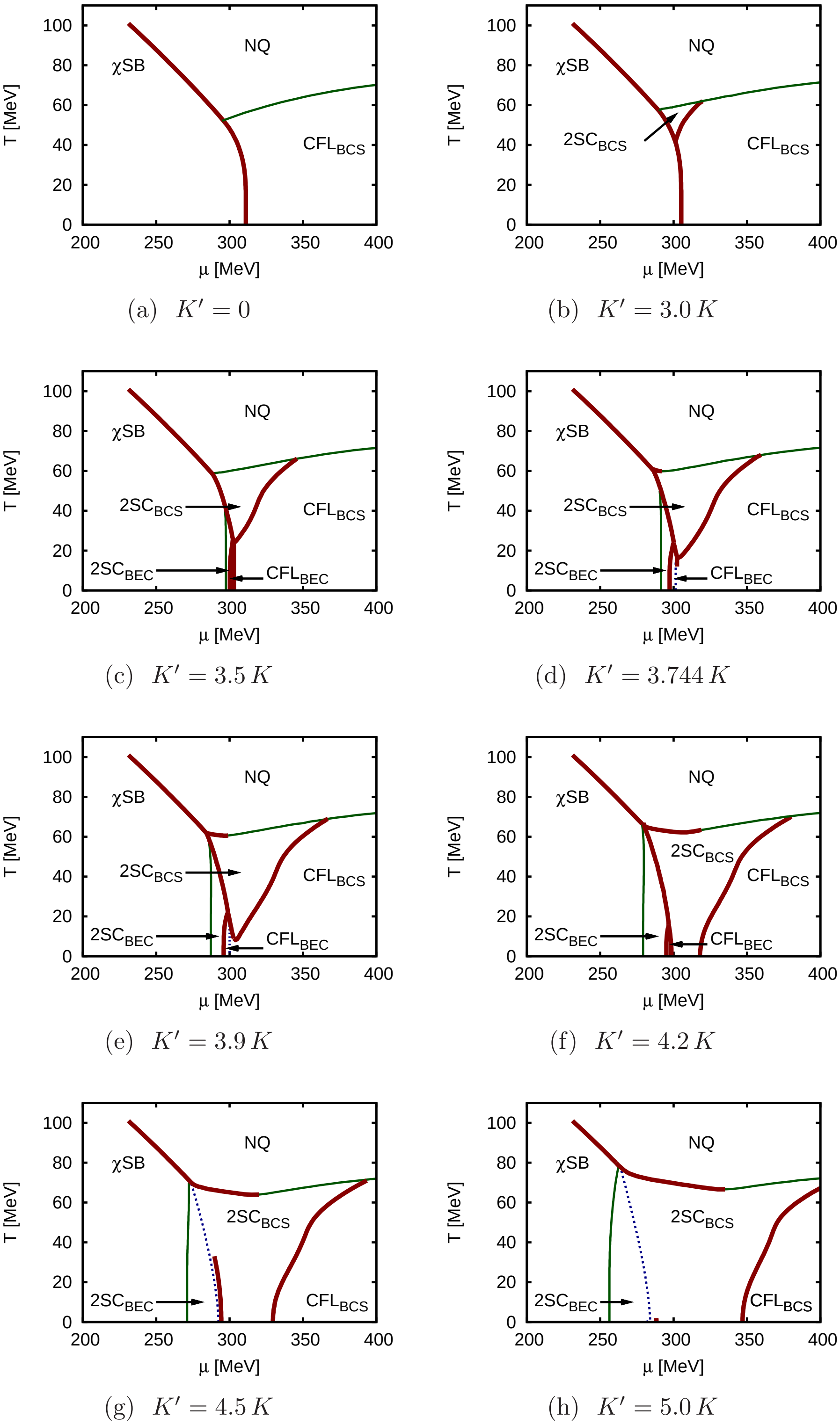

(a) $K' = 0$

(b) $K' = 3.0\,K$

(c) $K' = 3.5\,K$

(d) $K' = 3.744\,K$

(e) $K' = 3.9\,K$

(f) $K' = 4.2\,K$

(g) $K' = 4.5\,K$

(h) $K' = 5.0\,K$

Figure 5.5.: The $\mu - T$ phase diagram for different values of K'/K and equal bare quark masses. (parameter set IV)

voring the 2SC phase over the CFL phase by looking into the numerical results. With s_{22} being the only non-zero diquark condensate in the 2SC phase, it is clear from Eq. (5.14) that only the dynamical strange quark mass M_s but not M_u or M_d receive a contribution related to the six-point coupling K'. On the other hand the growing M_s has an effect on the gap parameter $\Delta_{22}^{(s)}$, cf. Eq. (5.15), trough the chiral condensate ϕ_s. This amplifying effect works better in the 2SC phase than in the CFL phase, since the 2SC pairing pattern allows for a large chiral condensate of one flavor while the two other flavors can form Cooper-pairs. In the more symmetric CFL phase this separation is not possible. In Fig. 5.6 we show the dependence of the dynamical quark masses and the gap parameters on the six-point coupling K' for the 2SC and CFL solutions at $T = 0$ and $\mu = 310$ MeV. One can clearly see that the gap parameter $\Delta_{22}^{(s)}$ and the mass M_s of the 2SC solution rise much faster than any other quantity. Comparing the ratio of $\Delta_{22}^{(s)}$ in the 2SC solution with the common gap parameter Δ in the CFL solution we see that this ratio rises from about 1.25 at $K' = 0$ to 2.0 at $K' = 4\,K$. If one neglects dynamical quark masses and the six-point interaction $\mathcal{L}_{\chi d}^{(6)}$ it can be shown that if $\Delta_{22}^{(s)}|_{\text{2SC}}$ is larger than about $\sqrt{3}\Delta|_{\text{CFL}}$ the 2SC phase becomes favored. From this perspective $\Delta_{22}^{(s)}|_{\text{2SC}}/\Delta|_{\text{CFL}} = 2$ is quite large and it seems plausible that this mechanism leads to the appearance of the 2SC phase. Nevertheless we have to keep in mind that the dynamical quark masses are essential in this situation and the considerations above can only be a rough estimate.

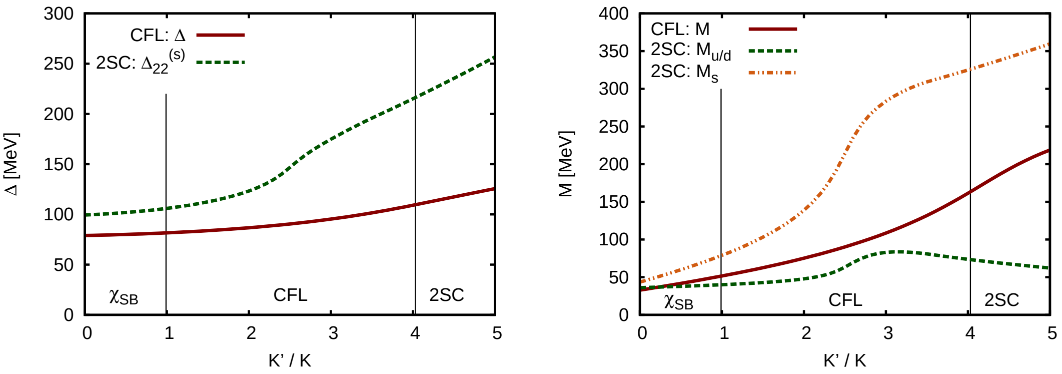

Figure 5.6.: The gap parameters $\Delta_{AA}^{(s)}$ (left panel) and the constituent quark masses M_f (right panel) in the 2SC and CFL solutions for equal bare quark masses at $T = 0$ and $\mu = 310$ MeV. The vertical line indicate the phase transitions in the phase diagram Fig. 5.3. (parameter set IV)

5.3.2. Realistic strange quark mass

Assuming that all quarks have the same mass, as we have done in the section above, is quite unrealistic, therefore we will now introduce a bare strange quark mass which is larger than the bare masses of the up and down quarks. We will now turn up the bare strange quark mass from $m_s = m_{u/d} = 5.5$ MeV to the "realistic" case $m_s = 140.7$ MeV, i.e. interpolating between the parameter sets IV and V (see Sect. 5.2.2). In Fig. 5.7 (left panel) we show the mutation of the phase diagram at $T = 0$ when the strange quark mass is turned up. For comparison with Fig. 5.2 we choose $K' = 4.2\,K$. With increasing m_s the onset of the $\mathrm{CFL}_{\mathrm{BCS}}$ phase, gets

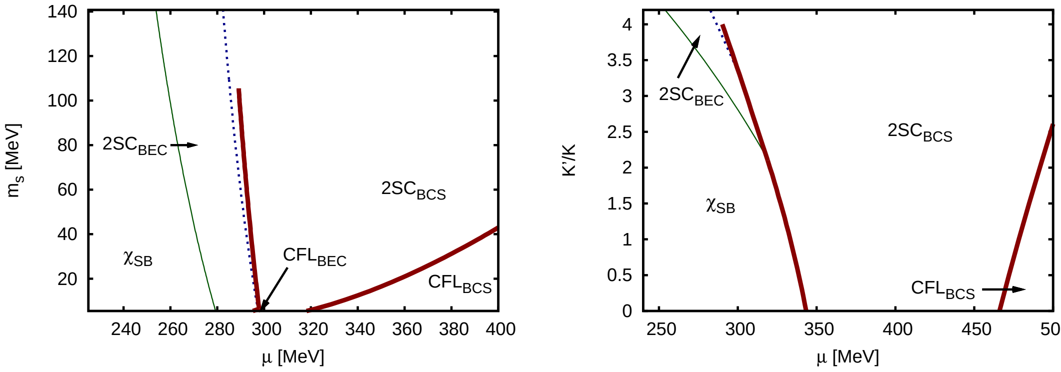

(a) $\mu - m_s$ (b) $\mu - K'/K$

Figure 5.7.: (a): the phase diagram in the $m_s - \mu$ plane at $T = 0$ and $K'/K = 4.2$. (Interpolation between parameter sets IV and V.) (b): the phase diagram in the $\mu - K'$ plane for $m_s = 140.7$ MeV and $T = 0$. (parameter set V)

pushed to higher quark chemical potentials. The area of the $2\mathrm{SC}_{\mathrm{BCS}}$ phase broadens with rising m_s. The mechanism behind this effect works like in the equal masses case described above with the difference that the strange quark mass now explicitly breaks the $SU(3)_{\mathrm{flavor}}$ symmetry, enhancing the binding between up and down quarks through a larger strange chiral condensates ϕ_s, cf. Eq. (5.15). The stronger effective quark-quark coupling leads to deeper bound quark pairs and shifts the onset of the BEC-like phase to lower quark chemical potential (cf. Sect 5.4). At $m_s \approx 105$ MeV the first-order phase transition between the 2SC phase with a large and the 2SC phase with a smaller chiral condensate turns into a crossover.

The right panel of Fig. 5.7 shows the phase diagram in the $\mu - K'$ plane for $m_s = 140.7$ MeV. As expected turning up K' activates the mechanisms enhancing the 2SC phases, moving the onset of the $2\mathrm{SC}_{\mathrm{BEC}}/2\mathrm{SC}_{\mathrm{BCS}}$ phase to lower and pushing the onset of the CFL phase to higher quark chemical potentials. As K' reaches

$4.0\,K$ the first-order phase transition between the two 2SC phases ends. The values at $K' = 4.2\,K$ in Fig. 5.7(a) agree with them at $m_s = 140.7$ MeV in Fig. 5.7(b).

To demonstrate the effect of the diquark and chiral condensate mixing six-point interaction, $\mathcal{L}^{(6)}_{\chi d}$, on the phase diagram with a realistic strange quark mass, we show a series of phase diagram for different values of K'/K in Fig. 5.8. Our starting point, the phase diagram with $K' = 0$ (Fig. 5.8(a)) agrees with the results in Ref. [16]. Increasing K' enlarges the 2SC area (Fig. 5.8(b), Fig. 5.8(c)) and at $K' = 2.5K$ the Bose-Einstein condensation starts (Fig. 5.8(d)). While the $2\mathrm{SC}_{\mathrm{BEC}}$ phase grows, the chiral phase transition gets weaker at large temperatures (Fig. 5.8(e), Fig. 5.8(f)) with the result that the CEP gets surrounded by a 2SC phase (Fig. 5.8(g)) and finally disappears completely (Fig. 5.8(h)). From these phase diagrams we see that when K' is varied the phase structure undergoes large changes. However the most severe changes happen at large values of K'/K, which might be unrealistic. At smaller values of K'/K the general phase structure is retained with an enhanced 2SC phase.

5.4. Bose-Einstein condensate of diquarks

In the sections above we saw the appearance of a Bose-Einstein condensate of bound quark pairs. A sufficiently strong attractive interaction between the quarks may form these bound state. In our Lagrangian (Eq. (3.1)) such an interaction is given by the term $\mathcal{L}^{(4)}_{d}$ (Eq. (3.3)), including $\mathcal{L}^{(6)}_{\chi d}$ (Eq. (5.13)) this gets enhanced by an effective four-point interaction. For the coupling in the ud-channel this gives the effective quark-quark coupling

$$H'_{ud} = H - \frac{K'}{4}\phi_s \tag{5.17}$$

and analog expressions in the other quark-quark channels. Below we calculate the mass of the diquark molecules in the chirally broken phase and study the effect of the bare strange quark mass m_s and the six-point coupling K' to understand the onset of the $2\mathrm{SC}_{\mathrm{BEC}}$ phase in the phase diagrams above. The calculation of the mass of such a bound quark-quark state is completely analogous to the calculation of an RPA-meson mass. We therefore use the same numerical framework used in Sect. 4.1 with the vertices

$$\Gamma^{s\uparrow}_{AA'} \equiv \begin{pmatrix} 0 & i\gamma_5\,\tau_A\,\lambda_{A'} \\ 0 & 0 \end{pmatrix}, \qquad \Gamma^{s\downarrow}_{AA'} \equiv \begin{pmatrix} 0 & 0 \\ i\gamma_5\,\tau_A\,\lambda_{A'} & 0 \end{pmatrix} \tag{5.18}$$

although an analytical treatment is possible to the same level as it is possible for the vacuum mesons in the NJL model.

As usual we start with equal bare quark masses. In Fig. 5.9(a) we show the dependence of the bound diquark mass $M_{D_{AA'}}$ in vacuum as a function of the six-point coupling strength K'. The index AA' labels the flavor (A) and color (A')

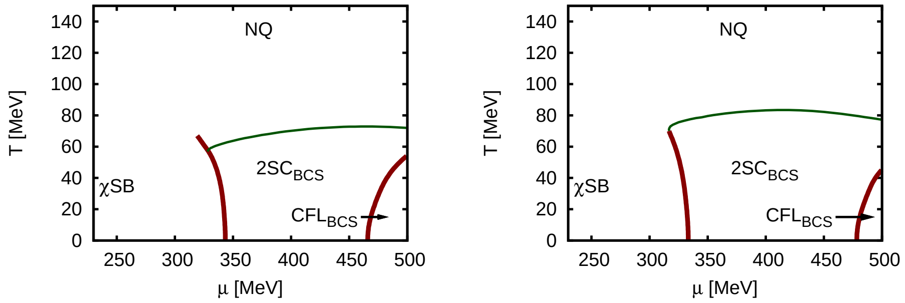

(a) $K' = 0$ (b) $K' = 1.0\,K$

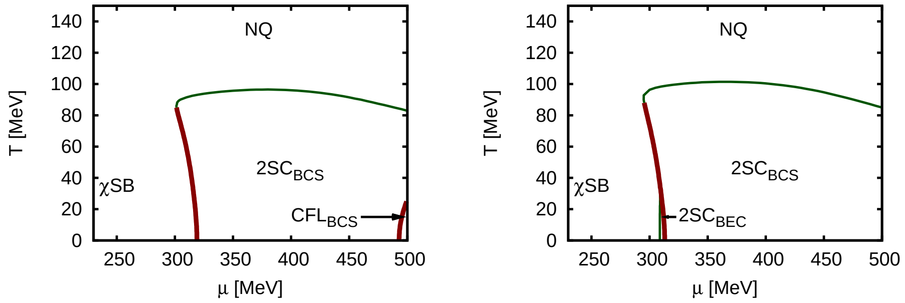

(c) $K' = 2.1\,K$ (d) $K' = 2.5\,K$

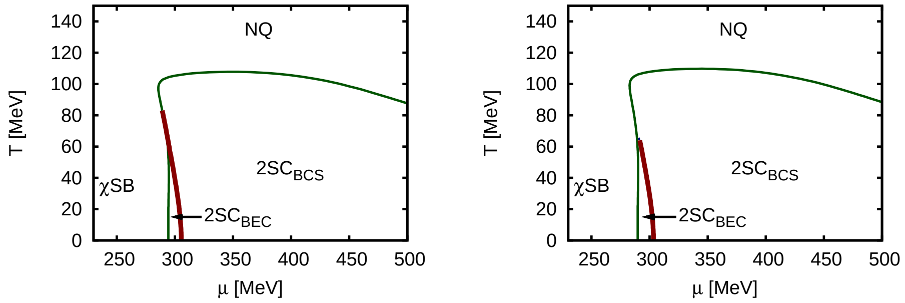

(e) $K' = 3.0\,K$ (f) $K' = 3.15\,K$

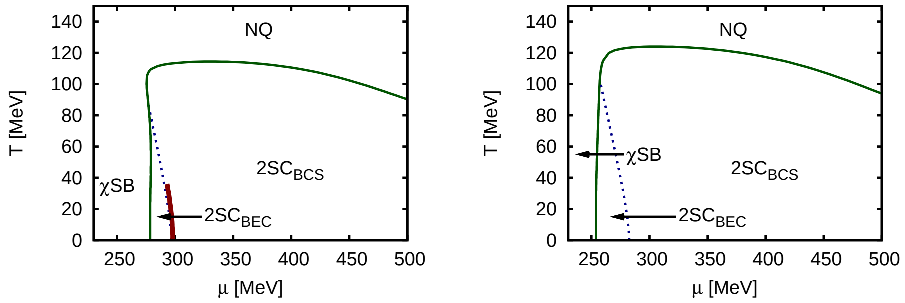

(g) $K' = 3.5\,K$ (h) $K' = 4.2\,K$

Figure 5.8.: The $\mu - T$ phase diagram for different values of K'/K and a realistic strange quark mass $m_s = 140.7$ MeV. (parameter set V)

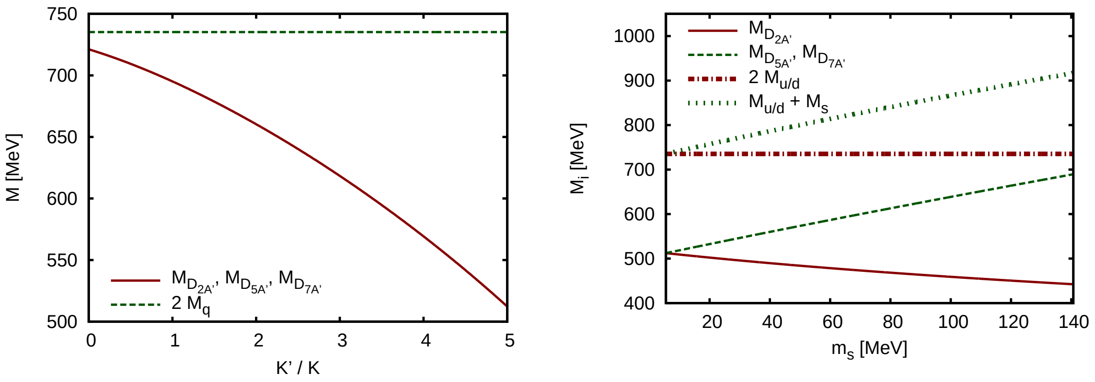

(a) (b)

Figure 5.9.: (a): the mass of the bound diquark pairs in vacuum for equal quark masses as a function of the coupling strength K'. (parameter set IV) (b): the masses of the bound diquark pairs in vacuum as functions of the strange quark mass at $K' = 5\,K$. In both panels the threshold for the decay into two quarks is also indicated. (Interpolation between parameter sets IV and V.)

structure of the quark pair. Since all quarks have the same mass also all diquark pairs have equal masses, with increasing K' the diquarks get deeper bound. In Fig. 5.9(b) we introduce a bare strange quark mass larger than the masses of the up and down quarks and work at $K' = 5\,K$. Keeping in mind that we adjusted G to keep the dynamical up and down quark masses constant, we observe that the masses of the diquark pairs containing a strange quark grow with similar speed as the strange quark mass grows. On the other hand the pair containing up and down quarks becomes deeper bound, this is due to the larger (negative) chiral condensates ϕ_s that comes along with the growing strange quark mass (cf. Eq. (5.17)). The deeper bound diquarks will condense earlier when the quark chemical potential is increased, therefore the phase transition between the χSB and the 2SC$_{\text{BEC}}$ phase in Fig. 5.7(a) moves leftwards with rising m_s.

Finally, we have a look on the condensation of these diquark pairs. As an example we choose the equal quark mass case at $K' = 5\,K$ and $T = 0$ (the corresponding phase diagram is shown in Fig. 5.5(h)). Note that we only calculate the masses of the diquark pairs up to the point where they condense. Containing two quarks the bound diquark pair is sensitive to twice the quark chemical potential. In Fig. 5.10 we see how the difference $M_{D_{AA'}} - 2\mu$ decreases linearly as the quark chemical potential rises and reaches zero at $\mu = 256.1$ MeV, exactly where the gap equation starts to give a non-vanishing value for the gap parameter $\Delta_{22}^{(s)}$. Here a BEC of red and green up and down quarks is formed. As the value of $\Delta_{22}^{(s)}$ rises with increasing

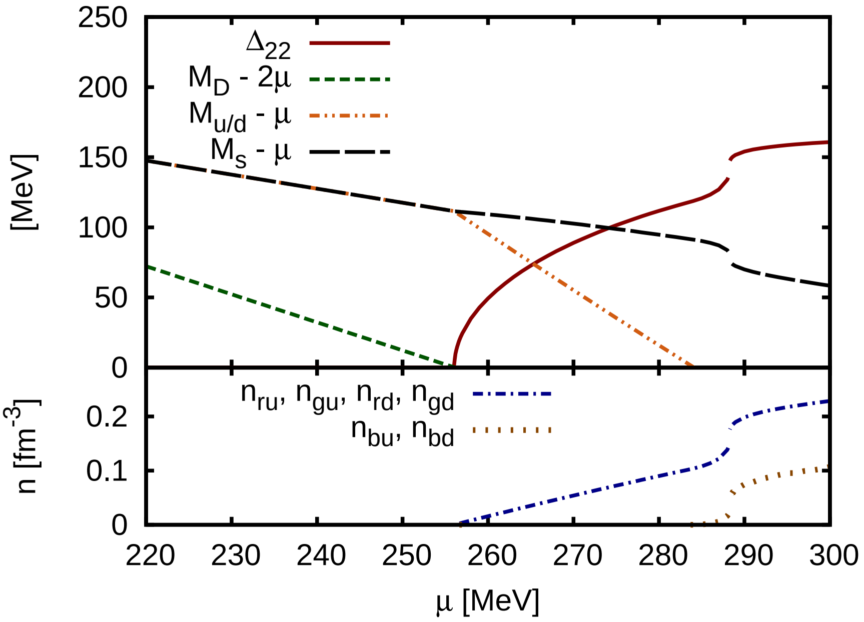

Figure 5.10.: The quark masses, bound diquark masses, gap parameter (upper part) and the quark number densities (lower part) in dependence of the quark chemical potential at $T = 0$ for equal bare quark masses and $K' = 5\,K$. This plot shows the situation on the zero-temperature axis in the phase diagram Fig. 5.5(h). (parameter set IV)

quark chemical potential the number density for the quarks contained in the BEC rises while there are still no blue and no strange quarks present. This "medium" of up and down quarks modifies the quark masses leading to the appearance of blue up and down quarks ($M_{u/d} - \mu = 0$) at $\mu = 284.9$ MeV. Looking at the number densities (Fig. 5.10) this is the point where the density of blue up and down quarks starts to take a non-zero value. At this point we draw the crossover line in the phase diagrams since from this point on "free" quarks are able to form BCS-pairs. At $\mu = 288.3$ MeV we see the "remains" of the chiral phase transition.

5.5. Connection to the Ginzburg-Landau results

The results of the Ginzburg-Landau analysis ([20, 21, 22]) do not show the competition of the CFL and 2SC phase and the possibility that the low-temperature CEP may be covered by the 2SC phase. At first sight this seems to contradict to our NJL model results. In this section we will show that this is a results of the parameterization used in the GL ansatz and that working with a more general GL ansatz in this situation is practically impossible.

As we already pointed out in Sect. 5.1, the two-flavor ansatz used in Refs. [20, 21, 22] differs from the situation in the 2SC phase of our three-flavor NJL model. In the NJL description the chiral strange quark condensate, which is completely neglected in the two-flavor GL ansatz (Eq. (5.11)), plays a crucial role. Its large magnitude effects, through the diquark coupling strength, the diquark condensate. The diquark condensate, on the other hand, has an effect on the strange quark masses and chiral condensate. To allow for these effects one has to include a strange chiral condensate that can differ from the other chiral condensates, $\Phi = \mathrm{diag}\,(\sigma, \sigma, \sigma_s)$. This leads to the following ansatz

$$\begin{aligned}\Omega_{2SC}\left(\sigma, \sigma_s, d\right) = & \left(\frac{a}{2}\frac{2\sigma^2+\sigma_s^2}{3} - \frac{c}{3}\sigma^2\sigma_s + \frac{b_1'}{4}\sigma^4 + \frac{b_2'}{4}\sigma_s^4 + \frac{b_1'-2b_2'}{2}\sigma^2\sigma_s^2\right) \\ & + \left(\frac{\alpha}{6}d^2 + \frac{\beta'}{4}d^4\right) - \frac{\gamma}{3}d^2\sigma_s + \lambda_1' d^2\sigma^2 + \lambda_2' d^2\sigma_s^2\,, \qquad (5.19)\end{aligned}$$

where the coefficients a, c, α, and γ are the same as in Eq. (5.10), and

$$\begin{aligned} b_1' &= \frac{1}{3}(2b_1+b_2)\,, & b_2' &= \frac{1}{6}(b_1+b_2)\,, \\ \beta' &= 4\left(2\beta_1+2\beta_2+\beta_3+\beta_4\right)\,, \\ \lambda_1' &= 2\left(2\lambda_2-\lambda_3\right)\,, & \lambda_2' &= 2\left(\lambda_1+\lambda_2\right)\,. \qquad (5.20)\end{aligned}$$

The inclusion of the strange chiral condensates increases the number of coefficients from five in Eq. (5.11) to nine. It is important to note that in this ansatz we have the γ-term, which was found to be responsible for the low-temperature end-point using Eq. (5.9) and is related to the transformed six-point interaction in our NJL-type model. This term is absent in Eq. (5.11) due to the missing σ_s. Setting $\sigma_s = 0$ will reduce Eq. (5.19) to Eq. (5.11). To investigate the competition of the CFL and 2SC phase one can compare Ω_{3F} and Ω_{2SC} (Eq. (5.9) and Eq. (5.19)), although this only give a useful answer when both, Ω_{3F} and Ω_{2SC}, give meaningful results, i.e. all condensates are sufficiently small. To perform the comparison both terms should by expressed using the same coefficients. We therefore relate the coefficients of Eq. (5.19) and Eq. (5.9) via

$$b = 3\left(b_1'-b_2'\right)\,, \qquad \lambda = 3\left(\lambda_1'+\lambda_2'\right)\,, \qquad \beta = 3\left(3\beta_1'+\beta_2'\right)\,, \quad \beta' = \beta_1'+\beta_2'$$

with

$$\beta_1' = 4\left(2\beta_1+\beta_4\right)\,, \quad \beta_2' = 4\left(2\beta_2+\beta_3\right)\,. \qquad (5.21)$$

To the perform a full Ginzburg-Landau analysis in this context one has to deal with these ten coefficients (a, c, b_1', b_2', α, β_1', β_2', γ, λ_1', λ_2'), which is practically impossible. However we can find an example with whose help we can show that the NJL-model results are indeed completely consistent with a general GL analysis.

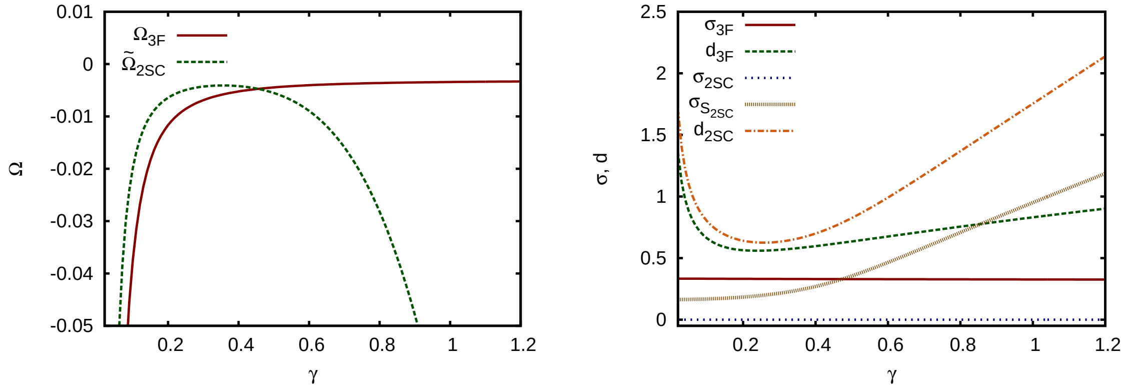

(a) free energies (b) condensates

Figure 5.11.: Results obtain for the example of a GL analysis of the CFL and 2SC phases described in the text (Sect. 5.5.1. (a): the GL free energies for the CFL solutions (solid) and the 2SC solutions (dashed) as functions of γ at the endpoint found in Ref. [20, 21, 22]. (b): the values of the condensates associated with the solutions in (a).

5.5.1. A GL example of CFL vs. 2SC

For this example we make some simplifying assumptions

- We neglect all λ-terms, i.e. $\lambda'_1 = \lambda'_2 = 0$. This was also assumed in Ref. [21] when using Eq. (5.9).
- We use $b'_1 = 2\,b/3$ and $b'_2 = b/3$, since this ansatz reproduces the NJL-model feature that the flavors do not mix when only four-point interactions are taken into account.
- We choose $\beta' = \beta/\left(3 \cdot 2^{2/3}\right)$ for the coupling in the diquark sector. This choice reproduces the relation $d_{\mathrm{2SC}} = 2^{1/3} d_{\mathrm{CFL}}$, with $\gamma = \lambda = 0$. This relation comes from weak coupling QCD [36] and usually also holds in the NJL model.
- We only allow for BCS-like 2SC solutions, i.e. we set $\sigma = 0$. This assumption is guided by the observation that we find a BCS-like 2SC phase in the phase diagram on the point where the end point should be.

With these assumptions the GL free energy for the 2SC phase simplifies to

$$\tilde{\Omega}_{2SC}\left(\sigma_s, d\right) = \left(\frac{a}{6}\sigma_s^2 + \frac{b}{12}\sigma_s^4\right) + \left(\frac{\alpha}{6}d^2 + \frac{\beta}{12 \cdot 2^{2/3}}d^4\right) - \frac{\gamma}{3}d^2\sigma_s\,. \tag{5.22}$$

We use this equation and Eq. (5.9) with $\lambda = 0$ to compare the free energies of the CFL and 2SC solutions. To reduce the number of coefficients we work at the location of the low-temperature critical end point found in Ref. [20, 21, 22]. This relates a and α to b, c, β and γ

$$a = \frac{c^2}{3b} + \frac{2\gamma^2}{\beta}\,, \qquad \alpha = -\frac{\beta c^2}{27\gamma b^2}\,. \tag{5.23}$$

Since an analytic study still is infeasible we choose numerical values for the remaining coefficients. Therefore we choose a scaling factor Λ of dimension energy which allows us to work in units of the corresponding power of Λ and to choose $b = c = \beta = 1$. Thereby the positivity of these coefficients can be motivated physically, cf. Ref. [21].

With all coefficients, except for γ, fixed we can study the free energy as a function of γ numerically. In Fig. 5.11(a) the free energies for the CFL and 2SC phase in our example are shown, at low γ the CFL phase is favored whereas at large γ the 2SC phase becomes favored. Looking at the associated condensates, in Fig. 5.11(b), we see that the diquark and chiral condensate increase much faster in the 2SC than in the CFL phase as functions of γ. Both these effects have also been observed in the NJL-model calculation, cf. Fig. 5.6, here as functions of K'. Although this example can not replace a full Ginzburg-Landau analysis it shows that the NJL-model results are consistent with a more general GL ansatz and there is no discrepancy between those two approaches.

6. $U(1)_A$ breaking and meson condensates

In this chapter we will investigate the effect of the transformed six-point interaction on the condensation of neutral kaons in the CFL phase and the phase diagram of charge neutral quark matter. In the previous chapter we were interested in the possible existence of a low-temperature critical end point and therefore varied K' between zero and $5\,K'$. The phase diagram changed dramatically when K' was large. We suppose that these large values are unrealistic and therefore work here with the assumption that K' is of the same order as K and choose K' between zero and $1.5\,K$. In the following we are only interested in K^0 since this is the only meson condensate which is realized in the phase diagram of neutral quark matter (with $K' = 0$).

6.1. The K^0 mass at non-zero K'

In Ref. [21] the authors used a low-energy effective theory to study the effect of the $U(1)_A$ breaking in the diquark sector on the masses of the Goldstone bosons. The two key results obtained in this model are: (i) the mixing of the two sets of Goldstone bosons ($\bar{q}q$ states and CFL mesons) enhances, (ii) the masses of the Goldstone bosons increase. In the following we will investigate these effects in the NJL model.

For the calculation of the meson masses in the NJL model we proceed as in Sect. 4.1.1 and include terms that originate from the transformed six-point interaction. In the first step we solve the gap equations and neutrality conditions for the CFL phase and then solve the Bethe-Salpeter equation

$$T = K + K\,J\,T. \tag{6.1}$$

The structure of the matrix J does not change when K' is introduced since no new operators appear. The values of J only depend on K' through the modified solutions of the gap equations. The matrix K, on the other hand, has some entries proportional to K'. The transformed six-point interaction contains, among others,

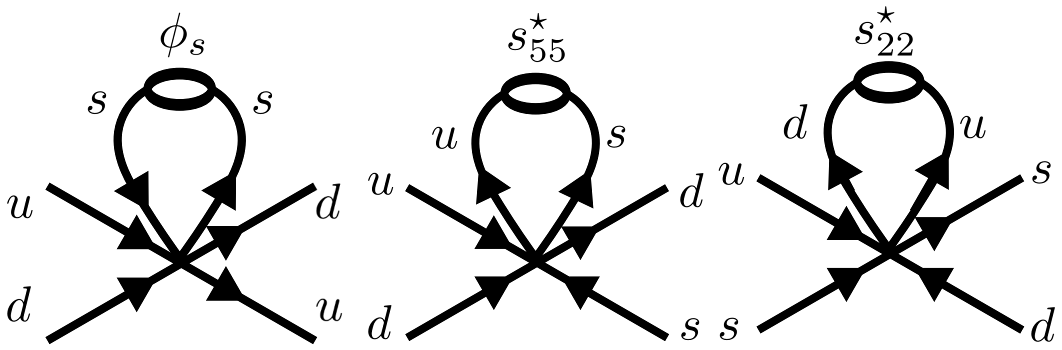

(a) $(K'\phi_s)\ \Gamma^\uparrow_{25} \otimes \Gamma^\downarrow_{25}$ (b) $\left(\frac{i}{2\sqrt{2}}K's_{55}\right)\ \Gamma^\downarrow_{25} \otimes t_{\bar{K}^0}$ (c) $\left(\frac{i}{2\sqrt{2}}K's_{22}\right)\ \Gamma^\downarrow_{52} \otimes t_{K^0}$

Figure 6.1.: Diagrammatic representations of some examples of contribution to the matrix K generated by the transformed six-point interaction. These terms are contributing to the diagonal (a) and off-diagonal (b),(c) parts of K.

the terms

$$\frac{K'}{4}\left(\bar{q}\tau_5\lambda_2 C\bar{q}^T\right)\ \left(q^T C\tau_5\lambda_2 q\right)\ \left(\bar{d}d\right)\ , \tag{6.2}$$

$$\frac{K'}{4}\left(\bar{q}\tau_2\lambda_5 C\bar{q}^T\right)\ \left(q^T C\tau_2\lambda_5 q\right)\ \left(\bar{s}s\right)\ . \tag{6.3}$$

These terms create effective four-point interactions

$$(K'\phi_d)\ \Gamma^\uparrow_{52} \otimes \Gamma^\downarrow_{52}\,, \tag{6.4}$$

$$(K'\phi_s)\ \Gamma^\uparrow_{25} \otimes \Gamma^\downarrow_{25}\,. \tag{6.5}$$

Figure 6.1(a) shows a diagrammatic representation of this kind of interaction. These additional terms weaken the quark-quark interaction in these pseudoscalar channels and hence give a larger meson mass. It is interesting to note that this is the same mechanism that enhances the interaction in the scalar quark-quark channel. The different sign is due to the fact that the scalar vertices (Eq. (5.18)) contain an imaginary unit that is not contained in the terms of the transformed six-point interaction. Further on also vertex-terms connecting $\bar{q}q$ meson states with CFL meson states appear.

These effective four-point interactions come from the terms

$$-\frac{K'}{4}\left(\bar{q}\tau_5\lambda_2 C\bar{q}^T\right)\left(q^T C\gamma_5\tau_2\lambda_2\right)\left(\bar{d}\gamma_5 s\right)\,, \tag{6.6}$$

$$-\frac{K'}{4}\left(\bar{q}\tau_5\lambda_5\gamma_5 C\bar{q}^T\right)\left(q^T C\tau_2\lambda_5\right)\left(\bar{d}\gamma_5 s\right)\,, \tag{6.7}$$

$$-\frac{K'}{4}\left(\bar{q}\tau_2\lambda_2\gamma_5 C\bar{q}^T\right)\left(q^T C\tau_5\lambda_2\right)\left(\bar{s}\gamma_5 d\right)\,, \tag{6.8}$$

$$-\frac{K'}{4}\left(\bar{q}\tau_2\lambda_5 C\bar{q}^T\right)\left(q^T C\gamma_5\tau_5\lambda_5\right)\left(\bar{s}\gamma_5 d\right) \tag{6.9}$$

in Eq. (5.13) and read

$$-\left(\frac{i}{2\sqrt{2}}K's_{22}\right)\Gamma^{\uparrow}_{52}\otimes t_{\bar{K}^0}\,, \tag{6.10}$$

$$\left(\frac{i}{2\sqrt{2}}K's_{55}\right)\Gamma^{\downarrow}_{25}\otimes t_{\bar{K}^0}\,, \tag{6.11}$$

$$\left(\frac{i}{2\sqrt{2}}K's_{22}\right)\Gamma^{\downarrow}_{52}\otimes t_{K^0}\,, \tag{6.12}$$

$$-\left(\frac{i}{2\sqrt{2}}K's_{55}\right)\Gamma^{\uparrow}_{25}\otimes t_{K^0}\,. \tag{6.13}$$

Here we use $t_{\bar{K}^0} = \frac{1}{2}(\tau_6 - i\tau_7)$ and $t_{K^0} = \frac{1}{2}(\tau_6 + i\tau_7)$. These terms (Eq. (6.10)–(6.13)) add off-diagonal components to the matrix K. However, this does not change the procedure qualitatively. As before, in Sect. 4.1.1, we solve for the poles of T and extract the mass and chemical potential of the meson.

Figure 6.2 shows the mass of the K^0 as a function of the strength of the transformed six-point interaction for the case of equal quark masses. Here we see that the mass rises drastically when K' is increased, from $m_{K^0} = 3.3$ MeV at $K' = 0$ to $m_{K^0} = 17.1$ MeV at $K' = 1.5\,K$. This effect is in agreement with the results of the Ginzburg-Landau analysis [21], where a rise of meson masses with in increased γ (for the meaning of γ see Eq. (5.9)) was predicted.

Interested in a more realistic case, we increase the bare strange quark mass to $m_s = 140.7$ MeV. In Fig. 6.3 the mass and chemical potential of the K^0 meson are shown as functions of the strange quark mass at $T = 0.1$ MeV for several values of K'/K. While the chemical potential changes only marginally when K' is varied the mass function changes more drastically. This shifts the condensation point to larger values of m_s.

Unfortunately the numerical calculation of the lower lying pole of T becomes unstable at larger m_s and the solution starts to jitter (cf. Fig. 6.3). To avoid this problem and to find the condensation point more precisely we plot $m_K - \mu_K = \omega_1$

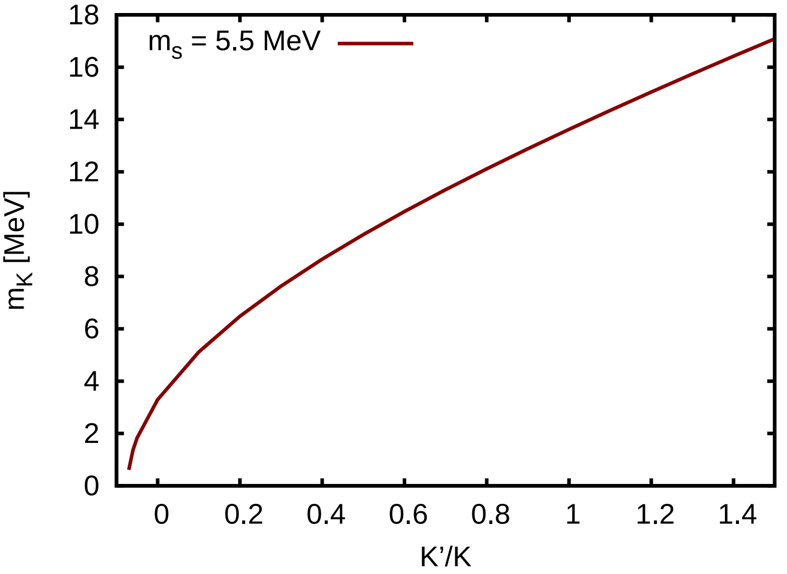

Figure 6.2.: The mass of the K^0 meson in the CFL phase at $\mu = 500$ MeV and $T = 0.1$ MeV as a function of K' for equal bare quark masses. (parameter set II)

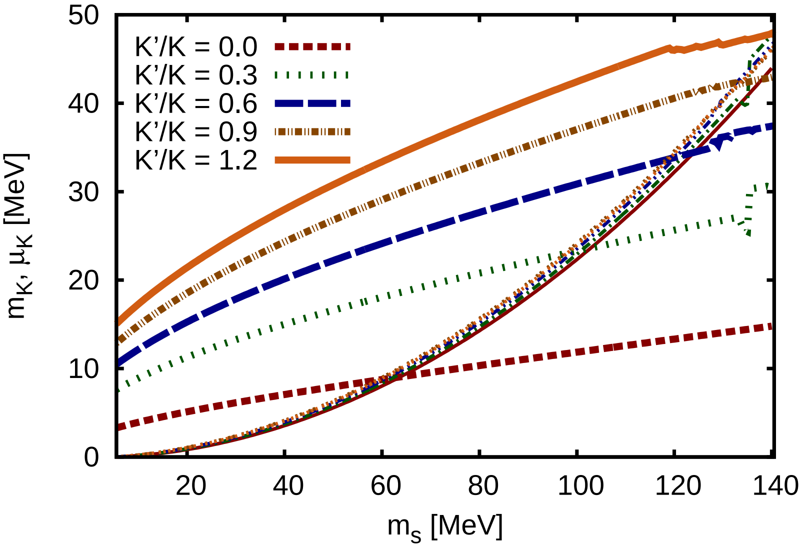

Figure 6.3.: The mass (thick lines) and the chemical potential (thin lines) of the K^0 meson as a function of the bare strange quark mass for several values of K'/K. The intersections can be seen more clearly in Fig. 6.4. (Interpolating between parameter sets II and I.)

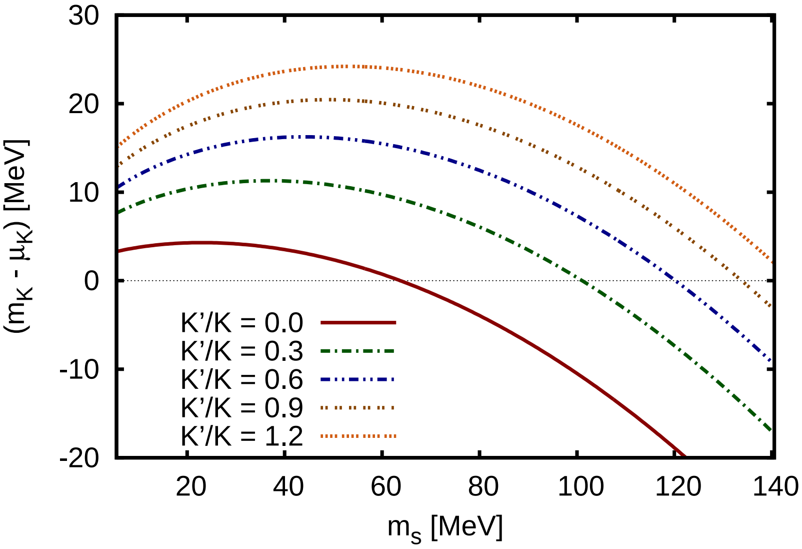

Figure 6.4.: The difference between the K^0 mass and its chemical potential in dependence of m_s for several values of K'/K. (Interpolating between parameter sets II and I.)

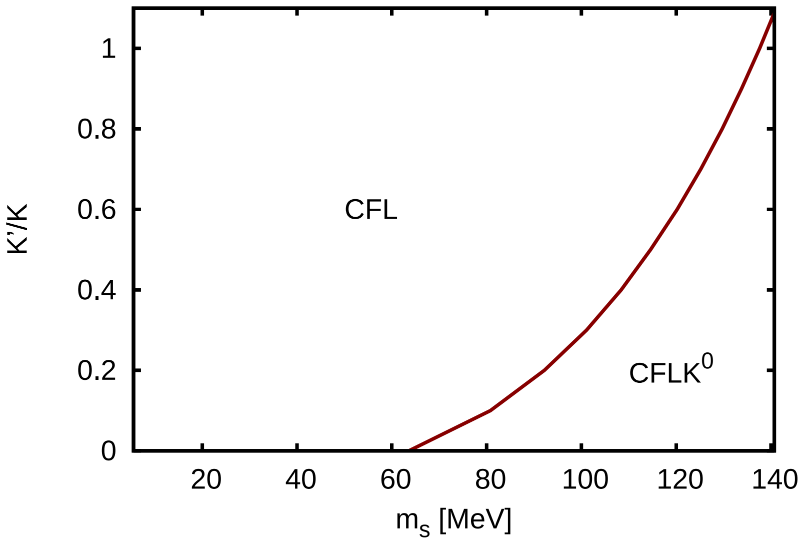

Figure 6.5.: The CFL/CFLK^0 phase diagram in the m_s–K'/K plane obtained by calculating the K^0 mass and its chemical potential. (Interpolating between parameter sets II and I.)

(cf. Eq. (4.23) and Eq. (4.24)) in Fig. 6.4. Here we see how the condensation point moves to higher values of m_s when K' is increased.

To illustrate this we show a phase diagram in the m_s–K'/K plane in Fig. 6.5. Here we consider only the CFL and the CFLK^0 phase and draw the phase boundary at the condensation point. This diagram shows how the onset of the CFLK^0 phase gets pushed to higher bare strange quark mass by an increasing K'.

This effect can also be investigated on the level of the thermodynamic potential by solving the gap equations. Therefore we need to introduce pseudoscalar diquark condensates in the context of the transformed six-point interaction.

6.2. Pseudoscalar diquark condensates and non-zero K'

To be able to solve the gap equations and to calculate the thermodynamic potential in the CFLK^0 phase for a non-zero value of K' we need to include the terms that arise from the transformed six-point interaction and contain pseudoscalar condensates in our mean-field Lagrangian. Only interested in the CFLK^0 phase we only consider the p_{25} and the p_{52} condensate.

Similar to the scalar diquark condensates there is also a contribution to the mass coming from the pseudoscalar diquark condensates. In the CFLK^0 phase this only affects the down and strange quark masses, cf. Fig. 6.6(a),

$$M_d = m_d - 4G\phi_d + 2K\phi_u\phi_s + \frac{K'}{4}\left(|s_{55}|^2 - |p_{52}|^2\right) , \tag{6.14}$$

$$M_s = m_s - 4G\phi_s + 3K\phi_u\phi_d + \frac{K'}{4}\left(|s_{22}|^2 - |p_{25}|^2\right) . \tag{6.15}$$

The pseudoscalar condensates also contribute to off-diagonal mass-like terms, namely

$$\frac{K'}{4}\left(-p_{52}^{\star}s_{22} + s_{55}^{\star}p_{25}\right)\bar{d}\gamma_5 s \, , \tag{6.16}$$

$$\frac{K'}{4}\left(-p_{25}^{\star}s_{55} + s_{22}^{\star}p_{52}\right)\bar{s}\gamma_5 d \, , \tag{6.17}$$

cf. Fig. 6.6(b). We call these contributions mass-like since they enter in the inverse propagator (Eq. (4.31)) as off-diagonal elements of the matrix M. While the elements on the diagonal can be seen as modification of the mass (cf. Eq. (6.14) and Eq. (6.15)), these off-diagonal elements are modification of the pseudoscalar quark-antiquark condensates $\langle\bar{s}\gamma_5 d\rangle$ and $\langle\bar{d}\gamma_5 s\rangle$. However, we continue to assume that the pseudoscalar quark-antiquark condensates are small and neglect them by setting

$$\langle\bar{q}_i i\gamma_5 q_j\rangle = 0 \qquad \forall\, q_i, q_j \, . \tag{6.18}$$

Again similar to the scalar diquark case the gap parameter gets modified by the transformed six-point interaction[1], cf. Fig. 6.6(c),

$$\Delta^{(p)}_{AB} = -2\left(H - \frac{K'}{4}\phi_{\bar{A}}\right) p_{AB}\,. \tag{6.19}$$

The above shown terms contribute the to inverse propagator S^{-1}. The mean-field approximation also gives an field-independent(cf. Eq. (4.32)) contribution, cf. Fig. 6.6(d),

$$\sum_{A,B=2,5,7} \frac{K'}{2}\phi_{\bar{A}}|p_{AB}|^2\,. \tag{6.20}$$

With these additional contribution we solve the gap equations, calculate the thermodynamic potential and proceed as before to obtain a phase diagram.

In Fig. 6.7 we the show the difference in thermodynamic potential to the normal phase for the CFL and CFLK^0 phase in dependence of K'/K. Here we see a second-order phase transition from the CFLK^0 to the CFL phase around $K' = 1.1\,K$, this agrees very well with the point estimated by calculating the meson mass and chemical potential, cf. Fig. 6.5.

6.3. The phase diagram with non-zero K'

In this section we will investigate the effect of the transformed six-point interaction on the phase diagram under neutrality conditions (Eq. (3.41)). Therefore we will proceed as in Sect. 4.3 but with non-vanishing values of K'.

First we have a look at one point of the phase diagram, namely $\mu = 500$ MeV, $T = 0$. Figure 6.8 shows the thermodynamic potential of the different phases[2]. As in Fig. 6.7 we see how the CFLK^0 phase disappears around $K' = 1.1\,K$. Since this point ($\mu = 500$ MeV, $T = 0$) lies in the lower right corner of the section of the phase diagram we usually draw, we do not expect any CFLK^0 phase in the plots of the phase diagram when $K' > 1.1\,K$.

Further increasing K' leads to a first-order phase transition from the CFL to the uSC phase at $K' = 4.9\,K$. The uSC turns into a 2SC phase by a second-order phase transition at $K' = 5.4\,K$. As we saw in Chapter 5, with increasing coupling of the transformed six-point interaction the pressure of the 2SC phase grows faster than the pressure of the CFL phase, so that the 2SC phase replaces the CFL phase at sufficiently large values of K'. Electric charge neutrality leads to the appearance of the uSC phase at a small intermediate range of K'.

---

[1] Here we use the same notation as in Sect. 5.2.1, i.e. $\bar{2} = s$, $\bar{5} = d$ and $\bar{7} = u$.

[2] Here we use K' up to $6\,K$ for a clearer presentation of the effects of the transformed six-point interaction. We still consider these large values of K' as unrealistic.

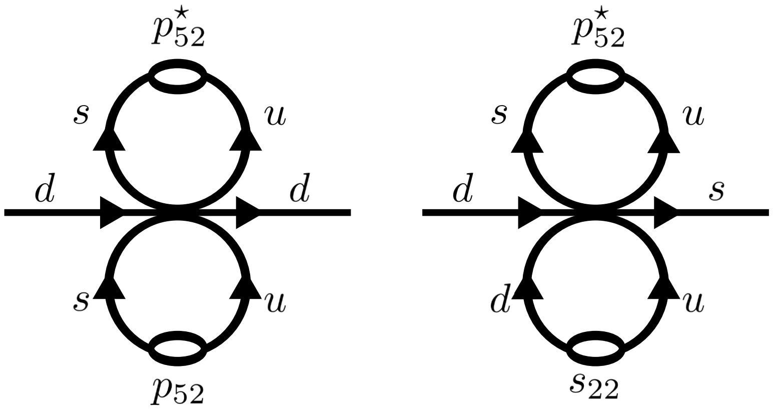
$p^\star_{52}$
s
u
d
d
s
u
p_{52}
$p^\star_{52}$
s
u
d
s
d
u
s_{22}

(a) mass

(b) off-diagonal mass-like

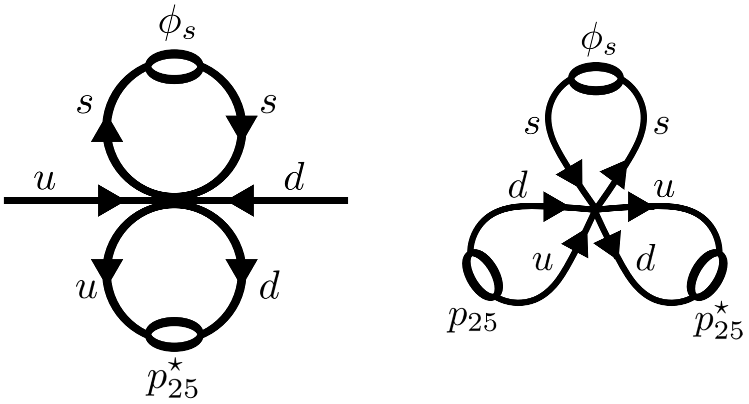
ϕ_s
s
s
u
d
u
d
$p^\star_{25}$
ϕ_s
s
s
d
u
u
d
p_{25}
$p^\star_{25}$

(c) off-diagonal in Nambu-Gorkov space

(d) field independent

Figure 6.6.: Examples for the contributions to the mean-field Lagrangian induced by the transformed six-point interaction in the presence of the pseudoscalar diquark condensates of the CFLK^0 phase. (a) a contribution to the dynamical down quark mass (M_d), (b) an off-diagonal mass-like term, (c) a contribution to the pseudoscalar gap parameter ($\Delta^{(p)\star}_{25}$) and (d) a contribution to the field independent term $\mathcal{V}$.

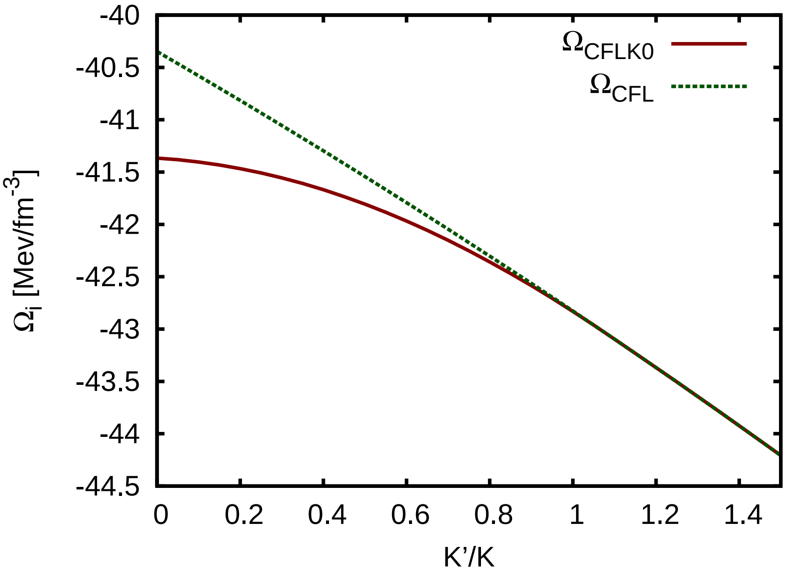

Figure 6.7.: The difference in thermodynamic potential of the CFL and the CFLK^0 phase to the normal phase as functions of K'/K. (parameter set I)

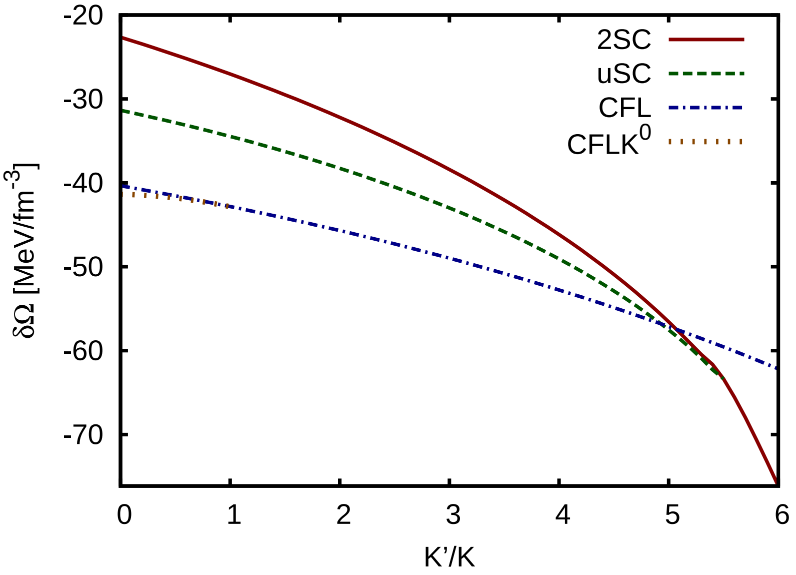

Figure 6.8.: The difference in thermodynamic potential of several phases at $\mu =$ 500 MeV and $T = 0$ to the normal phase in dependence of K'/K. (parameter set I)

Figure 6.9 shows the masses and diquark condensate in the different phases, still at $\mu = 500$ MeV and $T = 0$. In contrast to Fig. 5.6, we now use a realistic strange quark mass, enforce charge neutrality and work at a larger quark chemical potential. However, the basic behavior of the 2SC (Fig. 6.9(b)) and CFL (Fig. 6.9(d)) phase remains unchanged and can be explained by the mechanisms shown in Chapter 5. The uSC phase, not considered before, shows some interesting features. The presence of the $\Delta_{55}^{(s)}$ condensate gives a contribution to the down quark mass. This leads to a down quark mass that is a bit larger than the up quark mass and damps the amplifying effect involving the strange quark and the $\Delta_{22}^{(s)}$ diquark condensate, cf. Chapter 5. It is therefore no surprise that the $\Delta_{55}^{(s)}$ condensate is reduced in the uSC phase when K' is increased. When $\Delta_{55}^{(s)}$ finally vanishes the uSC phase turns into a 2SC phase.

In Fig. 6.10 and Fig. 6.11 we finally present the phase diagrams of neutral quark matter for different choices of K'. For comparison we show the phase diagram for $K' = 0$ (from Sect. 4.3) in Fig. 6.10(a) and then increase K' to $0.5\,K$ (Fig. 6.10(b)), $1\,K$ (Fig. 6.11(a)) and $1.5\,K$ (Fig. 6.11(b)).

Here we observe that the transformed six-point interaction induces a stronger diquark coupling. This leads to the expansion of the 2SC phase. The 2SC phase expands to higher temperatures as well as it replaces the area of normal quark matter at lower temperatures in the phase diagram. Further on the area of the gapless 2SC shrinks. These effects are comparable with the effect of the increased quark-quark coupling H comparing Fig. 4.3(b) and Fig. 4.5(b). Unlike in the case of an increased quark-quark coupling H, the enhancement induced by the transformed six-point interaction works differently in the various phases. Therefore the 2SC phase pushes the onset of the uSC to higher quark chemical potential. In turn, the uSC phase replaces parts of the CFL phase. This differs from the situation in Fig. 4.5(b) where the overall diquark coupling strength was increased. There the CFL profits and replaces parts of the uSC and parts of the 2SC phase. Beside these changes we observe, that the CFLK^0 phase disappears rapidly from the phase diagram. Further on we see, that with increasing K' first-order phase transitions are replaced by second-order phase transitions. This happens to the phase boundary between the 2SC and the uSC phase and to the lower part of the uSC–CFL transition.

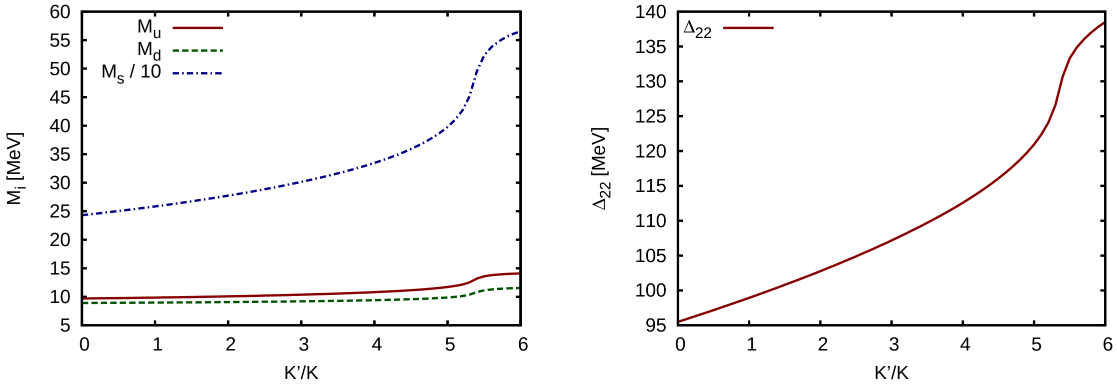

(a) 2SC masses (b) 2SC diquark condensate

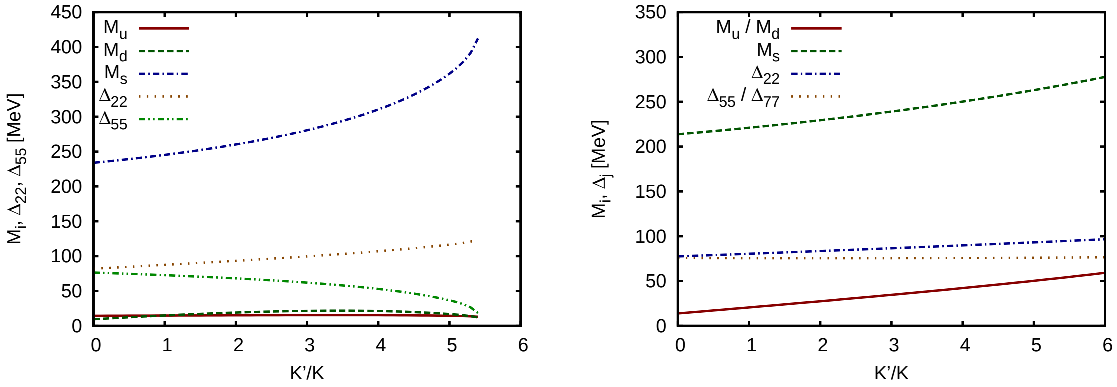

(c) uSC (d) CFL

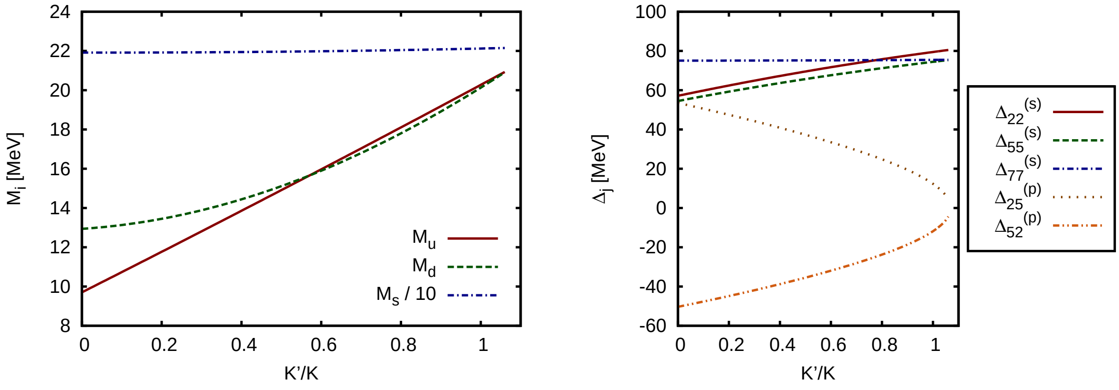

(e) CFLK^0 masses (f) CFLK^0 diquark condensates

Figure 6.9.: The quark masses and diquark condensates in different color superconducting phase as functions of K'/K for $\mu = 500$ MeV and $T = 0$. (parameter set I)

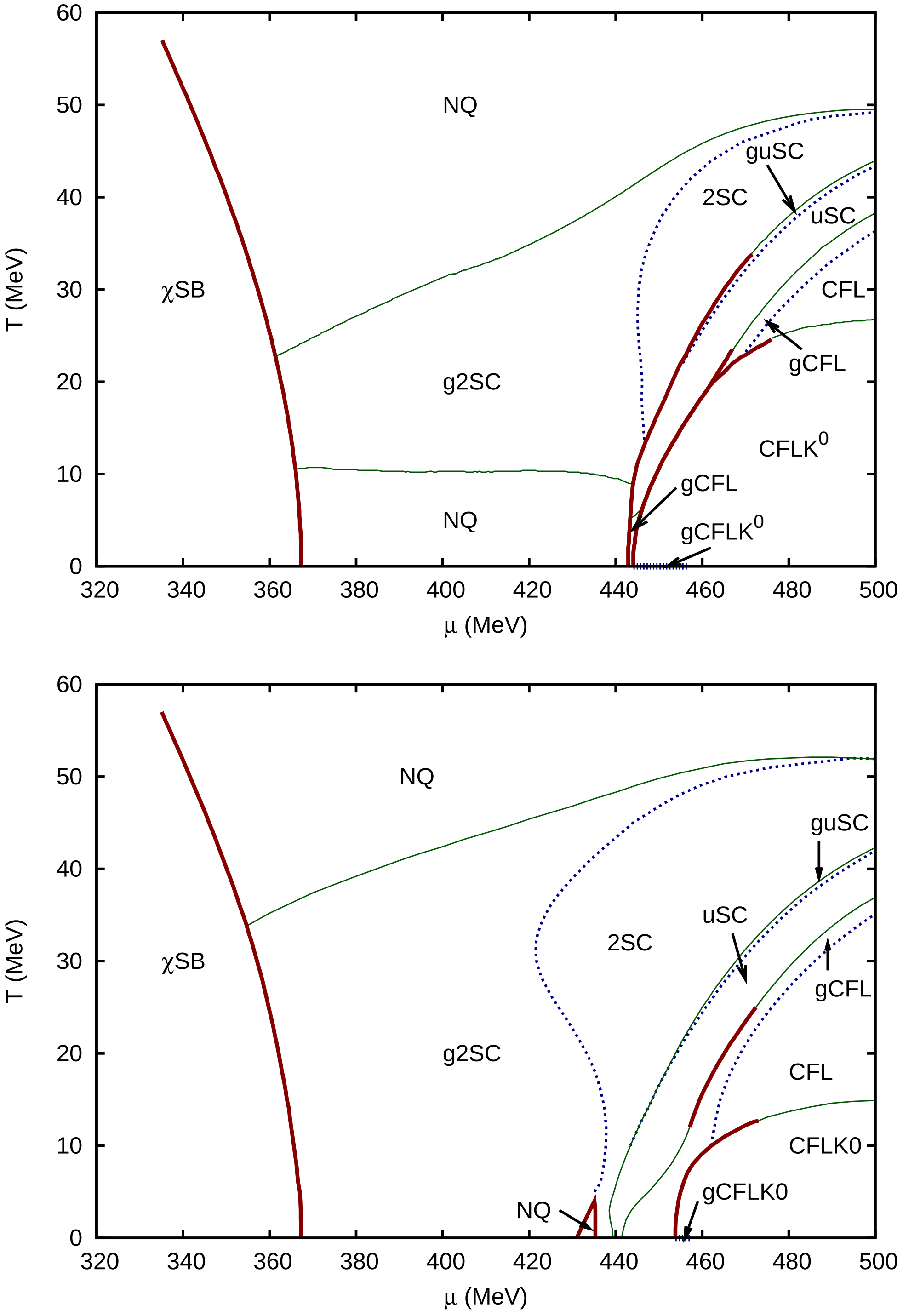

Figure 6.10.: The phase diagram of electric and color charge neutral quark matter for $K' = 0.0\,K$ (upper panel) and $K' = 0.5\,K$ (lower panel). Thick (red) solid lines denote first-order phase transitions, thin (green) lines second-order phase transitions and the dotted (blue) line the (dis)appearance of the gap in the excitations spectrum (transition to a gapless phase). Continued in Fig. 6.11. (parameter set I)

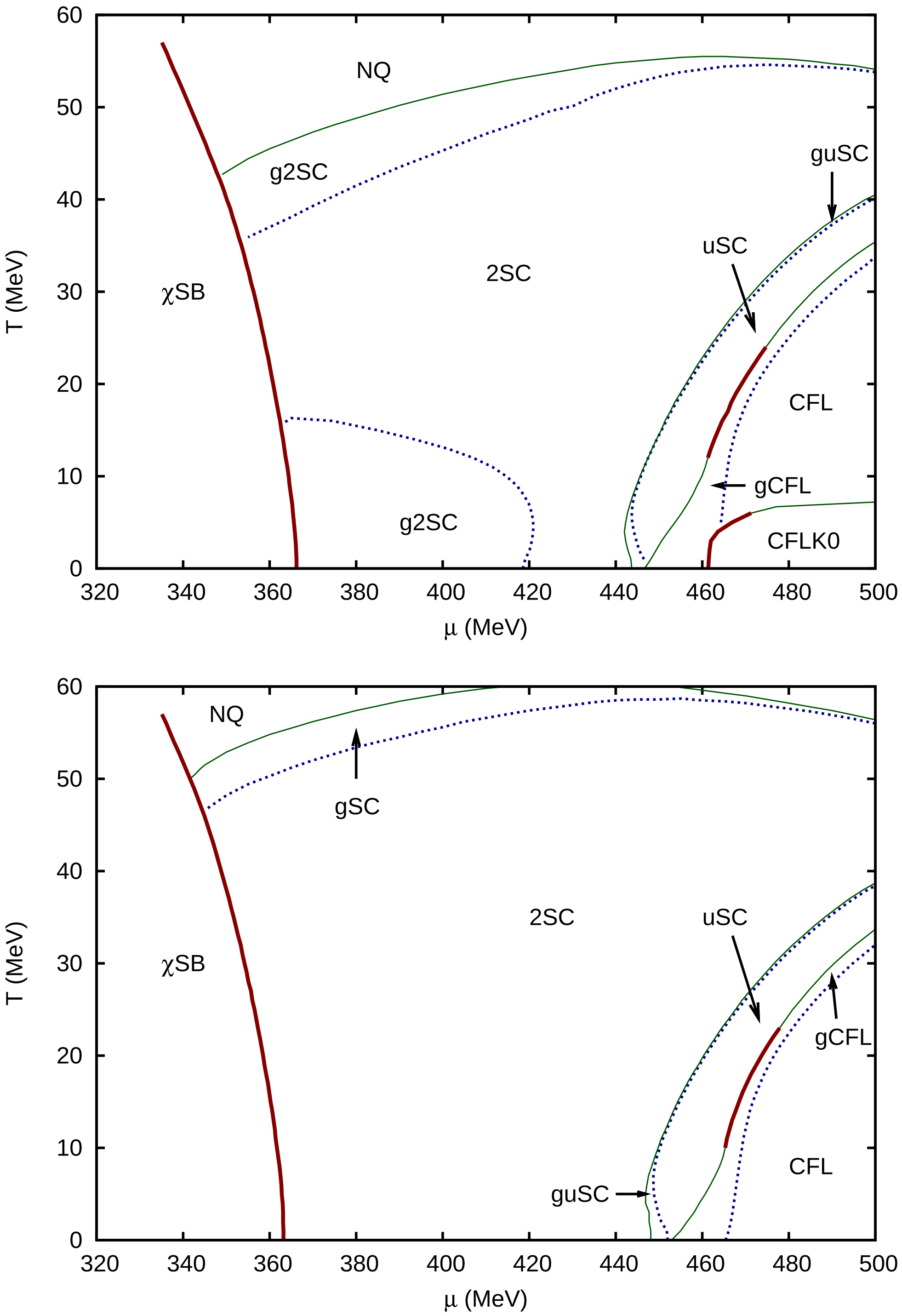

Figure 6.11.: Continuation of Fig. 6.10, showing the phase diagram for $K' = 1.0\,K$ (upper panel) and $K' = 1.5\,K$ (lower panel).

7. Summary, conclusions and outlook

In this study we investigated several features of the phase structure of homogeneous, electric and color charge neutral quark matter in β equilibrium. We used an NJL-type model to simulate QCD at a few times nuclear matter density and temperatures up to a few tens of MeV. These choices for temperature, quark chemical potential and neutrality are motivated by the possible existence of deconfined quark matter in the inner core of a neutron star.

In the first part of this work we studied the condensation of pseudoscalar Goldstone bosons in the CFL phase. The symmetry breaking due to the presence of diquark condensates in the CFL phase leads to an octet of pseudoscalar mesons, as the breaking of chiral symmetry does in vacuum. At the beginning of Chapter 4 we calculated the masses and chemical potentials of pions and kaons in the CFL phase by solving the Bethe–Salpeter equation. Unlike older studies we added the self-consistent treatment of the chiral condensates and the mixing of the $\bar{q}q$ meson states with the CFL meson states. This analysis shows the possible formation of a K^0 condensate in the CFL phase.

To obtain the phase diagram we minimized the mean-field thermodynamic potential by solving the gap equations. Here meson condensates where taken into account by allowing for pseudoscalar diquark condensates. Since the quark-quark coupling is basically unknown we use two different values for it to study the effect of quark-quark couplings with different strengths. In both cases a large part of the CFL phase is replaced by the CFLK^0 phase. The phase diagram with the smaller quark-quark coupling agrees in most parts with the results of Ref. [72]. In contrast to Ref. [72] we find a gapless CFLK^0 phase. This gapless phase is only realized at very low temperatures, a feature that can be explained by investigating the quasi-particle modes. Here remains the open question whether the gapless CFLK^0 phase also suffers from the same chromomagnetic instabilities as the gapless CFL and the gapless. On the other hand low-energy effective theory predicts [112] that all Meissner mass are real. Our numerical results also confirm the p2SC solution found in Ref. [72], however we find strong indications that this phase is an artifact of the mean-field approximation.

Further on we have investigated the effect of neutrino trapping on the phase structure. The idea behind this effect is that in the first few moments after the formation of a neutron star, the star is still several tens of MeV hot and neutrinos are trapped inside. In this situation lepton number is a conserved quantity. Our investigation is guided by the steps performed in Ref. [102] with the addition of pseudoscalar condensates. In a CFL phase without meson condensates color charge neutrality automatically leads to electric charge neutrality. Pseudoscalar condensates are of interest in this context, since the condensation of electrically charged mesons allows the quark part of the system to carry an electric charge while CFL pairing is realized. Indeed we find areas in the phase diagram where charged kaons condense in the CFL phase, when the electron lepton number chemical potential is sufficiently large.

In Chapter 5, inspired by a Ginzburg-Landau analysis [20, 21, 22], we introduced a $U(1)_A$ breaking six-point interaction that allows for the coupling of chiral and diquark condensates. This term is one of many that are possible in the NJL model but which are usually neglected. In this context we investigated the possible existence of a second, low-temperature critical end point on the chiral phase transition. For this purpose we dropped the neutrality conditions in this Chapter.

Unlike the NJL study in Ref. [81] we allow for flavor dependent chiral and diquark condensates. Even with equal bare quark masses the area where a low-temperature critical end point may lie gets covered by a 2SC phase. This is due to a mutual amplification of the chiral strange quark condensate and the diquark condensate containing up and down quarks. Besides this amplification the axial anomaly also induces an effective four-point interaction leading to the appearance of a Bose-Einstein condensate of bound quark pairs. In the case of equal bare quark masses, the absence of the low-temperature critical end point might be the result of our specific choice of parameters, however when one introduces a more realistic strange quark mass the situation becomes absolutely clear. Here the 2SC covers a large part of the phase diagram, this area grows when the coupling strength of the transformed six-point interaction is increased and there is no trace of a low-temperature critical end point. For both choices of the bare strange quark mass we find that the phase structure changes dramatically when the coupling is increased to large values (i.e. $K' = 3\,K \ldots 5\,K$).

The effect of the transformed six-point interaction on the phase diagram of electrically and color charge neutral quark matter was studied in Chapter 6. Here we proceeded analogously to Chapter 4, first we calculated the mass of the K^0 and studied the effects of the transformed six-point interaction. Increasing the strength of the transformed six-point interactions leads to a larger kaon mass. A large kaon mass suppresses the appearance of the CFLK^0 phase. In the next step, we calculate the phase diagram of neutral quark matter and include the transformed six-point interaction. As predicted, the CFLK^0 phase disappears from the phase diagram. The other phases behave similarly as in Chapter 5, the area of the 2SC phase grows, slowly suppressing the uSC and CFL phase.

In this thesis we have seen that the NJL model is a great tool to investigate the basic structures and mechanisms in a color superconductor. Whereas a Ginzburg-Landau analysis is only based on symmetries and leaves much room for interpretation, the parameters of the NJL model can be fitted to vacuum observables. Unfortunately this cannot be done for all parameters and it is so far unclear how all these parameters depend on temperature and density. The comparison of our results with weak coupling, low-energy effective theory and Dyson-Schwinger results ensure us that we choose reasonable values for the couplings. However, this might not be good enough since the QCD phase diagram, at least at low temperatures, changes quickly when parameters are varied. Therefore it must be a primary goal of future investigations to eliminate this uncertainty. NJL model studies show a lot of interesting possible phases that might be realized. Besides the homogeneous phase presented in this work, these are mixed and crystalline phases as well as the formation of a Goldstone-boson current, spin-one pairing and more. To get some quantitatively reliable answers, it is necessary to better constrain the parameters of the NJL model or the use methods with better known parameters. Only this can bring us closer to the real phase diagram of cold and dense quark matter. So there is quite a lot to do until the mysteries of a neutron star's inner core can be solved.

A. Conventions

We use natural units

$$\hbar = c = k_B = 1 \tag{A.1}$$

and the metric

$$g^{00} = 1, \quad g^{11} = g^{22} = g^{33} = -1, \quad g^{ij} = 0 \,\forall\, i \neq j\,. \tag{A.2}$$

Using the Pauli matrices, defined as

$$\sigma_1 = \begin{pmatrix} 0 & 1 \\ 1 & 0 \end{pmatrix}, \quad \sigma_2 = \begin{pmatrix} 0 & -i \\ i & 0 \end{pmatrix}, \quad \sigma_3 = \begin{pmatrix} 1 & 0 \\ 0 & -1 \end{pmatrix}, \tag{A.3}$$

we define the γ-matrices in Dirac representation

$$\gamma^0 = \begin{pmatrix} \mathbb{1} & 0 \\ 0 & -\mathbb{1} \end{pmatrix} \qquad \gamma^i = \begin{pmatrix} 0 & \sigma_i \\ -\sigma_i & 0 \end{pmatrix} \; i \in \{1,2,3\},$$

$$\gamma^5 = \begin{pmatrix} 0 & \mathbb{1} \\ \mathbb{1} & 0 \end{pmatrix} = i\gamma^0\,\gamma^1\,\gamma^2\,\gamma^3\,, \tag{A.4}$$

which obey the relations

$$\{\gamma^\mu, \gamma^\nu\} = \gamma^\mu\gamma^\nu + \gamma^\nu\gamma^\mu = 2g^{\mu\nu} \qquad \text{and} \quad \{\gamma^5, \gamma^\mu\} = 0\,. \tag{A.5}$$

Further on we use the γ-matrices to define the charge conjugation operator

$$C = i\gamma^2\gamma^0\,, \tag{A.6}$$

which obeys the following useful relations

$$C = -C^{-1} = -C^T = -C^\dagger\,, \tag{A.7}$$

$$C\gamma^\mu C^{-1} = -\left(\gamma^\mu\right)^T\,. \tag{A.8}$$

To describe structures in color and flavor space we use the Gell-Mann matrices. For a clean notation we denote them with τ_a in flavor space and with λ_a in color space,

$$\tau_1,\,\lambda_1 = \begin{pmatrix} 0 & 1 & 0 \\ 1 & 0 & 0 \\ 0 & 0 & 0 \end{pmatrix}, \qquad \tau_2,\,\lambda_2 = \begin{pmatrix} 0 & -i & 0 \\ i & 0 & 0 \\ 0 & 0 & 0 \end{pmatrix}, \quad \tau_3,\,\lambda_3 = \begin{pmatrix} 1 & 0 & 0 \\ 0 & -1 & 0 \\ 0 & 0 & 0 \end{pmatrix},$$

$$\tau_4,\,\lambda_4 = \begin{pmatrix} 0 & 0 & 1 \\ 0 & 0 & 0 \\ 1 & 0 & 0 \end{pmatrix}, \qquad \tau_5,\,\lambda_5 = \begin{pmatrix} 0 & 0 & -i \\ 0 & 0 & 0 \\ i & 0 & 0 \end{pmatrix}, \quad \tau_6,\,\lambda_6 = \begin{pmatrix} 0 & 0 & 0 \\ 0 & 0 & 1 \\ 0 & 1 & 0 \end{pmatrix},$$

$$\tau_7,\,\lambda_7 = \begin{pmatrix} 0 & 0 & 0 \\ 0 & 0 & -i \\ 0 & i & 0 \end{pmatrix}, \qquad \tau_8,\,\lambda_8 = \frac{1}{\sqrt{3}} \begin{pmatrix} 1 & 0 & 0 \\ 0 & 1 & 0 \\ 0 & 0 & -2 \end{pmatrix},$$

and add (A.9)

$$\tau_0 = \sqrt{\frac{2}{3}} \begin{pmatrix} 1 & 0 & 0 \\ 0 & 1 & 0 \\ 0 & 0 & 1 \end{pmatrix}. \tag{A.10}$$

B. Parameter sets

	m_u [MeV]	m_d [MeV]	m_s [MeV]	$G\Lambda^2$	$K\Lambda^5$	$H\Lambda^2$	Λ [MeV]
set I	5.5	5.5	140.7	1.835	12.36	1.37625	602.3
set II	5.5	5.5	5.5	1.918	12.36	1.37625	602.3
set III	5.5	5.5	140.7	1.835	12.36	1.835	602.3
set IV	5.5	5.5	5.5	1.918	12.36	1.74	602.3
set V	5.5	5.5	140.7	1.835	12.36	1.74	602.3

Table B.1.: The five sets of parameters used in this work.

Here we give an overview of all parameter sets used in this work. The sets I, II and III are introduced in Sect. 3.6, the sets IV and V in Sect. 5.2.2.

When we are interested in quantities as functions of the bare strange quark mass m_s, we vary m_s between 5.5 MeV and 140.7 MeV. We follow [81] and adjust the coupling G so that a dynamical vacuum mass for the up and down quarks of $M_{u/d} = 367.6$ MeV is reproduced for every value of m_s. This varies G as shown in Fig. B.1. The parameter sets I and II (IV and V) are chosen such that this method interpolates between them.

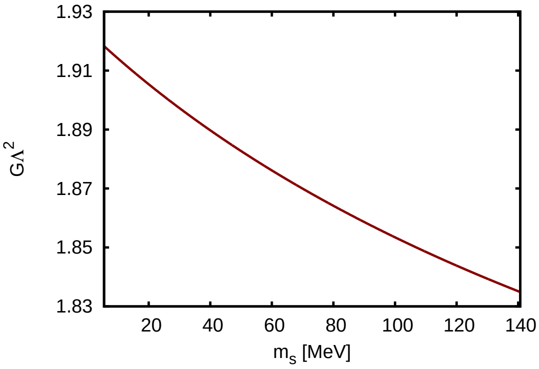

Figure B.1.: The coupling $G\Lambda^2$ as a function of m_s.

C. The transformed six-point interaction

Evaluating the sum over A and A' in Eq. (5.13) gives

$$\begin{aligned}\mathcal{L}_\chi^{(6)} = \frac{K'}{8}\sum_{\pm}\sum_{B}\Big\{ \quad & \left(\bar{q}\tau_7\lambda_B\left(1\pm\gamma_5\right)C\bar{q}^T\right)\left(q^T C\tau_7\lambda_B\left(1\pm\gamma_5\right)q\right)\left(\bar{u}\left(1\pm\gamma_5\right)u\right)\\ & -\left(\bar{q}\tau_7\lambda_B\left(1\pm\gamma_5\right)C\bar{q}^T\right)\left(q^T C\tau_5\lambda_B\left(1\pm\gamma_5\right)q\right)\left(\bar{u}\left(1\pm\gamma_5\right)d\right)\\ & +\left(\bar{q}\tau_7\lambda_B\left(1\pm\gamma_5\right)C\bar{q}^T\right)\left(q^T C\tau_2\lambda_B\left(1\pm\gamma_5\right)q\right)\left(\bar{u}\left(1\pm\gamma_5\right)s\right)\\ & -\left(\bar{q}\tau_5\lambda_B\left(1\pm\gamma_5\right)C\bar{q}^T\right)\left(q^T C\tau_7\lambda_B\left(1\pm\gamma_5\right)q\right)\left(\bar{d}\left(1\pm\gamma_5\right)u\right)\\ & +\left(\bar{q}\tau_5\lambda_B\left(1\pm\gamma_5\right)C\bar{q}^T\right)\left(q^T C\tau_5\lambda_B\left(1\pm\gamma_5\right)q\right)\left(\bar{d}\left(1\pm\gamma_5\right)d\right)\\ & -\left(\bar{q}\tau_5\lambda_B\left(1\pm\gamma_5\right)C\bar{q}^T\right)\left(q^T C\tau_2\lambda_B\left(1\pm\gamma_5\right)q\right)\left(\bar{d}\left(1\pm\gamma_5\right)s\right)\\ & +\left(\bar{q}\tau_2\lambda_B\left(1\pm\gamma_5\right)C\bar{q}^T\right)\left(q^T C\tau_7\lambda_B\left(1\pm\gamma_5\right)q\right)\left(\bar{s}\left(1\pm\gamma_5\right)u\right)\\ & -\left(\bar{q}\tau_2\lambda_B\left(1\pm\gamma_5\right)C\bar{q}^T\right)\left(q^T C\tau_5\lambda_B\left(1\pm\gamma_5\right)q\right)\left(\bar{s}\left(1\pm\gamma_5\right)d\right)\\ & +\left(\bar{q}\tau_2\lambda_B\left(1\pm\gamma_5\right)C\bar{q}^T\right)\left(q^T C\tau_2\lambda_B\left(1\pm\gamma_5\right)q\right)\left(\bar{s}\left(1\pm\gamma_5\right)s\right)\Big\}\,.\end{aligned} \tag{C.1}$$

The $(1\pm\gamma_5)$ terms lead to all combinations with zero or two γ_5's for each term. In this lengthy notation the flavor structure of the transformed six-point interaction can be identified more easily than in the more compact form given in the text (Eq. (5.13)).

D. On the numerical details

D.1. Momentum integrals in the gCFL/gCFLK^0 phase

To solve the gap equations (Eq. (3.29), Eq. (4.33)) and the neutrality conditions (Eq. (3.41)) and to calculate the thermodynamic potential Eq. (3.17) it is necessary to integrate over the three-momentum. Since the angular integration can be performed trivially only a one-dimensional integral is left. At the momenta where one of the quasi-particle modes hits zero the integrand might be discontinuous (at $T = 0$) or changes very fast (at $T > 0$). It is therefore advantageous to know the values of the momenta where this happens and to perform the integral in intervals where the integrand is continuous.

Luckily, in the CFL phase only modes connected to the small 4×4 - blocks in the inverse propagator become gapless. Gapless means, that one of the eigenvalues vanishes and therewith

$$\det S^{-1}_{4\times 4} = 0\,. \tag{D.1}$$

Due to the spherical symmetric situation the determinate is a polynomial of second order in p^2. In a fully gapped phase this has no real roots, but in a gapless phase the two real positive roots are the numbers we are interested in.

This procedure is similar to the one used in Ref. [113] where a condition for the existence of a gapless phase was derived

$$\Delta^{(s)} \leq \frac{|\bar{\mu}\delta\mu - \bar{M}\delta M|}{\sqrt{\bar{\mu}^2 - \delta M^2}} \tag{D.2}$$

with

$$\bar{M} = (M_1 + M_2)/2\,, \qquad \delta M = (M_1 - M_2)/2\,, \tag{D.3}$$

$$\bar{\mu} = (\mu_1 + \mu_2)/2\,, \qquad \delta\mu = (\mu_1 - \mu_2)/2\,. \tag{D.4}$$

Here M_1 and M_2 (μ_1 and μ_2) are the masses (chemical potentials) of the quarks related the the diquark condensates $\Delta^{(s)}$.

In the (g)CFLK^0 phase the situation is more complex, here the modes carrying a $\tilde{Q} = \pm 1$ charge are connected to the 8×8 - blocks and the $\tilde{Q} = 0$ modes to the 20 × 20 block in the inverse propagator. It is not obvious if a condition like Eq. (D.2) can be found for the gCFLK^0 phase, but it is still possible to calculate the determinants of the 8 × 8 blocks and find the (quite lengthy) analytical expressions for the roots of $\det S^{-1}_{8\times 8}(p^2) = 0$. This is hopeless for the 20 × 20 block. Therefore it is possible to handle the integrals at $T = 0$ for the gCFLK^0 phase ($\tilde{Q} = +1$ mode gapless) but not for the gCFLK$^{0\,\star}$ phase ($\tilde{Q} = 0$ mode gapless). Unlike the gCFLK^0 phase the gCFLK$^{0\,\star}$ phase does not only exist at very low temperatures and we can conclude from our analysis at a small but non-zero temperature that this phase is never preferred (Fig. 4.11).

D.2. Solving the gap equations in the gCFLK^0 phase

The key step for constructing a phase diagram is to solve the gap equations (Eq. (3.29), Eq. (4.33)) in order to find a minimum of the thermodynamic potential. For the fully gapped phases the solution of the gap equations is a true minimum but for the gapless phases the solution of the gap equations might be a maximum with respect to variations of one or more condensates [60]. Only varying the condensates and keeping the system neutral at the same time gives a minimum.

For the gCFLK^0 phase (in the phase diagrams Fig. 4.3(b) and Fig. 4.5(b)) the solution is a maximum with respect to $\Delta^{(s)}_{55}$, $\Delta^{(p)}_{52}$ and ϕ_s. So coming from the gapped phase, where the solution lies in a minimum, going to the gapless phase, where it lies on a maximum, the solution has to lie at an inflection point when the quasiparticle mode touches zero. Such an inflection point is very hard (impossible) to find numerically and, even worse, a small variation of the condensates or charge chemical potentials lets the solution disappear completely.

In a gapless phase where the blocking region is very small the neutral gapless solution lies on a maximum in the direct neighborhood of a minimum for a gapped non-neutral solution. This makes it difficult to find a solution for the gap equation for $T = 0$ everywhere in the gCFL and gCFLK^0 phase in the phase diagrams Fig. 4.3(b) and Fig. 4.5(b). In the phase diagrams with a non-zero lepton chemical potential Fig. 4.17 and Fig. 4.18 the blocking region broadens and the situation becomes manageable.

Since it is not possible to find a solution of the gap equations and neutrality conditions in the gCFL/gCFLK^0 phase with zero μ_L we investigate two extreme cases. First we neglect all electrons and look for the onset of the gapless phase and later find a solution for 250 artificial flavors of electrons. We do this since we expect that these two solutions give us an interval wherein the real, one electron flavor solution lies. We will see, that this works out and the values for the masses, gap parameters and charge chemical potential only differ marginally in the two solutions.

In a world without electrons it is possible to choose a value of $\mu_Q < 0$ that reduces the stress on the quark pairs and keeps the CFL/CFLK^0 solution fully gapped at every point of the phase diagram. This is not possible with leptons in the system, since the CFL/CFLK^0 phase is electrically charge neutral by itself a non-zero μ_Q will always introduce electric charge from the lepton part of the system. Therefore we are interested in the solution without leptons on the edge to the gapless region. This solution lies in direct neighborhood to the one electron flavor neutral gapless solution we were originally looking for and it is the closest point we can reach continuously from the gapped side. For given T and μ, we choose a μ_Q sufficiently large to find a gapped solution (neglecting electrons), then we change the charge chemical potentials from μ_3, μ_8 and μ_Q to

$$\mu_{\tilde{Q}} = \frac{4}{9}\left(\mu_Q - 2\mu_3 - \frac{\sqrt{3}}{2}\mu_8\right) , \tag{D.5}$$

$$\mu_X = \frac{1}{18}\left(-\mu_Q + 2\mu_3 - 4\sqrt{3}\mu_8\right) , \tag{D.6}$$

$$\mu_Y = \frac{1}{18}\left(-\mu_Q - 2\mu_3\right) . \tag{D.7}$$

Since there are no $\tilde{Q}$ charges in the gapped CFL/CFLK^0 phase we can vary $\mu_{\tilde{Q}}$ without any effect on the solution of the gap equations or neutrality conditions. In the CFL phase we choose $\mu_{\tilde{Q}}$ in such a way that the right side of Eq. (D.2) takes the same values as the gap parameter on the left side (onset of the gapless regime). For the CFLK^0 phase it is slightly more complicated since no condition Eq. (D.2) exists. Here we track the positions of the roots of $\det S^{-1}_{8\times 8}\left(p^2\right)$ in the complex momentum plane and find the onset of the gapless phase when the distance of one pole to its complex conjugate partner vanishes.

For a gapless solution follow the idea of Ref. [61] and introduce 250 (unphysical) flavors of electrons. This broadens the blocking region artificially and moves the minimum of the non-neutral gapped solution and the maximum of the neutral gapless solution apart. The 250 electron flavors have only a very small effect on the quark part of the system. The green dashed line in Fig. D.1 shows the quasi-particle dispersion relation for the gapless $\tilde{Q} = +1$ mode in the gCFLK^0 phase (at $T = 0$ and $\mu = 450$ MeV) for 250 electron flavors. There is only a small deviation from the solid (red) line, which shows the mode for the situation without electrons at the onset of the gapless region (details on the construction of the solution for the solid (red) mode were given above). For the physical case of one electron flavor we expect a mode very close the red solid mode but with a very narrow blocking region. In the values of the diquark condensates, chiral condensates and charge chemical potential we barely see a difference between the solution related to the 250 and the zero electron flavor case and therefore use the zero electron solution for most of our calculations. The 250 electron flavor solution ensures us, that the solution in the gapless regime exists.

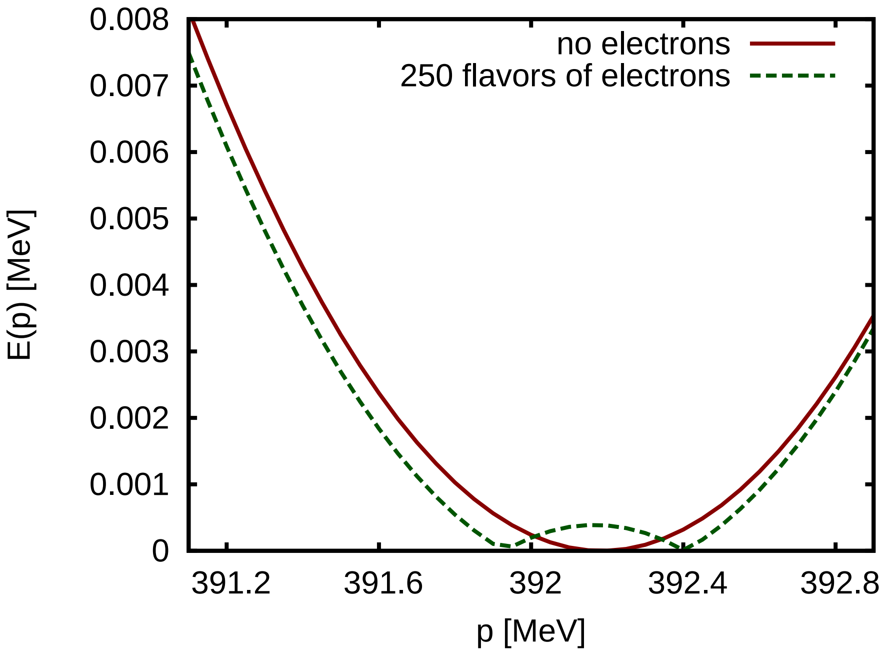

Figure D.1.: The gapless $\tilde{Q} = +1$ mode in the gCFLK^0 phase at $T = 0$ and $\mu = 450$ MeV for $H = 3/4\,G$. The dashed (green) line shows the situation with 250 electron flavors, while the solid (red) line shows the situation with no electron when the solution lies directly at the onset of the gapless phase.

E. The accidental axial symmetry in the (p)2SC phase

Here we will present more details in the accidental axial symmetry of the mean-field thermodynamic potential leading to the appearance of the p2SC phase described in Sect. 4.3.3. For vanishing masses $M_u = M_d = 0$ and in the absence of charge chemical potentials the mean-field thermodynamic potential Eq. (3.17) is invariant under the axial color transformations

$$q \to \exp\left(i\theta \frac{\lambda_7}{2}\gamma_5\right) q \,, \tag{E.1}$$

if the transformation is limited to the non-strange sector. In the 2SC phase the inverse propagator can be decomposed into 4×4 blocks for the quarks involved in the pairing and 2×2 blocks for the unpaired quarks. In the p2SC phase the blocks containing the paired quarks are larger (6×6) since all colors participate in the pairing. The 2×2 blocks are related to the strange quarks and since we limit the transformation to the non-strange sector and the strange and non-strange sectors decouple completely (since $M_u = M_d = 0 \Rightarrow \phi_u = \phi_d = 0$), we can ignore the 2×2 blocks. The four 6×6 blocks take the form

$$\left(S^{\pm}_{u_b-d_r-u_g}\right)^{-1} = \begin{pmatrix} p_0 \pm \mu_u & -p & -\Delta_{25}^{(p)} & 0 & 0 & 0 \\ -p & p_0 \pm \mu_u & 0 & \Delta_{25}^{(p)} & 0 & 0 \\ -\Delta_{25}^{(p)} & 0 & p_0 \mp \mu_d & p & 0 & \mp\Delta_{22}^{(s)} \\ 0 & \Delta_{25}^{(p)} & -p & p_0 \mp \mu_d & \pm\Delta_{22}^{(s)} & 0 \\ 0 & 0 & 0 & \pm\Delta_{22}^{(s)} & p_0 \pm \mu_u & -p \\ 0 & 0 & \mp\Delta_{22}^{(s)} & 0 & -p & p_0 \pm \mu_u \end{pmatrix} \tag{E.2}$$

and

$$\left(S^{\pm}_{d_b-u_r-d_g}\right)^{-1} = \left[\left(S^{\pm}_{u_b-d_r-u_g}\right)^{-1} \text{ with } u \leftrightarrow d\right] \tag{E.3}$$

with μ_u (μ_d) being the chemical potential for the up (down) quarks. Relevant for the thermodynamic potential is the determinant of the inverse propagator

$$\begin{aligned}\det\left[\left(S^{\pm}_{u_b-d_r-u_g}\right)^{-1}\right] = &\left[(p_0 \pm \mu_u)^2 + p^2\right] \\ &\times\left[((p_0 \mp \mu_d) \pm p)\,((p_0 \pm \mu_u) \mp p) - (\Delta^{(s)}_{22})^2 - (\Delta^{(p)}_{25})^2\right] \\ &\times\left[((p_0 \mp \mu_d) \mp p)\,((p_0 \pm \mu_u) \pm p) - (\Delta^{(s)}_{22})^2 - (\Delta^{(p)}_{25})^2\right]\end{aligned} \tag{E.4}$$

and the analogous result from Eq. (E.3) with μ_u and μ_d interchanged. The determinant only depends on the sum of the squares of the diquark condensates ($\Delta^{(s)}_{22}, \Delta^{(p)}_{25}$) and so does the field independent part ($\mathcal{V}$, Eq. (3.14)) of the thermodynamic potential. This makes the mean-field thermodynamic potential invariant under Eq. (E.1).

Bibliography

[1] W. Baade, F. Zwicky, "Supernovae and cosmic rays," Phys. Rev. **45**, 138 (1934).

[2] J. Chadwick, "Possible existence of a neutron," Nature **129**, 312 (1932).

[3] A. Hewish, S. J. Bell, J. D. H. Pilkington, P. F. Scott and R. A. Collins, "Observation of a rapidly pulsating radio source," Nature **217**, 709 (1968).

[4] M. Gell-Mann, "A Schematic Model Of Baryons And Mesons," Phys. Lett. **8**, 214 (1964).

[5] G. Zweig, "An SU(3) Model For Strong Interaction Symmetry And Its Breaking," CERN-TH-401.

[6] J. C. Collins and M. J. Perry, "Superdense Matter: Neutrons Or Asymptotically Free Quarks?," Phys. Rev. Lett. **34**, 1353 (1975).

[7] N. Cabibbo and G. Parisi, "Exponential Hadronic Spectrum And Quark Liberation," Phys. Lett. B **59**, 67 (1975).

[8] D. J. Gross and F. Wilczek, "Asymptotically Free Gauge Theories. 1," Phys. Rev. D **8**, 3633 (1973).

[9] H. D. Politzer, "Reliable perturbative results for strong interactions?," Phys. Rev. Lett. **30**, 1346 (1973).

[10] Y. Nambu, "Quasi-particles and gauge invariance in the theory of superconductivity," Phys. Rev. **117**, 648 (1960).

[11] J. Goldstone, "Field Theories With Superconductor Solutions," Nuovo Cim. **19**, 154 (1961).

[12] J. Goldstone, A. Salam and S. Weinberg, "Broken Symmetries," Phys. Rev. **127**, 965 (1962).

[13] L. McLerran and R. D. Pisarski, "Phases of Cold, Dense Quarks at Large N_c," Nucl. Phys. A **796**, 83 (2007) [arXiv:0706.2191 [hep-ph]].

[14] Y. Nambu and G. Jona-Lasinio, "Dynamical model of elementary particles based on an analogy with superconductivity. I," Phys. Rev. **122** (1961) 345.

[15] Y. Nambu and G. Jona-Lasinio, "Dynamical model of elementary particles based on an analogy with superconductivity. II," Phys. Rev. **124**, 246 (1961).

[16] M. Buballa, "NJL model analysis of dense quark matter" Phys. Rept. **407**, 205 (2005) [arXiv:hep-ph/0402234].

[17] S. B. Rüster, V. Werth, M. Buballa, I. A. Shovkovy and D. H. Rischke, "The phase diagram of neutral quark matter: Self-consistent treatment of quark masses," Phys. Rev. D **72**, 034004 (2005) [arXiv:hep-ph/0503184].

[18] D. Blaschke, S. Fredriksson, H. Grigorian, A. M. Öztas and F. Sandin, "The phase diagram of three-flavor quark matter under compact star Phys. Rev. D **72**, 065020 (2005) [arXiv:hep-ph/0503194].

[19] H. Abuki and T. Kunihiro, "Extensive study of phase diagram for charge neutral homogeneous quark matter affected by dynamical chiral condensation: Unified picture for thermal unpairing transitions from weak to strong coupling," Nucl. Phys. A **768**, 118 (2006) [arXiv:hep-ph/0509172].

[20] T. Hatsuda, M. Tachibana, N. Yamamoto and G. Baym, "New critical point induced by the axial anomaly in dense QCD," Phys. Rev. Lett. **97**, 122001 (2006) [arXiv:hep-ph/0605018].

[21] N. Yamamoto, M. Tachibana, T. Hatsuda and G. Baym, "Phase structure, collective modes, and the axial anomaly in dense QCD," Phys. Rev. D **76**, 074001 (2007) [arXiv:0704.2654 [hep-ph]].

[22] G. Baym, T. Hatsuda, M. Tachibana and N. Yamamoto, "The axial anomaly and the phases of dense QCD," J. Phys. G **35**, 104021 (2008) [arXiv:0806.2706 [nucl-th]].

[23] H. Basler and M. Buballa, "NJL model of homogeneous neutral quark matter: Pseudoscalar diquark condensates revisited," Phys. Rev. D **81**, 054033 (2010) [arXiv:0912.3411 [hep-ph]].

[24] H. Basler and M. Buballa, "Role of 2SC pairing in a three-flavor NJL model with axial anomaly," Phys. Rev. D **82**, 094004 (2010) [arXiv:1007.5198 [hep-ph]].

[25] J. Bardeen, L. N. Cooper and J. R. Schrieffer, "Microscopic Theory Of Superconductivity," Phys. Rev. **106**, 162 (1957).

[26] J. Bardeen, L. N. Cooper and J. R. Schrieffer, "Theory Of Superconductivity," Phys. Rev. **108**, 1175 (1957).

[27] D. Bailin and A. Love, "Superfluidity And Superconductivity In Relativistic Fermion Systems," Phys. Rept. **107**, 325 (1984).

[28] S. D. H. Hsu, "Color superconductivity in high density quark matter," arXiv:hep-ph/0003140.

[29] K. Rajagopal and F. Wilczek, "The condensed matter physics of QCD," arXiv:hep-ph/0011333.

[30] M. G. Alford, "Color superconducting quark matter," Ann. Rev. Nucl. Part. Sci. **51**, 131 (2001) [arXiv:hep-ph/0102047].

[31] D. K. Hong, "Aspects of color superconductivity," Acta Phys. Polon. B **32**, 1253 (2001) [arXiv:hep-ph/0101025].

[32] G. Nardulli, "Effective description of QCD at very high densities," Riv. Nuovo Cim. **25N3**, 1 (2002) [arXiv:hep-ph/0202037].

[33] S. Reddy, "Novel phases at high density and their roles in the structure and evolution of neutron stars," Acta Phys. Polon. B **33**, 4101 (2002) [arXiv:nucl-th/0211045].

[34] T. Schäfer, "Quark matter," arXiv:hep-ph/0304281.

[35] H. c. Ren, "Color superconductivity of QCD at high baryon density," arXiv:hep-ph/0404074.

[36] D. H. Rischke, "The quark-gluon plasma in equilibrium," Prog. Part. Nucl. Phys. **52**, 197 (2004) [arXiv:nucl-th/0305030].

[37] M. Huang, "Color superconductivity at moderate baryon density," Int. J. Mod. Phys. E **14**, 675 (2005) [arXiv:hep-ph/0409167].

[38] I. A. Shovkovy, "Two lectures on color superconductivity," Found. Phys. **35**, 1309 (2005) [arXiv:nucl-th/0410091].

[39] M. G. Alford, A. Schmitt, K. Rajagopal and T. Schäfer, "Color superconductivity in dense quark matter," Rev. Mod. Phys. **80**, 1455 (2008) [arXiv:0709.4635 [hep-ph]].

[40] D. Bailin and A. Love, "Superfluid Quark Matter," J. Phys. A **12**, L283 (1979).

[41] M. G. Alford, K. Rajagopal and F. Wilczek, “QCD at finite baryon density: Nucleon droplets and color superconductivity,” Phys. Lett. B **422**, 247 (1998) [arXiv:hep-ph/9711395].

[42] R. Rapp, T. Schäfer, E. V. Shuryak and M. Velkovsky, “Diquark Bose condensates in high density matter and instantons,” Phys. Rev. Lett. **81**, 53 (1998) [arXiv:hep-ph/9711396].

[43] P. W. Anderson, “Plasmons, gauge invariance, and mass,” Phys. Rev. **130**, 439 (1963).

[44] P. W. Higgs, “Broken symmetries and the masses of gauge bosons,” Phys. Rev. Lett. **13**, 508 (1964).

[45] M. G. Alford, K. Rajagopal and F. Wilczek, “Color-flavor locking and chiral symmetry breaking in high density QCD,” Nucl. Phys. B **537**, 443 (1999) [arXiv:hep-ph/9804403].

[46] R. D. Pisarski and D. H. Rischke, “Why color-flavor locking is just like chiral symmetry breaking,” arXiv:nucl-th/9907094.

[47] I. A. Shovkovy and L. C. R. Wijewardhana, “On gap equations and color flavor locking in cold dense QCD with three massless flavors,” Phys. Lett. B **470**, 189 (1999) [arXiv:hep-ph/9910225].

[48] A. Schmitt, Q. Wang and D. H. Rischke, “Mixing and screening of photons and gluons in a color superconductor,” Phys. Rev. D **69**, 094017 (2004) [arXiv:nucl-th/0311006].

[49] T. Schäfer, “Quark hadron continuity in QCD with one flavor,” Phys. Rev. D **62**, 094007 (2000) [arXiv:hep-ph/0006034].

[50] A. Schmitt, “The ground state in a spin-one color superconductor,” Phys. Rev. D **71**, 054016 (2005) [arXiv:nucl-th/0412033].

[51] M. G. Alford, J. A. Bowers and K. Rajagopal, “Crystalline color superconductivity,” Phys. Rev. D **63**, 074016 (2001) [arXiv:hep-ph/0008208].

[52] J. A. Bowers and K. Rajagopal, “The crystallography of color superconductivity,” Phys. Rev. D **66**, 065002 (2002) [arXiv:hep-ph/0204079].

[53] R. Casalbuoni and G. Nardulli, “Inhomogeneous superconductivity in condensed matter and QCD,” Rev. Mod. Phys. **76**, 263 (2004) [arXiv:hep-ph/0305069].

[54] D. Nickel and M. Buballa, "Solitonic ground states in (color-) superconductivity," Phys. Rev. D **79**, 054009 (2009) [arXiv:0811.2400 [hep-ph]].

[55] F. Neumann, M. Buballa and M. Oertel, "Mixed phases of color superconducting quark matter," Nucl. Phys. A **714**, 481 (2003) [arXiv:hep-ph/0210078].

[56] E. V. Gorbar, M. Hashimoto and V. A. Miransky, "Gluonic phase in neutral two-flavor dense QCD," Phys. Lett. B **632**, 305 (2006) [arXiv:hep-ph/0507303].

[57] T. Schäfer, "P-wave meson condensation in high density QCD," Phys. Rev. Lett. **96**, 012305 (2006) [arXiv:hep-ph/0508190].

[58] G. Sarma, "On the influence of a uniform exchange field acting on the spins of the conduction electrons in a superconductor", J. Phys. Chem. Solids **24** 8, 1029 (1963).

[59] I. Shovkovy and M. Huang, "Gapless two-flavor color superconductor," Phys. Lett. B **564**, 205 (2003) [arXiv:hep-ph/0302142].

[60] M. Huang and I. Shovkovy, "Gapless color superconductivity at zero and at finite temperature," Nucl. Phys. A **729**, 835 (2003) [arXiv:hep-ph/0307273].

[61] M. Alford, C. Kouvaris and K. Rajagopal, "Evaluating the Gapless Color-Flavor Locked Phase," Phys. Rev. D **71**, 054009 (2005) [arXiv:hep-ph/0406137].

[62] M. Alford, P. Jotwani, C. Kouvaris, J. Kundu and K. Rajagopal, "Astrophysical implications of gapless color-flavor locked quark matter: A hot water bottle for aging neutron stars," Phys. Rev. D **71**, 114011 (2005) [arXiv:astro-ph/0411560].

[63] R. Casalbuoni, R. Gatto, M. Mannarelli, G. Nardulli and M. Ruggieri, "Meissner masses in the gCFL phase of QCD," Phys. Lett. B **605**, 362 (2005) [Erratum-ibid. B **615**, 297 (2005)] [arXiv:hep-ph/0410401].

[64] K. Fukushima, "Analytical and numerical evaluation of the Debye and Meissner masses in dense neutral three-flavor quark matter," Phys. Rev. D **72**, 074002 (2005) [arXiv:hep-ph/0506080].

[65] H. Kleinert, "On The Hadronization Of Quark Theories," Theories, Lectures presented at the Erice Summer Institute 1976; in: Understanding the Fundamental Constituents of Matter, A. Zichichi (ed.), Plenum Press, New York 1978, p. 289.

[66] T. Hatsuda and T. Kunihiro, "Possible Critical Phenomena Associated With The Chiral Symmetry Breaking," Phys. Lett. B **145**, 7 (1984).

[67] M. K. Volkov, “Meson Lagrangians In A Superconductor Quark Model,” Annals Phys. **157**, 282 (1984).

[68] U. Vogl and W. Weise, “The Nambu and Jona Lasinio model: Its implications for hadrons and nuclei,” Prog. Part. Nucl. Phys. **27**, 195 (1991).

[69] S. P. Klevansky, “The Nambu-Jona-Lasinio model of quantum chromodynamics,” Rev. Mod. Phys. **64**, 649 (1992).

[70] T. Hatsuda and T. Kunihiro, “QCD phenomenology based on a chiral effective Lagrangian,” Phys. Rept. **247**, 221 (1994) [arXiv:hep-ph/9401310].

[71] K. Fukushima, “Chiral effective model with the Polyakov loop,” Phys. Lett. B **591**, 277 (2004) [arXiv:hep-ph/0310121].

[72] H. J. Warringa, “The phase diagram of neutral quark matter with pseudoscalar condensates in the color-flavor locked phase,” arXiv:hep-ph/0606063.

[73] M. Kobayashi and T. Maskawa, “Chiral symmetry and eta-x mixing,” Prog. Theor. Phys. **44**, 1422 (1970).

[74] M. Kobayashi, H. Kondo and T. Maskawa, “Symmetry breaking of the chiral u(3) x u(3) and the quark model,” Prog. Theor. Phys. **45**, 1955 (1971).

[75] G. ’t Hooft, “Computation of the quantum effects due to a four-dimensional pseudoparticle,” Phys. Rev. D **14**, 3432 (1976) [Erratum-ibid. D **18**, 2199 (1978)].

[76] J.I. Kapusta, “Finite-temperature field theory,” (Cambridge University Press, 1989).

[77] S. B. Rüster, “The phase diagram of neutral quark matter,” PhD Thesis, arXiv:nucl-th/0612090.

[78] P. Amore, M. C. Birse, J. A. McGovern and N. R. Walet, “Color superconductivity in finite systems,” Phys. Rev. D **65**, 074005 (2002) [arXiv:hep-ph/0110267].

[79] M. Buballa and I. A. Shovkovy, “A note on color neutrality in NJL-type models,” Phys. Rev. D **72**, 097501 (2005) [arXiv:hep-ph/0508197].

[80] P. Rehberg, S. P. Klevansky and J. Hüfner, “Hadronization in the SU(3) Nambu-Jona-Lasinio model,” Phys. Rev. C **53**, 410 (1996) [arXiv:hep-ph/9506436].

[81] H. Abuki, G. Baym, T. Hatsuda and N. Yamamoto, “The NJL model of dense three-flavor matter with axial anomaly: the low temperature critical point and BEC-BCS diquark crossover,” Phys. Rev. D **81**, 125010 (2010) [arXiv:1003.0408 [hep-ph]].

[82] N. J. Evans, J. Hormuzdiar, S. D. H. Hsu and M. Schwetz, "On the QCD ground state at high density," Nucl. Phys. B **581**, 391 (2000) [arXiv:hep-ph/9910313].

[83] J. S. Bell and R. Jackiw, "A PCAC puzzle: pi0 → gamma gamma in the sigma model," Nuovo Cim. A **60**, 47 (1969).

[84] S. L. Adler, "Axial vector vertex in spinor electrodynamics," Phys. Rev. **177**, 2426 (1969).

[85] R. Casalbuoni and R. Gatto, "Effective theory for color-flavor locking in high density QCD," Phys. Lett. B **464**, 111 (1999) [arXiv:hep-ph/9908227].

[86] D. T. Son and M. A. Stephanov, "Inverse meson mass ordering in color-flavor-locking phase of high density QCD," Phys. Rev. D **61**, 074012 (2000) [arXiv:hep-ph/9910491].

[87] T. Schäfer, "Mass terms in effective theories of high density quark matter," Phys. Rev. D **65**, 074006 (2002) [arXiv:hep-ph/0109052].

[88] P. F. Bedaque and T. Schäfer, "High Density Quark Matter under Stress," Nucl. Phys. A **697**, 802 (2002) [arXiv:hep-ph/0105150].

[89] D. B. Kaplan and S. Reddy, "Novel phases and transitions in quark matter," Phys. Rev. D **65**, 054042 (2002) [arXiv:hep-ph/0107265].

[90] E. E. Salpeter, H. A. Bethe, "A Relativistic equation for bound state problems," Phys. Rev. **84**, 1232-1242 (1951).

[91] V. Kleinhaus, M. Buballa, D. Nickel and M. Oertel, "Pseudoscalar Goldstone bosons in the color-flavor locked phase at moderate densities," Phys. Rev. D **76**, 074024 (2007) [arXiv:0707.0632 [hep-ph]].

[92] V. Kleinhaus and M. Buballa, "Pseudoscalar bosonic excitations in the color-flavor locked phase at moderate densities," Phys. Rev. D **79**, 014016 (2009) [arXiv:0808.3490 [hep-ph]].

[93] V. Kleinhaus, "Color superconductivity: Phase Diagrams and Goldstone Bosons in the Color-Flavor Locked Phase," PhD Thesis, Darmstadt 2009.

[94] D. Ebert and K. G. Klimenko, "Diquarks in the color-flavor locked phase of dense quark matter," Phys. Rev. D **75**, 045005 (2007) [arXiv:hep-ph/0611385].

[95] D. Ebert, K. G. Klimenko and V. L. Yudichev, "Mass spectrum of diquarks and mesons in the color–flavor locked phase of dense quark matter," Eur. Phys. J. C **53**, 65 (2008) [arXiv:0705.2666 [hep-ph]].

[96] M. Rho, A. Wirzba and I. Zahed, “Generalized pions in dense QCD,” Phys. Lett. B **473**, 126 (2000) [arXiv:hep-ph/9910550].

[97] M. Rho, E. V. Shuryak, A. Wirzba and I. Zahed, “Generalized Mesons in Dense QCD,” Nucl. Phys. A **676**, 273 (2000) [arXiv:hep-ph/0001104].

[98] M. Buballa, “NJL-model description of Goldstone boson condensation in the color-flavor Phys. Lett. B **609**, 57 (2005) [arXiv:hep-ph/0410397].

[99] M. M. Forbes, “Kaon condensation in an NJL model at high density,” Phys. Rev. D **72**, 094032 (2005) [arXiv:hep-ph/0411001].

[100] D. Blaschke, D. Gomez Dumm, A. G. Grunfeld and N. N. Scoccola, “Color neutral ground state of 2SC quark matter,” arXiv:hep-ph/0507271.

[101] M. Prakash, I. Bombaci, M. Prakash, P. J. Ellis, J. M. Lattimer and R. Knorren, “Composition and Structure of Protoneutron Stars,” Phys. Rept. **280**, 1 (1997) [arXiv:nucl-th/9603042].

[102] S. B. Rüster, V. Werth, M. Buballa, I. A. Shovkovy and D. H. Rischke, “The phase diagram of neutral quark matter: The effect of neutrino trapping,” Phys. Rev. D **73**, 034025 (2006) [arXiv:hep-ph/0509073].

[103] A. W. Steiner, S. Reddy and M. Prakash, “Color-neutral superconducting quark matter,” Phys. Rev. D **66**, 094007 (2002) [arXiv:hep-ph/0205201].

[104] M. Kitazawa, T. Koide, T. Kunihiro and Y. Nemoto, “Chiral and color superconducting phase transitions with vector interaction in a simple model,” Prog. Theor. Phys. **108**, 929 (2002) [arXiv:hep-ph/0207255].

[105] Z. Zhang, K. Fukushima and T. Kunihiro, “Number of the QCD critical points with neutral color superconductivity,” Phys. Rev. D **79**, 014004 (2009) [arXiv:0808.3371 [hep-ph]].

[106] Z. Zhang and T. Kunihiro, “Vector interaction, charge neutrality and multiple chiral critical point structures,” Phys. Rev. D **80**, 014015 (2009) [arXiv:0904.1062 [hep-ph]].

[107] A. Schmitt, S. Stetina and M. Tachibana, “Ginzburg-Landau phase diagram for dense matter with axial anomaly, strange quark mass, and meson condensation,” arXiv:1010.4243 [hep-ph].

[108] M. Matsuzaki, “Spatial structure of quark Cooper pairs in a color superconductor,” Phys. Rev. D **62**, 017501 (2000) [arXiv:hep-ph/9910541].

[109] H. Abuki, T. Hatsuda and K. Itakura, “Structural change of Cooper pairs and momentum-dependent gap in color superconductivity,” Phys. Rev. D **65**, 074014 (2002) [arXiv:hep-ph/0109013].

[110] M. Kitazawa, D. H. Rischke and I. A. Shovkovy, “Bound diquarks and their Bose-Einstein condensation in strongly coupled quark matter,” Phys. Lett. B **663**, 228 (2008) [arXiv:0709.2235 [hep-ph]].

[111] D. Blaschke and D. Zablocki, “Bound States and Superconductivity in Dense Fermi Systems,” Phys. Part. Nucl. **39**, 1010 (2008) [arXiv:0812.0589 [hep-ph]].

[112] A. Gerhold, T. Schäfer and A. Kryjevski, “Goldstone boson currents in a kaon condensed CFL phase,” Phys. Rev. D **75**, 054012 (2007) [arXiv:hep-ph/0612181].

[113] F. Sandin and A. M. Öztas, “Condition for gapless color-antitriplet excitations in NJL models,” Phys. Rev. C **73**, 035203 (2006) [arXiv:hep-ph/0512087].

Danksagung

An dieser Stelle möchte ich den vielen Menschen, die direkt oder indirekt zum Gelingen dieser Arbeit beigetragen haben, danken.

An erste Stelle danke ich Prof. Jochen Wambach für die Gelegenheit diese Arbeit anfertigen zu können und sowie für seine andauernde Unterstützung.

Besonderer Dank gebührt Dr. Michael Buballa für die Betreuung dieser Arbeit, für sein Interesse an meiner Arbeit und für die vielen hilfreichen Diskussionen zu physikalischen und numerischen Fragen.

Für die sehr angenehme Arbeitsatmosphäre im 4. und 5. Stock, und inzwischen auch auf der anderen Straßenseite, möchte ich allen Mitgliedern der Theoriegruppen des Institutes für Kernphysik danken. Hier geht ein besondere Dank an meine Zimmerkollegen Jens Müller, Sabine Reinhardt, Jan Lücker, Felix Schmitt (wenn es auch nur ein paar Wochen waren) und Anneke Günther, sowie an Markus Hild für seine Besuche und Snickers. Nicht zu vergessen die Besatzung des “Pausenraumes” 420, Klaus Heckmann, Christian Kellerman, Tobias Göcke und Thorsten Zöller, hier wurde über Gott und die Welt diskutiert und oft gab es auch Erdnüsse. Des Weiteren möchte ich auch unserem Fussball-Team für die lustigen Stunden auf dem Feld danken, hierzu noch eine Bemerkung: “Hingefallen ist er ganz von alleine, der Chrisitan!”.

Teilweise finanziert wurde diese Arbeit durch das Helmholtz International Center for FAIR. Auch danke ich der Helmholtz Graduate School for Hadron and Ion Research für die Reisekostenunterstützung sowie die abwechslungsreichen Veranstaltungen an denen ich im letzen Jahr teilnehmen konnte. In diesem Zusammenhang möchte ich Prof. Dirk Rischke dafür danken, dass er diese Arbeit im *PhD Committee* begleitet hat.

Meinen Eltern danke ich für die anhaltende Unterstützung während meines gesamten Studiums. Abschließend möchte ich meiner Freundin Lidia für ihre Unterstützung und ihr Verständnis, besonders in der Schlussphase, danken.

Lebenslauf

Name:	Hannes Gregor Steffen Basler
Geburtsdatum:	5. Juni 1981
Geburtsort:	Bad Soden am Taunus
Staatsangehörigkeit:	deutsch
Familienstand:	ledig

Bildungsweg

07/1987 – 06/1991	Diesterweg Grundschule, Frankfurt am Main
07/1991 – 06/2000	Ziehenschule, Gymnasium, Frankfurt am Main
06/2000	Abitur
10/2000 – 03/2007	Studium der Physik an der TU Darmstadt
07/2003 – 06/2004	ERASMUS-Austauschprogramm an Norges Teknisk-Naturvitenskapelige Universitet, Trondheim, Norwegen
03/2007	Diplom
seit 07/2007	Promotionsstudium an der TU Darmstadt und Anfertigung der Dissertation
seit 07/2007	Wissenschaftlicher Mitarbeiter am Insitut für Kernphysik